REVIEW

Check for updates

Recent progress in the preparation and environmental applications of functionalized adsorbent hydrogel: a review

Huda Salman Alkhaldi, [a] Muneer Baata, [b] Fawziah Alhajri, [a] A. M. Elbasiony, [c] Mohammed S. Almoiqli, [b] Mohamed Madani [a] and Mohamed Mohamady Ghobashy *[d]

This review highlights recent advancements in the preparation and environmental applications of functionalized adsorbent hydrogels, with a focus on their role in addressing global water pollution and scarcity. Hydrogels, with their unique three-dimensional crosslinked structures and exceptional water retention capabilities, have emerged as versatile materials for water purification. The review encompasses various synthesis methods, including chemical cross-linking and radiation-induced polymerization, and examines their mechanisms for pollutant removal, including adsorption, ion exchange, electrostatic interactions, and photocatalytic degradation. Additionally, integrating nanomaterials into hydrogels enhances their mechanical properties and contaminant-removal efficiency. The review also discusses innovative applications, including solar-driven water remediation, microbial inactivation, and simultaneous water and power generation. These advancements position hydrogels as sustainable and efficient solutions for global water security challenges.

1. Introduction

Access to clean water remains one of humanity's most pressing challenges, with over 1.2 billion people currently lacking direct access to safe drinking water due to widespread pollution and water scarcity.[1] The contamination of water bodies by heavy metals, dyes, pharmaceuticals, microplastics, and various organic pollutants continues to escalate, driven by rapid industrialization, urbanization, and anthropogenic activities.[2] This critical situation necessitates the development of efficient, cost-effective, and environmentally sustainable water treatment technologies.[3] Among the numerous water purification approaches available, adsorption and photocatalytic technologies have emerged as particularly promising solutions due to their operational simplicity, high performance, and economic viability. Fig. 1 illustrates the multifaceted nature of water pollution challenges and the diverse treatment strategies

currently employed to address them. The figure demonstrates that hydrogel-based materials represent a significant advancement in this field, offering unique advantages through their three-dimensional crosslinked structures and exceptional water-retention capabilities.

Hydrogels play a pivotal role in water purification due to their exceptional water absorption capacity and tunable physicochemical properties, which enable the efficient removal of contaminants such as heavy metals, dyes, and organic pollutants.[4,5] Functionalized adsorbent hydrogels have gained considerable attention as next-generation water treatment materials due to their remarkable structural flexibility, chemical stability, and abundance of hydrophilic functional groups, including carboxylic, amino, and hydroxyl groups. These characteristics enable hydrogels to remove various contaminants through multiple mechanisms, while their biocompatibility and renewable precursors enhance their environmental sustainability. The integration of nanomaterials into hydrogel matrices has further expanded their capabilities, creating nanocomposite systems with enhanced mechanical properties, improved mass transport, and synergistic functionality for both adsorption and photocatalytic applications.[6]

Recent progress has demonstrated that these advanced materials can simultaneously address multiple water quality challenges through integrated approaches combining adsorptive removal, photocatalytic degradation, antimicrobial disinfection, and solar-driven desalination processes.[5,7] The versatility of their contaminant removal mechanisms spanning

a Department of Physics, College of Science and Humanities-Jubail, Imam Abdulrahman Bin Faisal University, Jubail, Saudi Arabia. E-mail: hsalkaldi@iau.edu.sa; fsalhajri@iau.edu.sa; mmadani@iau.edu.sa

b Desalination Technologies Institute (DTI), King Abdulaziz City for Science and Technology, Riyadh, 11442, Saudi Arabia. E-mail: mbaata@kacst.gov.sa; almoiqli@kacst.gov.sa

c Department of Chemistry, College of Science, Northern Border University (NBU), Arar, Saudi Arabia. E-mail: amr.albeasieny@nbu.edu.sa

d Radiation Research of Polymer Department, National Center for Radiation Research and Technology (NCRRT), Atomic Energy Authority, P. O. Box. 29, Nasr City, Cairo, Egypt. E-mail: Mohamed.ghobashy@eaea.org.eg
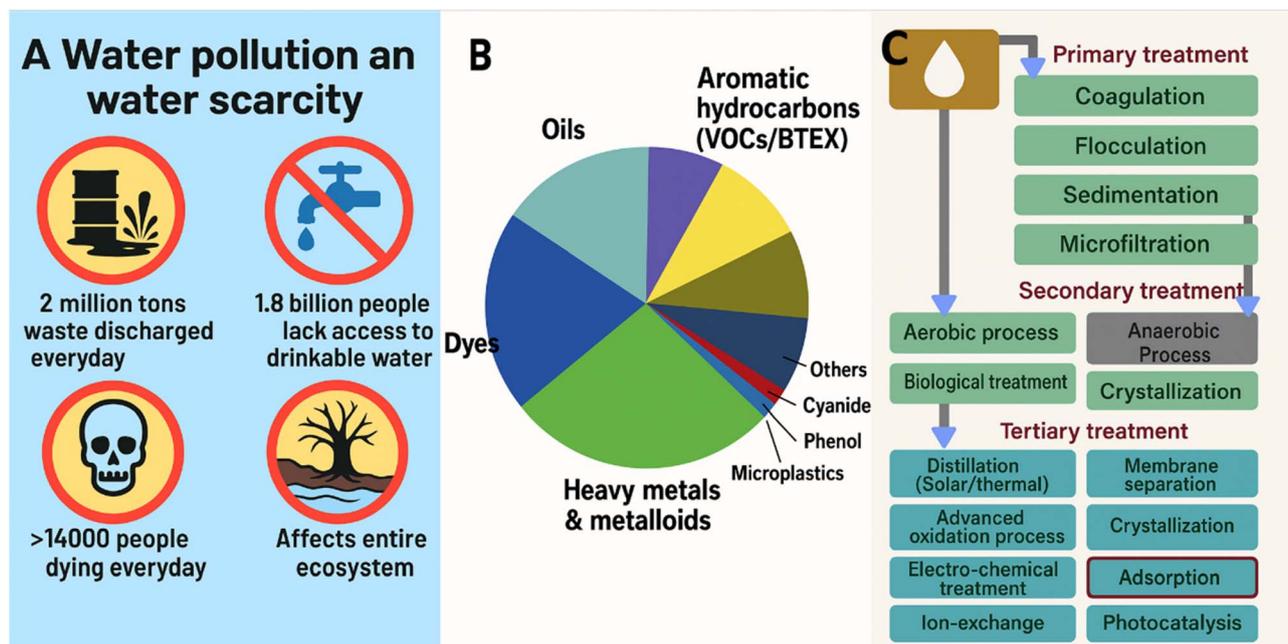
Fig. 1 Summary of water pollution and available treatment technologies. (A) Worldwide water pollution and water scarcity statistics from the Global Water Intelligence Report (2014), highlight the critical shortage of clean water access affecting over 1.2 billion people worldwide. (B) Various water pollutants commonly found in contaminated water bodies, including heavy metals, dyes, pharmaceuticals, microplastics, volatile organic compounds, and biological contaminants that pose significant health risks. (C) Primary, secondary, and tertiary water treatment practices are employed to eliminate inorganic, organic, and biological contaminants from wastewater, showcasing the multi-stage approach required for comprehensive water purification and the positioning of advanced treatment technologies in addressing complex pollution challenges.

ion exchange, complexation, electrostatic interactions, and surface adsorption positions functionalized hydrogels as transformative materials for comprehensive water treatment solutions.[8] This review synthesizes current knowledge of hydrogel preparation methodologies, environmental applications, and underlying performance mechanisms, providing essential insights into how these innovative materials are revolutionizing water treatment strategies and advancing global water security initiatives. The exceptional recyclability of hydrogels represents a significant advantage for sustainable water treatment applications, as many hydrogel systems maintain their adsorption efficiency across multiple regeneration cycles without performance degradation, thereby supporting both economic viability and environmental sustainability. Hydrogel performance can be substantially enhanced by strategically incorporating nanomaterials into their polymer matrices, creating advanced nanocomposite systems with superior properties that further optimize their water treatment capabilities.[6] This enhancement approach involves integrating diverse organic and inorganic nanomaterials, including carbonaceous structures such as graphene and carbon nanotubes; metal-based compounds such as metal oxides and sulfides; magnetic particles; nanoclays; layered double hydroxides; emerging materials such as MXenes and metal–organic frameworks; and bio-based nanocellulose. Incorporating these nanomaterials fundamentally alters the hydrogel architecture by promoting extensive cross-linking between polymer chains and nanofillers, simultaneously reducing the mesh size and

creating numerous interconnected pores that facilitate enhanced mass and charge transport. This structural modification results in dramatically increased surface areas and improved polymer–water interactions, contributing to superior adsorption and photocatalytic performance.[9] The synergistic combination of nanomaterial properties with the inherent advantages of hydrogel networks creates multifunctional materials that excel in water treatment applications, particularly as photocatalysts, where the high porosity and specific surface area provide abundant active sites for reactant adsorption and subsequent degradation reactions.

Traditionally, hydrogels are synthesized *via* chemical methods using crosslinkers (*e.g.*, N,N'-methylenebisacrylamide) and initiators, which can introduce toxic residues, necessitating post-synthesis purification.[10,11] In contrast, radiation-assisted methods, such as gamma irradiation, electron beam, and microwave techniques, offer cleaner alternatives by inducing crosslinking without the use of chemical additives. Gamma irradiation, for instance, produces hydrogels from polymers such as carboxymethyl cellulose or poly(acrylic acid) with high purity and inherent sterilization, making them ideal for biomedical and environmental applications.[12,13] Electron beam irradiation enables rapid, directional synthesis of hydrogels with tailored porosity for pollutant adsorption, while microwave methods achieve fast polymerization with minimal energy consumption.[14,15] Radiation-synthesized hydrogels, such as starch-acrylic acid or chitosan-based networks, exhibit enhanced adsorption capacities and reusability, making them

eco-friendly solutions for wastewater treatment.[16,17] These methods not only reduce environmental contamination but also optimize hydrogel performance by controlling crosslinking density, demonstrating superior water-purification efficiency compared to conventional chemical approaches.[14]

As illustrated in Fig. 2, the advancement of functionalized adsorbent hydrogels represents a significant breakthrough in sustainable water treatment technologies. Recent progress has demonstrated that these materials can be synthesized *via* chemical and radiation-induced crosslinking, enabling precise control over their three-dimensional network structures and functional properties. The versatility of hydrogels in water treatment applications is evident in their multifaceted mechanisms of action, including adsorptive removal of pollutants *via* ion exchange, complexation, electrostatic interactions, and surface complexation.

Integrating photocatalytic degradation with solar-driven desalination processes highlights the emerging trend toward multifunctional hydrogel systems that simultaneously address multiple water-quality challenges.[18,19] Furthermore, incorporating antimicrobial properties expands their utility beyond contaminant removal to comprehensive water disinfection applications. The various contaminant removal mechanisms from physical adsorption to chemical complexation demonstrate the adaptability of hydrogel platforms for treating a diverse range of water pollutants. The incorporation of high-performance nanomaterials (NMs) such as graphene, metal–organic frameworks (MOFs), and MXenes into hydrogels is widely championed for creating next-generation adsorbents with enhanced capacity and selectivity for water treatment;[20] however, this performance-centric narrative often overlooks the critical caveat that these advanced materials can introduce significant environmental risks, including the potential for nanomaterial leaching, generation of reactive oxygen species, and long-term ecotoxicity to aquatic organisms, raising pressing concerns about their true lifecycle impact and challenging the sustainable credentials of the resulting nanocomposite hydrogels without rigorous design for degradation and disposal.[21,22] This review synthesizes the current state of knowledge on hydrogel preparation methodologies, their environmental applications, and the mechanisms governing their performance, providing a comprehensive foundation for understanding how these advanced materials are revolutionizing water treatment strategies and advancing global water security initiatives.

2. Polymer–based hydrogels and their synthesis approaches

Hydrogels are emerging as pioneering materials in water purification due to their exceptional ability to absorb and retain large volumes of water and contaminants. Their three-dimensional, hydrophilic polymer networks enable them to efficiently remove a wide range of pollutants, including heavy metals and organic contaminants, from water. For instance, chitosan-based hydrogels have demonstrated high adsorption capacities, making them particularly effective in wastewater treatment applications.[23,24] Recent advancements have led to the development of multifunctional hydrogels with tunable properties, enabling the rapid and selective absorption of both organic and inorganic micropollutants. These hydrogels can outperform traditional adsorbents, such as activated carbon, by adsorbing pollutants up to 10 times faster, even in the presence of background water hardness.[25] Hydrogels can be synthesized using both chemical and radiation methods, each with distinct advantages. Chemical cross-linking is a widely used method that forms permanent covalent bonds between polymer chains. This process typically requires a monomer, an initiator, and
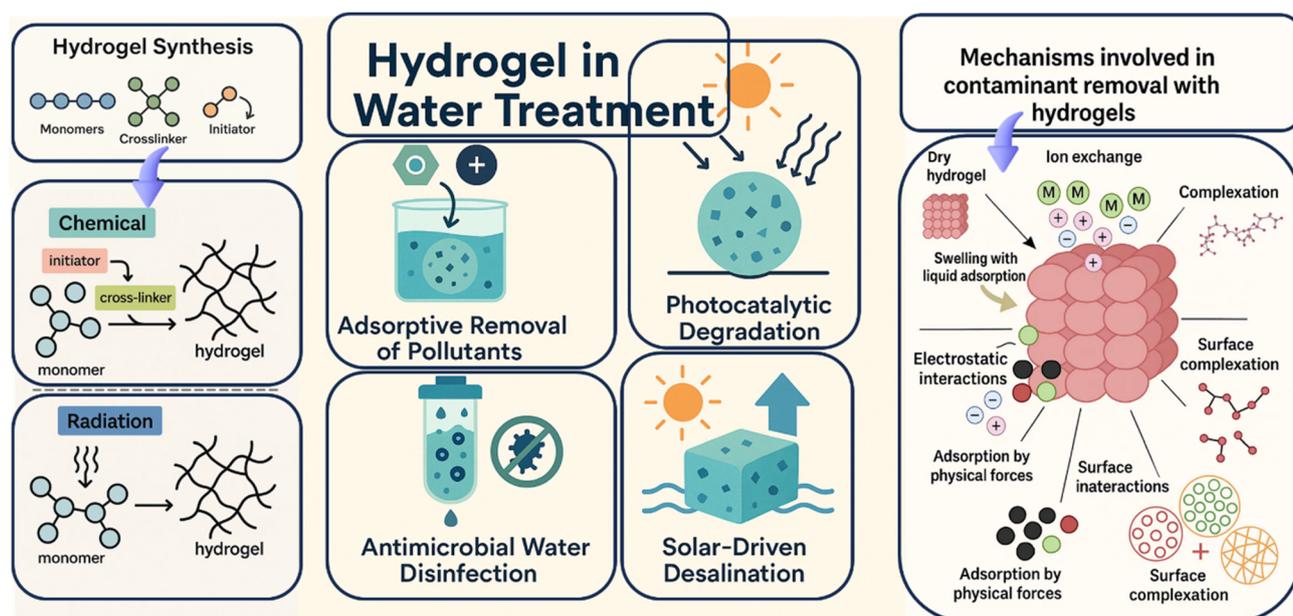

Fig. 2 Comprehensive overview of hydrogel synthesis and environmental applications in water treatment.

a cross-linking agent, and results in hydrogels with excellent mechanical strength and stability. The degree of cross-linking can be tailored to produce hydrogels with specific properties, such as stiffness or flexibility, depending on their intended application.[26,27] Radiation-induced methods, on the other hand, utilize high-energy sources, such as gamma rays, electron beams, or ultraviolet (UV) light, to initiate cross-linking within hydrophilic polymer networks. One of the key advantages of radiation methods is the ability to simultaneously sterilize the hydrogel and control the cross-link density without the need for additional chemical reagents, which is particularly beneficial for biomedical and environmental applications. Gamma radiation, for example, generates radicals on polymer chains, resulting in covalent bond formation and the formation of a stable hydrogel structure. The extent of cross-linking and thus the hydrogel's physical properties can be precisely controlled by adjusting the radiation dose.[28,29] Both chemical and radiation methods have facilitated the development of hydrogels with tailored properties for water purification. The versatility of synthesis enables customization of hydrogels to target specific contaminants or function effectively across various environmental conditions. As research continues to advance, hydrogels are expected to play an increasingly significant role in sustainable water treatment technologies, offering efficient, rapid, and adaptable solutions for global water purification challenges.[28,30]

Chemical and radiation methods differ fundamentally in how they initiate and control hydrogel formation, each offering unique advantages and limitations. Chemical methods for hydrogel synthesis typically involve the use of initiators and crosslinking agents to form covalent bonds between polymer chains. In this approach, hydrophilic monomers are polymerized and cross-linked simultaneously or sequentially, often in the presence of chemical additives such as initiators (to initiate polymerization) and cross-linkers (to connect polymer chains). This process enables precise control over the hydrogel's mechanical strength and structural properties, making it highly versatile for a wide range of applications. However, a significant drawback of chemical methods is the potential for residual toxicity due to unreacted initiators or cross-linkers, which may compromise the purity and biocompatibility of the final hydrogel product.[14,26]

In contrast, radiation methods utilize high-energy sources, such as gamma rays, electron beams, or ultraviolet light, to directly initiate the formation of free radicals within the polymer or monomer solution. These free radicals then induce polymerization and cross-linking without the need for additional chemical reagents. Radiation-induced hydrogel synthesis offers several distinct advantages: it eliminates the risk of residual toxic chemicals, allows simultaneous sterilization during production, and can be applied to a wide range of vinyl monomers and natural polymers.[28,29] The degree of cross-linking and, consequently, the hydrogel's physical properties can be finely tuned by adjusting the radiation dose and conditions, such as temperature and polymer concentration.[28] For example, gamma radiation is particularly effective due to its high energy, enabling efficient cross-linking and the formation of hydrogels with desirable swelling and absorption

properties.[14] Additionally, radiation methods can produce hydrogels with nanoscale structures, offering enhanced surface area and improved absorption and retention. This is especially advantageous for biomedical and environmental applications, where purity, biocompatibility, and performance are critical.[28]

2.1. Chemical synthesis of hydrogel

Chemical synthesis is one of the most common and versatile methods for producing polymer-based hydrogels. This approach involves the formation of permanent covalent bonds between polymer chains *via* chemical cross-linking. The synthesis typically requires three main components: a monomer (or a preformed polymer), an initiator to start the polymerization reaction, and a cross-linking agent to link the polymer chains and form a stable three-dimensional network. The choice of monomer and cross-linker enables precise tailoring of hydrogel properties, including mechanical strength, porosity, swelling capacity, and responsiveness to environmental stimuli. For example, using hydrophilic monomers such as acrylamide or acrylic acid yields hydrogels that can absorb large volumes of water, making them ideal for water purification applications. Chemical cross-linking offers excellent control over the structural integrity and functional characteristics of the resulting hydrogel. By adjusting the cross-link density, hydrogels can be engineered to exhibit specific stiffness, elasticity, or permeability, depending on the intended application. Additionally, functional groups can be incorporated into the hydrogel matrix to enhance their affinity for specific contaminants, such as heavy metals or organic pollutants.

Common methods include free radical polymerization, in which initiators such as ammonium persulfate (APS) and tetramethylethylenediamine (TEMED) generate reactive species to propagate monomer chains, often using crosslinking agents such as N,N'-methylenebisacrylamide (MBA) or poly(ethylene glycol) diacrylate (PEGDA) to establish permanent junctions.[31] Solution polymerization is widely employed, with monomers dissolved in aqueous or organic solvents under controlled temperatures and pH. Alternatively, advanced techniques such as click chemistry (*e.g.*, azide–alkyne cycloaddition) enable precise, rapid crosslinking with high specificity, minimizing side reactions.[32] Reversible addition-fragmentation chain-transfer (RAFT) polymerization and atom transfer radical polymerization (ATRP) are also utilized to design hydrogels with tunable architectures and responsive properties.[33] These methods allow customization of mechanical strength, porosity, and stimuli-responsive behavior (*e.g.*, pH and temperature), which are critical for applications in drug delivery, tissue engineering, and biosensing.[34] The choice of monomers, crosslinkers, and synthesis conditions directly influences hydrogel functionality, necessitating careful optimization for specific biomedical or industrial applications.

The chemical synthesis of hydrogels encompasses a diverse array of strategies to tailor their properties for specialized applications. Beyond conventional free radical polymerization, methods such as Michael addition allow for thiol- and acrylate-

based monomers to react under mild conditions, forming biocompatible networks suitable for cell encapsulation.[35] Photopolymerization, using light-activated initiators (*e.g.*, Irgacure 2959) [36] and UV exposure, enables spatially controlled hydrogel formation, which is advantageous for 3D bioprinting and *in situ* gelation.[37] Enzyme-mediated crosslinking, such as horseradish peroxidase (HRP)-catalyzed reactions, provides bioorthogonal control for fabricating hydrogels with minimal cytotoxicity, making them ideal for tissue regeneration.[38] Schiff base formation between amine and aldehyde groups (*e.g.*, chitosan and oxidized dextran) creates dynamic, self-healing hydrogels useful for injectable drug delivery systems.[39] Thiol–ene "click" chemistry enables rapid, oxygen-tolerant crosslinking of hydrogels with tunable mechanical properties, which are applied in wound dressings.[40] Additionally, polycondensation reactions (*e.g.*, polyurethane hydrogels) use diisocyanates and polyols to form elastomeric networks for industrial coatings.[41] Emerging approaches include dendrimer-based hydrogels, in which hyperbranched polymers serve as multifunctional crosslinkers to create nanoporous structures for gene delivery, and supramolecular hydrogels, which leverage host–guest interactions (*e.g.*, cyclodextrin-adamantane) to create stimuli-responsive scaffolds.[42] Hybrid systems combining covalent and ionic crosslinking (*e.g.*, alginate-polyacrylamide) enhance toughness for load-bearing applications.[43] These methods highlight the versatility of chemical synthesis in engineering hydrogels with precise functionality.

2.1.1. Click polymerization reaction. Click polymerization is a highly efficient and versatile chemical process for synthesizing polymers *via* modular, selective reactions under mild conditions. Originating from the "click chemistry" concept introduced by Sharpless and colleagues, this approach emphasizes highly yielding reactions, broad scope, and generates minimal by-products. A notable example in polymer science is the copper(I)-catalyzed azide–alkyne cycloaddition (CuAAC), which forms stable 1,2,3-triazole linkages. This reaction is particularly advantageous for forming well-defined polymer networks due to its rapid kinetics, orthogonality, and compatibility with various functional groups. Click polymerization is widely applied in the design of hydrogels, drug delivery systems, and functional materials, offering precise control over molecular architecture and enhancing material performance.

Barbucci *et al.*[44] developed a hydrogel system *via* thiol–maleimide coupling, in which thiolated hyaluronic acid (HA-SH) reacts with maleimide-functionalized poly(ethylene glycol) (PEG-MAL). This Michael-type addition forms highly specific, biocompatible networks under physiological conditions. The rapid gelation enables injectable applications and supports the viability of encapsulated cells, making it particularly suitable for cartilage tissue engineering. These hydrogels facilitate chondrocyte proliferation and matrix deposition, promoting cartilage repair. The mild reaction avoids the formation of toxic byproducts, thereby preserving the bioactivity of incorporated molecules. Due to its efficiency and tunability, this coupling is widely used in regenerative medicine.

Kelvin *et al.*[45] demonstrated the use of strain-promoted azide–alkyne cycloaddition (SPAAC) to form hydrogels for

wound healing. Dibenzocyclooctyne (DBCO)-functionalized polyethylene glycol (PEG) was reacted with azide-modified peptides in a metal-free, bioorthogonal process. This catalyst-free "click" chemistry avoids copper-related cytotoxicity, allowing safe *in vivo* applications. The fast, efficient crosslinking under mild conditions enables the encapsulation of sensitive biological molecules and cells. Resulting hydrogels promote tissue regeneration and reduce inflammation at wound sites. SPAAC offers a powerful platform for developing injectable, *in situ*-forming biomaterials for therapeutic delivery and tissue repair.

Ossipov *et al.*[46] utilized copper-catalyzed azide–alkyne cycloaddition (CuAAC) to create tunable hydrogels for 3D cell culture. By combining azide-modified gelatin with alkyne-functionalized PEG in the presence of Cu(I) catalyst, they achieved robust crosslinked networks. The reaction proceeds under aqueous conditions, enabling high structural definition and mechanical adaptability. Despite the requirement for copper, cytotoxicity was mitigated by using chelating agents and post-gelation washing. The system supports cell encapsulation with preserved viability and provides fine control over hydrogel stiffness, which is essential for studying cell behavior in tissue engineering. CuAAC remains a benchmark in bioorthogonal chemistry for its versatility and efficiency.

Lin *et al.*[47] developed thiol–ene photopolymerized hydrogels for corneal tissue engineering. Thiolated collagen was crosslinked with ene-functionalized polyethylene glycol diacrylate (PEGDA) under UV light, forming biocompatible and optically clear matrices. The reaction allows spatial and temporal control, enabling a precise microarchitecture essential for directing cellular organization. Rapid gelation and minimal cytotoxicity make this approach ideal for encapsulating delicate cells. The resulting hydrogels closely mimic the properties of the native corneal extracellular matrix, thereby supporting the growth and function of epithelial cells. Thiol–ene systems are highly efficient and tunable, making them suitable for tissue scaffolding and regenerative applications requiring structural fidelity.

Fairbanks *et al.*[48] employed thiol–yne click chemistry to fabricate high-strength hydrogels. Multi-armed PEG-yne was reacted with dithiol linkers, resulting in a densely crosslinked network with superior mechanical properties compared to thiol–ene systems. This increased crosslinking density enhances load-bearing capabilities, making these hydrogels suitable for applications such as cartilage or bone repair. The photoinitiated reaction proceeds rapidly and with minimal side reactions, preserving biological functionality. The system's tunability and strength enable it to support cellular growth in mechanically dynamic environments, underscoring its value in regenerative medicine and biomedical engineering, where structural integrity is crucial.

DeForest *et al.*[49] introduced a tetrazine-norbornene inverse electron demand Diels–Alder (IEDDA) reaction for ultrafast hydrogel formation. Tetrazine-modified hyaluronic acid (HA) was reacted with norbornene-functionalized PEG, enabling gelation within 1 minute. This catalyst-free, highly specific reaction enables *in situ* applications, particularly in injectable

drug delivery systems. The resulting hydrogels are cytocompatible and form under physiological conditions, supporting cell viability and drug encapsulation. The ultrafast kinetics of IEDDA reactions make them advantageous in time-sensitive biomedical contexts, such as localized therapy and tissue regeneration. This method exemplifies the potential of bioorthogonal chemistry for next-generation hydrogel systems.

Hoyle et al.[40] demonstrated the Michael addition reaction between thiol and acrylate for hydrogel synthesis. Thiolated chitosan was crosslinked with acrylated PEG under base-catalyzed conditions to form pH-responsive hydrogels for oral drug delivery. This reaction occurs under mild conditions, without the need for external initiators or catalysts, thereby maintaining biomolecule integrity. The resulting hydrogels swell and degrade in response to pH changes, enabling targeted release in specific gastrointestinal environments. Michael addition provides reliable, versatile crosslinking for drug delivery systems, enabling precise modulation of release profiles and material properties. Its efficiency and biocompatibility make it ideal for the design of therapeutic biomaterials.

Podgórski et al.[50] developed dynamic hydrogels through thiol-vinyl sulfone coupling. Vinyl sulfone-modified hyaluronic acid (HA) was crosslinked with dithiothreitol (DTT), forming self-healing networks suitable for vocal fold regeneration. Covalent bonding allows reversible network formation, enabling repeated damage repair. This adaptable gel structure supports cell adhesion and proliferation while mimicking the mechanical behavior of soft tissues. The hydrogel's tunable viscoelasticity and resilience make it ideal for dynamic environments such as vocal folds, where repeated mechanical stress occurs. Thiol-vinyl sulfone chemistry thus offers promising solutions in soft tissue repair and regenerative medicine.

Yue et al.[51] utilized thiol-methacrylate photoclick chemistry to construct cell-laden hydrogels for bioprinting liver tissue. Methacrylated gelatin (GelMA) was crosslinked with thiolated poly (ethylene glycol) (PEG) under UV light, forming a biocompatible network with excellent printability. The system enables precise spatial patterning, a crucial step for replicating complex tissue structures. Photoclick reactions proceed rapidly and under mild conditions, preserving cell viability and function. The resulting hydrogels support hepatocyte growth and matrix deposition, demonstrating utility in tissue engineering and disease modeling. This approach combines tunable mechanical properties with high-resolution fabrication, advancing 3D bioprinting applications.

Wang et al.[52] reported on thiol-isocyanate coupling to generate fast-setting hydrogels for hemostatic wound dressings. Thiolated alginate was reacted with polyisocyanate crosslinkers to form robust hydrogels in seconds. The reaction proceeds under ambient conditions without external stimuli, enabling rapid application during emergencies. These hydrogels provide strong tissue adhesion, efficiently seal wounds, and reduce blood loss. Additionally, the materials support cellular infiltration and tissue regeneration. This coupling method offers a practical platform for developing next-generation bioadhesives and wound care products, combining speed, biocompatibility, and mechanical integrity.

Table 1 summarizes key click polymerization reactions employed in hydrogel synthesis, highlighting their reagent systems, structural features, and representative examples from the reviewed literature. The table categorizes reactions such as SPAAC (using dibenzocyclooctyne and azide-PEG) and CuAAC (relying on propargyl-alcohol and sodium azide with copper catalysts), emphasizing their roles in creating biocompatible or high-efficiency networks. Dynamic strategies, such as the Diels–Alder reaction (furan–maleimide pairs) and oxime/hydrazone (aminooxy-ketone linkages), illustrate reversible crosslinking for stimuli-responsive hydrogels. Renewable reagents, including limonene-derived alkynes, vanillin-based bis-acetoacetates, and epoxidized plant oils, underscore the shift toward sustainable feedstocks. Notably, multicomponent reactions (e.g., Ugi and Biginelli) demonstrate versatility in monomer diversity but face scalability challenges. This comparative overview bridges reaction mechanisms.

2.1.2. Schiff base polymerization reaction. Schiff base polymerization involves the formation of polymers through condensation reactions between amine and aldehyde or ketone functional groups, forming imine (C=N) linkages. This reaction is typically carried out under mild conditions, often in aqueous or alcoholic solvents, and does not require additional catalysts, making it attractive for environmentally friendly and biocompatible applications. The resulting imine bonds confer dynamic, reversible properties to the polymer network, which can be advantageous in stimuli-responsive systems, self-healing materials, and controlled drug-release applications. Schiff base polymerization enables the incorporation of a wide range of functional monomers, allowing for the design of customizable polymeric materials with tailored physical, chemical, and biological properties.

Kim et al.[67] developed pH-responsive hydrogels using Schiff base chemistry between chitosan and oxidized dextran. The aldehyde groups on oxidized dextran react with the amine groups on chitosan to form dynamic imine bonds. These hydrogels demonstrate controlled degradation under acidic conditions, making them suitable for targeted drug delivery in tumor microenvironments. Their injectable nature and biocompatibility further support clinical applications. The pH-dependent degradation profile ensures minimal side effects in healthy tissues. Overall, the study highlights the potential of these chitosan–dextran hydrogels for smart, stimuli-responsive therapeutic systems.

Li et al.[68] created injectable gelatin–oxidized alginate hydrogels for cartilage tissue engineering. Oxidized alginate, containing aldehyde groups, reacts with lysine residues in gelatin to form stable Schiff base crosslinks. The resulting hydrogels exhibit self-healing properties, supporting cellular infiltration and integration with host tissues. Their viscoelastic behavior and tunable mechanical properties make them suitable for soft tissue repair. In addition, the mild gelation conditions preserve the bioactivity of encapsulated cells or biomolecules. These features make this system highly promising for minimally invasive cartilage regeneration strategies.

Deng et al.[69] engineered adhesive hydrogels by crosslinking benzaldehyde-functionalized hyaluronic acid with chitosan

Table 1 Kinds of click polymerization reactions for hydrogel synthesis

Reaction type	Common reagent and catalyst examples	Mechanism	Advantages	Disadvantages	Hydrogel example	Ref.
SPAAC	Dibenzocyclooctyne (DBCO) + azide-PEG	Strain-promoted azide–alkyne cycloaddition without copper catalyst	- Biocompatible (no Cu residue) - Fast gelation in aqueous media	- Expensive strained cyclooctyne reagents - Multi-step synthesis required	HA-PEG hydrogel: cyclooctyne-modified HA + azide-PEG at pH = 7.4 PBS and 37 °C	45
CuAAC	Propargyl alcohol + sodium azide (CuSO$_4$/NaAsc)	Copper-catalyzed azide–alkyne cycloaddition	- High efficiency - Orthogonal reactivity	- Cytotoxic Cu residues - Requires purification	Dendronized cellulose: CuAAC-grafted PAMAM dendrons on cellulose	53
Thiol–ene	PETMP (pentaerythritol tetrathiol) + allyl ethers (DMPA initiator)	Radical-mediated addition of thiols to alkenes	- Fast UV curing - Catalyst-free options	- Oxygen inhibition	Cellulose films: vinyl-silane cellulose + methyl thioglycolate	54
Diels-Alder (DA)	Furan + maleimide	Thermally reversible [4 + 2] cycloaddition	- Reversible crosslinking - No byproducts	- High retro-DA temperatures	Vanillin-based networks: acetal-containing diallyl vanillin + dithiols	55
Thiol–Michael	PEG-SH + acrylate-functionalized PCL (Et$_3$N catalyst)	Base-catalyzed thiol addition to electron-deficient alkenes	- Mild conditions - High conversion	- pH-sensitive (basic conditions)	PCL grafts: PEG-SH + acryloyl-functionalized PCL	56
Thiol–ene	1,6-Hexanedithiol + limonene-derived alkyne	Radical-mediated addition of two thiols to alkynes	- High crosslinking density	- Complex stoichiometry	Limonene polythioethers: plant oil-derived alkynes + dithiols	57
Perfluoroaryl click	Pentafluorophenyl ester + amine	Nucleophilic substitution on pentafluorophenyl esters	- Catalyst-free - High reactivity	- Requires basic pH	Poly(pentafluorophenyl acrylate): modified with bio-alcohols (e.g., geraniol)	58
Inverse DA (iEDDA)	Tetrazine-PEG + norbornene	Norbornene-tetrazine cycloaddition	- Fast in water - Bioorthogonal	- Tetrazine instability	PEG-Tz hydrogels: tetrazine-PEG + norbornene crosslinkers	59
Multicomponent (Ugi)	FDCA + diaminodecane + isocyanide + aldehyde	One-pot amine–aldehyde–isocyanide–carboxylic acid reaction	- Atom-economical - Diverse monomers	- Scalability challenges	FDCA polyamides: 2,5-furandicarboxylic acid + diaminodecane	60
Oxime/hydrazone	Aminooxy dextran + ketone-modified chitin	Carbonyl + aminooxy/ hydrazide condensation	- Dynamic bonds - Biocompatible	- Slow gelation	Chitin/dextran hydrogels: oxime-linked polysaccharides	61
Passerini polycondensation	Methyl 10-undecenoate + dialdehyde + isocyanide	Three-component (diacid, dialdehyde, isocyanide) polymerization	- Renewable monomers (e.g., castor oil) - Hyperbranched structures	- Limited mechanical strength	Hyperbranched polyesters: methyl 10-undecenoate + dithiols	62
Biginelli reaction	Vanillin-derived bis-acetoacetate + urea + aldehyde	Three-component (bis-acetoacetate, urea, aldehyde) polycondensation	- High thermal stability - Renewable (e.g., vanillin)	- Broad polydispersity	Poly(3,4-dihydropyrimidin-2(1H)-one)s: vanillin-derived monomers	63
Amino-yne click	Propiolated castor oil + hexamethylene diamine	Aza-Michael addition to propiolated oils	- Solvent-free - Ultra-fast (<5 min)	- Limited monomer scope	Propiolated castor oil: reacted with multifunctional amines	64
Salicylhydroxamate-boronic acid	Salicylhydroxamate polymer + phenylboronic acid	Boronate ester formation	- pH-responsive - Biocompatible	- Sensitivity to competitive ligands	Protein–polymer nanoassemblies: polymer–protein conjugates for intracellular delivery	65
Thiol-epoxy click	Epoxidized linseed oil + gallic acid–thiol	Ring-opening of epoxides with thiols	- High mechanical strength - Renewable (epoxidized oils)	- Slow kinetics	Gallic acid–thiol networks: crosslinked with epoxidized linseed oil	66

through Schiff base bonds. The aldehyde–amine reaction enables rapid gelation and strong tissue adhesion, rendering the hydrogels suitable for diabetic wound healing. Their biocompatibility and biodegradability enable safe degradation *in vivo* while promoting cell proliferation and vascularization. The hydrogels also exhibit moisture retention and antibacterial properties, key for effective chronic wound treatment. This platform demonstrates potential for clinical translation in the management of difficult-to-heal diabetic ulcers.

Zhao *et al.*[70] synthesized antibacterial hydrogels by reacting branched polyethylenimine (PEI) with oxidized pullulan. The Schiff base linkages between the aldehyde and amine groups form a stable hydrogel matrix that can sustain antibacterial activity. Due to PEI's intrinsic antimicrobial properties and pullulan is biocompatibility, these hydrogels are effective as wound dressings for infected skin injuries. Their mechanical integrity and ease of application make them practical for clinical use. Additionally, their structure supports a balance of moisture and promotes healing.

Chen *et al.*[71] reported the development of biodegradable hydrogels formed from carboxymethyl chitosan and dialdehyde starch *via* Schiff base crosslinking. The resulting hydrogels are environmentally friendly and designed for agricultural use, particularly in nutrient delivery. Their slow degradation in soil conditions ensures prolonged nutrient release, promoting sustainable crop growth. The material exhibits biocompatibility and non-toxicity, making it ideal for eco-safe applications. This innovative approach addresses controlled agrochemical release while reducing environmental impact.

Zhang *et al.*[72] developed injectable hydrogels by crosslinking oxidized hyaluronic acid with chitosan. Schiff base interactions yield a dynamic, self-healing gel suitable for osteoarthritis therapy. These hydrogels mimic the extracellular matrix, offering joint tissues a lubricating and protective environment. Their biocompatibility, ease of injection, and capacity to encapsulate anti-inflammatory drugs make them a strong candidate for localized, sustained treatment. The study demonstrates the potential of minimally invasive delivery systems for the management of joint disease.

Liu *et al.*[73] introduced bioactive hydrogels formed from silk fibroin and oxidized cellulose nanocrystals (CNCs). Schiff base bonding between the aldehyde groups on CNCs and the amine groups of silk fibroin yields robust, biocompatible scaffolds. These hydrogels exhibit enhanced mechanical strength and support osteoblast activity, making them ideal for bone regeneration. The combination of renewable materials and biological performance makes them suitable for orthopedic tissue engineering.

Zhong *et al.*[74] fabricated pH-sensitive hydrogels by crosslinking oxidized pectin with polyvinylamine (PVAm). Schiff base formation allows the hydrogel to respond to the pH variations in the gastrointestinal tract. The system remains stable under stomach acidity but swells and releases drugs in the colon. This selective behavior makes it effective for colon-targeted drug delivery. The hydrogels also demonstrate biocompatibility and high loading efficiency, making them promising for oral pharmaceutical applications.

Liu *et al.*[75] created antioxidant hydrogels from tannic acid and chitosan through aldehyde–amine crosslinking. These hydrogels exhibit potent radical scavenging activity, which is beneficial for treating oxidative stress-induced skin injuries. The material supports cell proliferation and wound closure while reducing inflammation. Hydrogels are effective wound dressings, offering strong mechanical integrity and biodegradability. Their multifunctionality positions them as advanced therapeutic materials for skin regeneration.

Yang *et al.*[76] designed antimicrobial hydrogels using oxidized poly(ethylene glycol) (PEG) and ε-polylysine. The Schiff base formation between the aldehyde groups of PEG and the amine-rich polylysine yields a hydrogel with inherent antibacterial properties. These materials are suitable for biomedical surface coatings, reducing the risk of infection on medical devices. The hydrogels exhibit strong adhesion and sustained antimicrobial effects, making them ideal for long-term implantable applications.

2.1.3. Enzyme-mediated crosslinking polymerization. Enzyme-mediated crosslinking polymerization is a bioinspired approach that utilizes enzymes to catalyze the formation of covalent bonds between polymer chains, leading to the development of crosslinked polymer networks. This method is particularly attractive due to its high specificity, mild reaction conditions (such as physiological pH and temperature), and reduced toxicity, making it an ideal choice for biomedical applications. Common enzymes used include horseradish peroxidase (HRP), tyrosinase, and transglutaminase, which catalyze the oxidative coupling or amide bond formation between functional groups, such as phenols, amines, and thiols. Enzyme-mediated crosslinking is frequently employed in the synthesis of hydrogels for tissue engineering, wound healing, and drug delivery, offering excellent biocompatibility, tunable mechanical properties, and the potential for *in situ* gelation.

Ehrbar *et al.*[77] developed fibrin hydrogels using thrombin to enzymatically convert fibrinogen into fibrin monomers, which spontaneously self-assemble into a fibrous hydrogel network. This mimics the body's natural clotting process, making the material highly suitable for wound healing and tissue regeneration. The hydrogels are biologically active, supporting cell adhesion and proliferation, and offer a versatile platform for regenerative medicine. The modular nature of the system allows incorporation of biochemical cues to guide cellular behavior. This enzymatic method provides spatiotemporal control over gelation, making it a valuable tool in designing cell-instructive scaffolds.

Yung *et al.*[78] demonstrated the formation of gelatin-based hydrogels using microbial transglutaminase (mTG), which catalyzes the formation of ε-(γ-glutamyl)lysine isopeptide bonds between gelatin's lysine and glutamine residues. This enzymatic crosslinking yields robust, biocompatible hydrogels with tunable stiffness, making them ideal for 3D cell culture and tissue engineering. The approach allows fine control of mechanical properties by adjusting enzyme concentration and reaction time. Importantly, the mild reaction conditions preserve cell viability, supporting *in situ* applications. These

hydrogels mimic the extracellular matrix (ECM), facilitating cellular infiltration, proliferation, and differentiation, which is crucial for regenerative medicine and drug screening platforms.

Farokhi et al.[79] created silk fibroin hydrogels by using tyrosinase to catalyze the oxidative coupling of tyrosine residues, forming di-tyrosine crosslinks. The resulting hydrogels are mechanically strong and exhibit excellent biocompatibility, making them promising candidates for load-bearing applications such as bone regeneration. The enzymatic method ensures gentle processing conditions that preserve bioactivity. These hydrogels can be fabricated into complex shapes, and their degradation rates can be modulated by altering protein concentration or enzyme exposure. The platform also enables the incorporation of bioactive molecules to enhance cellular responses, thereby expanding their utility in tissue engineering.

Sakai et al.[80] employed horseradish peroxidase (HRP) to crosslink phenol-modified hyaluronic acid (HA) in the presence of hydrogen peroxide (H_2O_2), forming stable, covalent phenol–phenol bonds. The resulting hydrogels are injectable, cell-compatible, and exhibit excellent biocompatibility for various biomedical applications, including tissue engineering and drug delivery. This HRP-mediated crosslinking occurs under physiological conditions, preserving encapsulated cells and bioactive agents. The hydrogels are also highly tunable in terms of gelation time, stiffness, and degradation, providing versatility for various therapeutic needs. Their shear-thinning and self-healing properties enhance their utility in minimally invasive procedures. Rodriguez et al.[81] utilized lysyl oxidase to generate collagen hydrogels with enhanced stiffness and biofunctionality. The enzyme oxidizes lysine residues to allysine, which subsequently forms covalent crosslinks that resemble the natural ECM architecture. These hydrogels offer structural integrity and support cell adhesion and migration, making them well-suited for skin regeneration and wound healing. The method mimics in vivo matrix remodeling, producing scaffolds that are both mechanically resilient and biologically instructive. By modulating enzyme activity, researchers can tailor the properties of gels to match the specific environments of various tissues. Pishesha et al.[82] designed peptide hydrogels via Sortase A-mediated ligation, in which the enzyme covalently links LPXTG-tagged peptides to polyglycine motifs. This modular strategy enables the formation of programmable, protein-engineered hydrogels for drug delivery and regenerative applications. The biocompatible process operates under mild conditions, offering site-specific crosslinking and allowing precise control over network architecture. The system supports the incorporation of functional motifs for targeting, degradation, or bioactivity. These hydrogels offer tunable mechanical properties and biological responses, with potential for in vivo therapeutic use and controlled release systems. Zhang et al.[83] developed self-assembling peptide hydrogels triggered by alkaline phosphatase, which dephosphorylates precursor peptides, inducing β-sheet formation and hydrogelation. This enzymatic approach enables spatiotemporal control over gelation, making it useful for bone regeneration and 3D cell culture. The mild reaction conditions preserve the functionality of incorporated biomolecules. These hydrogels exhibit excellent

biocompatibility and can support osteogenic differentiation. The platform enables in situ gel formation, suitable for injectable therapies. The system's responsiveness to enzyme concentration and substrate design enhances its utility for precision tissue-engineering applications. Schneider et al.[84] introduced a hybrid hydrogel system where Factor XIIIa enzymatically crosslinks fibrin to hyaluronic acid (HA), combining the bioactivity of fibrin with the viscoelastic properties of HA. The resulting hydrogels exhibit enhanced mechanical integrity and resilience, making them suitable for cartilage tissue engineering. Factor XIIIa forms stable covalent bonds under physiological conditions, allowing for in situ gelation and cell encapsulation. The system supports chondrogenic cell growth and extracellular matrix production, demonstrating promise for joint repair. It also enables the incorporation of bioactive factors for controlled release and tissue-specific functionality. Jaros et al.[85] explored casein hydrogels formed by microbial transglutaminase (mTG), which catalyzes crosslinking between casein proteins. These food-grade, biocompatible hydrogels are utilized as edible scaffolds for cultured meat production. The enzymatic method produces stable, elastic networks capable of supporting cell adhesion and proliferation. The mechanical properties and degradation of the hydrogel can be tuned by adjusting enzyme activity or protein concentration. Their origin from dairy proteins facilitates their integration into food systems, offering a sustainable, animal-free platform for developing structured meat alternatives and other bioengineered food products.

Gu et al.[86] engineered glucose-responsive hydrogels using a dual-enzyme system comprising glucose oxidase (GO_x) and horseradish peroxidase (HRP). GO_x oxidizes glucose to gluconic acid and H_2O_2, which HRP then uses to crosslink phenol-modified polymers, forming hydrogels that respond to glucose fluctuations. These smart materials are designed for closed-loop insulin delivery, releasing insulin in response to rising glucose levels. The system mimics pancreatic function, offering precise glucose management for diabetes therapy. The hydrogels demonstrate excellent biocompatibility, responsiveness, and stability, representing a significant advancement in intelligent drug delivery systems.

2.2. Radiation-crosslinked hydrogels

Radiation-crosslinked hydrogels are three-dimensional polymer networks that are crosslinked by ionizing radiation (e.g., gamma rays, electron beams, or X-rays). This method avoids the use of chemical initiators or crosslinking agents, making it advantageous for producing pure, biocompatible hydrogels with applications in medicine, agriculture, and environmental engineering.

Radiation crosslinking is a powerful alternative to chemical coupling methods for hydrogel formation, using high-energy radiation to form three-dimensional polymer networks without the need for additional crosslinking agents. This process begins with ionization, where radiation energy breaks chemical bonds within polymer chains, predominantly C–H or C–C bonds, generating free radicals. These highly reactive

species, located on adjacent polymer chains, subsequently recombine to form covalent crosslinks. The process occurs simultaneously throughout the material, creating uniformly distributed junction points that transform the polymer solution into a stable, three-dimensional network with enhanced mechanical properties and swelling behavior.

The efficiency of radiation crosslinking depends significantly on several key factors. Radiation dose directly correlates with crosslink density; however, excessive doses may trigger competing chain-scission reactions, potentially compromising network integrity. The polymer structure plays a crucial role, with hydrophilic polymers, such as poly(vinyl alcohol) (PVA) and poly(ethylene glycol) (PEG), demonstrating superior crosslinking efficiency compared to their hydrophobic counterparts. The irradiation environment substantially affects network formation: aqueous solutions promote radical mobility and subsequent crosslinking, whereas oxygen-rich environments may inhibit the process through competitive radical scavenging reactions.

Gamma radiation, typically from Co-60 or Cs-137 isotopes, is the most widely used radiation for hydrogel synthesis. Its exceptional penetration depth enables uniform crosslinking throughout thick samples, making it ideal for preparing bulk hydrogels. This radiation simultaneously sterilizes the material during processing, offering a significant advantage for biomedical applications. Gamma-crosslinked PVA hydrogels, typically prepared using doses between 25–50 kGy, have demonstrated remarkable success as wound dressings due to their excellent biocompatibility, appropriate moisture retention, and transparency that facilitates wound monitoring.

Electron beam (E-beam) radiation offers an attractive alternative to gamma sources, providing significantly faster processing times often reducing treatment duration from hours to minutes or even seconds. This high-throughput capability makes E-beam crosslinking particularly valuable for industrial-scale production. However, E-beam radiation exhibits less penetration than gamma rays, potentially creating crosslinking gradients in thicker materials. This characteristic can be advantageously exploited to create hydrogels with mechanical property gradients mimicking natural tissue interfaces, such as the cartilage–bone junction, by carefully controlling beam energy and sample orientation.

Ultraviolet (UV) radiation offers a milder crosslinking approach, typically requiring photoinitiators to achieve a sufficient radical concentration for effective network formation. While offering precise spatial control through masking or photolithographic techniques, UV crosslinking generally achieves lower penetration depths compared to gamma or E-beam radiation. This limitation restricts UV applications primarily to thin hydrogel films or surface modifications. However, the exceptional spatial control enables the creation of complex micropatterns within hydrogels, facilitating the development of advanced tissue-engineering scaffolds with precisely defined cellular microenvironments and microfluidic devices with intricate channel architectures.

Radiation crosslinking offers several distinct advantages over conventional chemical methods. The process eliminates potentially toxic chemical crosslinkers and catalysts, significantly enhancing biocompatibility for medical applications. The simultaneous sterilization during processing streamlines manufacturing for implantable or wound-contacting materials. Additionally, radiation allows for the crosslinking of pre-formed devices or within sealed packages, preserving sterility and enabling the processing of complex-shaped articles. However, radiation facilities require substantial capital investment and specialized safety protocols, which may limit accessibility compared to chemical approaches.

The applications of radiation-crosslinked hydrogels span numerous biomedical fields. Wound dressings represent the most established commercial application, with PVA hydrogel dressings offering exceptional exudate absorption, bacterial barrier properties, and atraumatic removal. Drug delivery systems benefit from radiation crosslinking's ability to incorporate therapeutic agents during network formation, without the chemical reactions that might degrade sensitive compounds. Tissue engineering applications leverage radiation's capacity to create cell-compatible scaffolds with tunable mechanical properties and degradation profiles. Additionally, radiation-crosslinked hydrogels are finding growing applications in biosensors, where their controlled swelling behavior enables the detection of various analytes through dimensional changes or shifts in optical properties.

Recent innovations in radiation crosslinking technology include the development of stimuli-responsive systems that combine radiation techniques with smart polymers. These advanced materials respond to environmental triggers, such as temperature, pH, or specific biomolecules, enabling applications ranging from controlled drug release to tissue-engineering scaffolds that adapt to cellular activity. Furthermore, hybrid approaches combining radiation with other crosslinking mechanisms can yield synergistic effects, leading to hydrogels with enhanced mechanical properties or more precisely tailored degradation profiles. These continued advancements ensure radiation crosslinking remains at the forefront of hydrogel technology, offering unique capabilities for next-generation biomedical materials.

2.2.1. Gamma radiation-induced polymerization. Gamma radiation-induced polymerization is a high-energy, initiator-free technique used to synthesize and crosslink polymers, particularly hydrogels, by generating free radicals. When exposed to gamma rays, typically from sources like cobalt-60. The radiation ionizes water molecules in the reaction medium, producing reactive species such as hydroxyl radicals ($^{\bullet}OH$), hydrogen atoms ($^{\bullet}H$), and hydrated electrons (e^-_{aq}). These radicals initiate the polymerization of vinyl monomers (*e.g.*, acrylic acid, acrylamide) and simultaneously facilitate crosslinking to form three-dimensional networks. This method is advantageous for its ability to sterilize the final product, control the degree of crosslinking, and eliminate the need for chemical initiators or catalysts, making it particularly suitable for biomedical applications such as wound dressings, drug delivery systems, and tissue engineering scaffolds.

Poly(vinyl alcohol) (PVA) hydrogels synthesized through gamma radiation demonstrate remarkable properties for

wound management applications. Researchers have developed PVA wound dressings by irradiating aqueous PVA solutions with gamma doses of 25–40 kGy, creating transparent, elastic hydrogels with excellent fluid absorption capacity. These dressings maintain a moist wound environment while providing a bacterial barrier, significantly accelerating healing in both acute and chronic wounds. The controllable cross-linking density, achieved through radiation dose adjustment, enables customization of mechanical strength and water vapor transmission rates to suit different wound types.

Poly(N-isopropylacrylamide) (PNIPAAm) temperature-responsive hydrogels synthesized *via* gamma radiation exhibit precise thermal transition behavior, making them suitable for drug delivery applications. By irradiating NIPAAm monomer solutions at low temperatures (0–4 °C) with moderate doses (10–20 kGy), researchers create hydrogels demonstrating sharp volume transitions near body temperature. These materials show remarkable "on–off" release profiles for incorporated therapeutic agents, with minimal burst release compared to chemically crosslinked counterparts. Eliminating chemical initiators makes these systems suitable for delivering sensitive biopharmaceuticals, such as proteins and peptides.[87]

Carboxymethyl cellulose (CMC) superabsorbent hydrogels produced by gamma irradiation exhibit exceptional water-absorption capacity, making them suitable for agricultural applications. Scientists have developed these materials by irradiating concentrated CMC solutions with doses of 15–30 kGy, creating hydrogels that can absorb up to 500 times their dry weight in water. When incorporated into arid soils, these hydrogels significantly reduce irrigation frequency by storing water and releasing it gradually to plant roots. The biodegradability of these networks provides additional benefits by improving soil structure as they decompose.[88]

Poly(acrylic acid) (PAA) hydrogels synthesized by gamma radiation exhibit outstanding metal-ion adsorption properties for environmental remediation. Researchers have created these materials by irradiating acrylic acid solutions with doses of 20–35 kGy, producing highly porous networks with abundant carboxyl groups. These hydrogels effectively remove heavy metal contaminants, such as lead, cadmium, and mercury, from industrial wastewater *via* ion exchange and chelation. The radiation technique enables the production of monolithic adsorbent blocks with superior mechanical integrity compared to conventional precipitation polymerization methods.[89]

Poly(ethylene glycol) (PEG) hydrogels fabricated *via* gamma irradiation serve as excellent tissue-engineering scaffolds with tunable mechanical properties. Scientists have developed these materials by irradiating PEG diacrylate solutions containing cells with low doses (5–10 kGy), enabling simultaneous polymerization and cell encapsulation. The resulting constructs demonstrate exceptional cytocompatibility, characterized by high cell viability and suitable mechanical support for various tissue types. The radiation approach eliminates concerns of photoinitiator toxicity associated with conventional UV cross-linking methods.[90]

Chitosan-based antimicrobial hydrogels produced through gamma radiation offer promising solutions for infection control. Researchers have created these materials by irradiating acidic chitosan solutions with doses of 15–25 kGy, generating networks with enhanced antimicrobial properties against both Gram-positive and Gram-negative bacteria. The radiation process increases the availability of chitosan's cationic groups, improving interaction with microbial cell membranes. These hydrogels demonstrate particular efficacy against antibiotic-resistant strains, making them valuable for wound management in high-risk populations.[91]

Poly(vinyl pyrrolidone) (PVP) hydrogels synthesized *via* gamma radiation serve as excellent matrix systems for controlled drug release. Scientists have developed these materials by irradiating aqueous PVP solutions containing pharmaceutical agents with doses of 15–30 kGy, creating drug-loaded networks in a single step. These hydrogels exhibit sustained release profiles lasting from days to weeks, depending on the network density, which is controlled by radiation parameters. The exceptional biocompatibility and non-immunogenic properties of radiation-crosslinked PVP make these systems particularly valuable for ophthalmic and transdermal drug delivery applications.[92]

Alginate-based hydrogels fabricated through gamma irradiation offer remarkable advantages for cell encapsulation and bioprinting applications. Researchers have created these materials by irradiating sodium alginate solutions with carefully controlled doses (5–15 kGy), producing networks with excellent shape fidelity that do not rely on conventional calcium crosslinking. These hydrogels demonstrate enhanced stability under physiological conditions while maintaining appropriate porosity for nutrient diffusion. The radiation approach enables the preparation of cell-laden constructs with improved mechanical properties compared to ionically crosslinked alternatives.[93]

Gelatin methacrylate (GelMA) hydrogels synthesized *via* gamma radiation provide excellent platforms for 3D cell culture and tissue modeling. Scientists have developed these systems by irradiating GelMA solutions with low doses (8–12 kGy), creating networks with well-preserved bioactive motifs from the native collagen structure. The radiation approach avoids potential cytotoxicity concerns associated with photoinitiators in conventional UV crosslinking, enabling superior cell proliferation and differentiation. These hydrogels demonstrate exceptional versatility for modeling various tissue microenvironments, from soft neural tissue to stiffer cartilage constructs.[94]

Hyaluronic acid (HA) hydrogels produced through gamma irradiation demonstrate superior performance in viscosupplementation for osteoarthritis treatment. Researchers have created these materials by irradiating high-molecular-weight HA solutions with carefully optimized doses (5–10 kGy), thereby generating networks with viscoelastic properties that mimic those of natural synovial fluid. The radiation technique enables crosslinking without chemical modifications that might compromise HA's biological functions. Clinical studies with these hydrogels have demonstrated prolonged joint lubrication, improved shock absorption, and significant pain reduction compared to chemically cross-linked alternatives,

establishing them as next-generation options for managing degenerative joint conditions.[95]

2.2.2. Electron beam and UV-induced polymerization of hydrogel. Electron beam and UV-induced polymerization are two of the most sophisticated and widely used radiation-based techniques for hydrogel fabrication, each offering distinct advantages in polymerization control, crosslinking efficiency, and material properties. Electron beam polymerization uses high-energy electrons (typically 0.5–10 MeV) to generate free radicals directly within the monomer solution, enabling rapid, uniform cross-linking without the need for photoinitiators. This approach is particularly valuable for biomedical applications, where chemical purity is paramount. The penetration depth and energy distribution of electron beams can be precisely controlled to achieve uniform crosslinking throughout thick hydrogel samples. At the same time, the absence of oxygen inhibition enables polymerization under ambient conditions. Raza et al.[96] provided a comprehensive review of state-of-the-art irradiation technologies, including electron beam methods, for polymeric hydrogel fabrication. They discussed the advantages of electron beam irradiation, including the initiation of free radical formation that leads to covalent cross-linked networks under mild conditions. The review highlighted applications in drug release systems, emphasizing the method's efficacy in producing hydrogels with controlled swelling behavior and mechanical properties suitable for biomedical applications.

In contrast, UV-induced polymerization relies on the photochemical activation of photoinitiators through ultraviolet radiation (typically 280–400 nm), offering exceptional spatial and temporal control over the polymerization process, which is crucial for applications such as 3D printing and the photolithographic patterning of hydrogels. UV polymerization enables the creation of complex geometries with high resolution, as demonstrated in digital light processing (DLP) techniques, where precise light patterns can create intricate three-dimensional structures with feature sizes down to the micrometer scale. Both techniques enable real-time monitoring and control of the polymerization process, with UV methods offering the additional advantage of easy integration with computer-controlled light sources for automated manufacturing. The choice between electron beam and UV polymerization often depends on specific application requirements, with electron beam methods preferred for bulk hydrogel production where uniform properties throughout large volumes are essential. In contrast, UV methods excel in applications requiring precise spatial control, surface modification, or integration with additive manufacturing technologies. Demeter et al.[97] investigated electron-beam cross-linking of complex hydrogels composed of collagen, poly(vinyl pyrrolidone), and poly(ethylene oxide). By varying the concentration of poly(ethylene oxide), they analyzed the resulting hydrogel network structures using swelling degree measurements, rheological analysis, and Fourier Transform Infrared (FT-IR) spectroscopy. The study revealed that poly(ethylene oxide) concentration significantly influenced the mechanical properties and network architecture of the hydrogel, providing insights into tailoring hydrogel characteristics for specific biomedical applications.

Gupta et al.[98] developed a novel technique utilizing focused electron and X-ray beams for in-liquid crosslinking of hydrogels, enabling nanoscale 3D printing and encapsulation. This method enabled the direct fabrication of hydrogel structures within liquid environments, thereby overcoming traditional limitations associated with vacuum incompatibility. The approach facilitated the encapsulation of nanoparticles and live cells, demonstrating potential applications in tissue engineering and drug delivery. The study highlighted the versatility and precision of electron beam-induced crosslinking in the fabrication of advanced hydrogels.

The study conducted by Ge et al.[99] introduced an innovative multimaterial 3D printing strategy aimed at fabricating hybrid structures that combine highly stretchable hydrogels with a wide range of UV-curable polymers. The primary motivation for this work was to overcome longstanding limitations in the design and performance of hydrogel–polymer composites, particularly for biomedical devices, soft robotics, and flexible electronics. Traditional fabrication methods for such hybrids often relied on silicone rubbers and simple laminate geometries, limiting both mechanical tunability and functional complexity of the resulting structures. Moreover, achieving strong interfacial bonding between hydrogels and non-silicone polymers especially those that are water-insoluble and UV-curable proved particularly challenging due to differences in chemical structure, polymerization mechanisms, and the tendency of hydrogels to swell or deform during processing. To address these issues, the researchers developed a digital light processing (DLP)-based 3D printing platform capable of producing intricate hydrogel–polymer composites with covalent bonding at the interfaces. A critical innovation in this approach was the partial polymerization of UV-curable polymers, which left reactive functional groups at the interface. These groups could then form covalent bonds with subsequently printed hydrogel layers, particularly those containing methacrylate groups. This method eliminated the need for adhesives or mechanical interlocks, enabling the seamless integration of dissimilar materials and enhancing both mechanical strength and device performance.

One of the UV-curable materials explored in the study was Tango, a soft elastomer commercially available from Stratasys Ltd Tango was used to fabricate soft robotic actuators and strain sensors. When bonded with the hydrogel, the resulting hybrid structures exhibited remarkable mechanical performance, including stretchability up to 500% without delamination. This high degree of elasticity, coupled with excellent fatigue resistance under repeated strain, made these hybrids ideal for wearable electronics and soft robotic applications. The robust covalent interface ensured structural integrity even under significant mechanical stress.

In contrast, the Vero rigid polymer, also from Stratasys, served a different role within hybrid composites. Vero was used to reinforce hydrogels in applications requiring higher stiffness, such as synthetic meniscus structures for biomedical implants. By strategically designing the polymer's microarchitecture, the researchers increased the hydrogel's stiffness by approximately 30-fold while retaining some stretchability. The composite's

localized mechanical properties could be finely tuned to 0.6–5 MPa, closely mimicking the mechanical gradients found in native biological tissues.

Agilus, another elastomeric polymer from Stratasys, was employed as a protective encapsulation layer for hydrogel-based ionic conductors. One major drawback of hydrogel-based electronics is their susceptibility to dehydration, which severely compromises their functionality. The Agilus layer effectively mitigated this problem by providing a stretchable yet impermeable barrier that preserved hydrogel hydration over extended periods. Mechanical testing revealed that the failure of the hydrogel-Agilus hybrid occurred within the hydrogel itself (cohesive failure), rather than at the interface, underscoring the strength of the covalent bonding achieved through their printing approach.

To demonstrate the versatility of their platform, the researchers also printed hybrid structures using polyethylene glycol diacrylate (PEGDA). By incorporating water-dispersible trimethylbenzoyl phosphine oxide (TPO) nanoparticles as photoinitiators, they achieved nearly 90% polymerization efficiency. The presence of residual monomers facilitated effective interfacial crosslinking with methacrylate-based UV-curable polymers, enabling high-resolution DLP printing of hydrogel–polymer networks with excellent mechanical and structural integration.

A particularly innovative application involved a methacrylate-based shape-memory polymer (SMP) derived from a modified version of VeroClear. This material was used to print cardiovascular stents that combined structural integrity, shape memory behavior, and drug-delivery functionality. Upon reaching body temperature (approximately 37 °C), the stent expanded and released its payload, modeled by a dye, over 3 hours, with 90% release efficiency. Notably, the interface between the SMP and the hydrogel remained intact throughout expansion and drug release, demonstrating the feasibility of using these hybrids in dynamic physiological environments.

Finally, the team explored an ABS-like rigid polymer from Kudo3D Ltd, typically used for structural components that
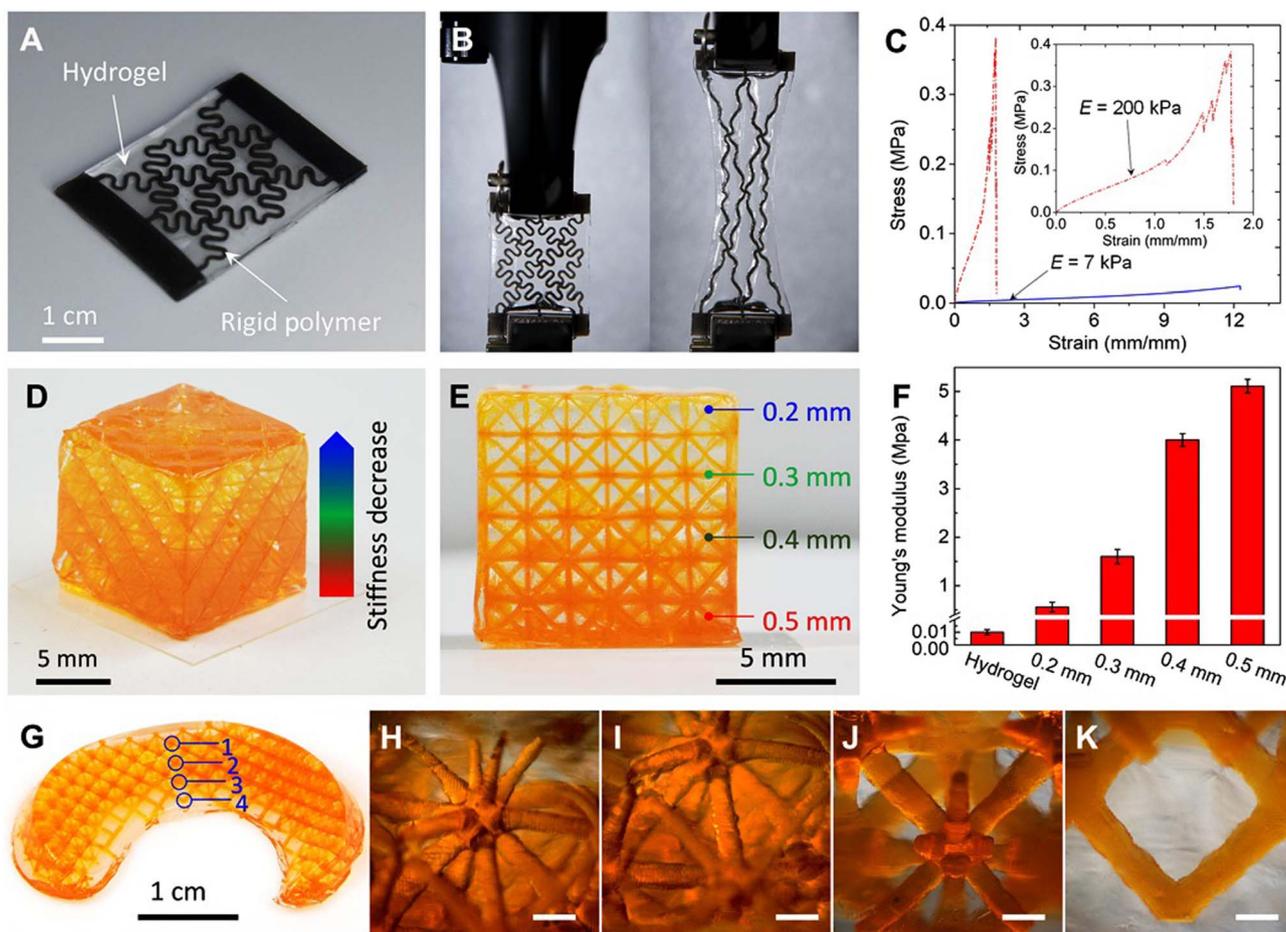

Fig. 3   3D printed hydrogel composites reinforced with rigid polymers and UV curable for enhanced mechanical performance. (A–C) Horseshoe-shaped Vero polymer enables a ∼30 times increase in stiffness while retaining stretchability. (D–F) Gradient-stiffness lattice structures modulate compressive modulus from ∼0.6 to 5 MPa. (G–K) A biomimetic meniscus with region-specific reinforcement replicates the native tissue's anisotropy, thereby mimicking its structure. Scale bars: 500 μm. Adapted from ref. 99 with permission from [American Association for the Advancement of Science (AAAS)], copyright 2021.

require high toughness and rigidity. When integrated with hydrogels, these polymers formed durable hybrid architectures suitable for load-bearing applications. The ability to print rigid-soft material combinations with robust interfaces broadens the scope of multimaterial design, enabling the fabrication of devices that incorporate both mechanical support and soft, functional components in a single printing process.

Fig. 3 powerfully illustrates how multi-material 3D printing, when combined with rational structural design, can overcome the inherent limitations of traditional hydrogels. By embedding programmable rigid elements within the soft matrix, the authors achieve high-performance composites that offer enhanced stiffness, maintained elasticity, and robust mechanical integrity. Furthermore, the biomedical potential of this platform is substantial, particularly in designing patient-specific orthopedic implants or soft tissue scaffolds with region-specific mechanical properties. The work not only addresses the hydrogel–tissue mismatch but also establishes a versatile blueprint for functional biofabrication.

Fig. 3A–C introduce a horseshoe-shaped VeroBlack polymer embedded in a highly stretchable AP hydrogel matrix (~80% water). The horseshoe design, with its inherent geometric compliance, provides a mechanically robust structure that accommodates large tensile deformations without compromising structural integrity. As demonstrated in Fig. 3C, this configuration achieves a 30-fold increase in stiffness (from ~10 kPa to ~300 kPa) while still allowing substantial elongation (~175% strain). Notably, no delamination occurs at the hydrogel–polymer interface, due to the strong covalent interfacial bonding, a key advantage over traditional fiber-reinforced hydrogels, which typically offer only unidirectional (1D) or planar (2D) reinforcement.

Fig. 3D–F introduce a gradient lattice reinforcement strategy using VeroClear polymer, where the rod diameters vary from 0.5 mm to 0.2 mm from bottom to top. This graded architecture enables spatially tunable stiffness, mimicking the natural tissue stiffness gradient observed in transitions such as tendon-to-bone junctions. Mechanical testing (Fig. 3F) reveals that increasing the rod diameter results in a higher compressive modulus, from ~0.6 MPa with 0.2 mm rods (closely matching unreinforced hydrogel), to ~2 MPa with 0.3 mm rods (tendon-like), and up to ~5 MPa with 0.5 mm rods (approaching cartilage stiffness). Significantly, the lattice-reinforced composites withstand compression without interfacial failure, confirming the durability of the material integration. This is the first demonstration of spatially programmable mechanical gradients in hydrogel composites enabled by digital light processing (DLP) 3D printing, which offers micron-level resolution and multimaterial deposition.

In Fig. 3G–K, a biomimetic meniscus prototype is shown, fabricated using the same hydrogel–rigid polymer strategy to replicate the anisotropic stiffness profile of native human meniscal tissue. As shown in Fig. 3G, the meniscus is printed with four distinct zones (Fig. 3H–K), each with a different lattice geometry to reflect natural mechanical gradients. Location 1 (outer edge, Fig. 3H) utilizes 0.5 mm rods to create a high-stiffness region (~5 MPa) for load-bearing purposes. In

contrast, the inner zone (Fig. 3K) utilizes 0.2 mm rods, resulting in a flexible zone (~0.6 MPa) that can accommodate motion and deformation. Intermediate zones (Fig. 3I and J) utilize 0.4 mm and 0.3 mm rods, respectively, to create a smooth transition in stiffness. This capability to spatially tune local mechanical properties within a single printed object represents a significant advancement in replicating the complex, heterogeneous biomechanics of real tissues.

2.3. Physically crosslinked hydrogels

Physically crosslinked hydrogels are a class of soft materials characterized by their three-dimensional polymer networks formed through non-covalent interactions such as hydrogen bonding, ionic interactions, hydrophobic associations, crystallization, or polymer chain entanglements. Unlike chemically or radiation-crosslinked hydrogels, which rely on covalent bonds to form permanent, irreversible structures, physically crosslinked hydrogels are held together by weaker, reversible forces. This key distinction makes physical hydrogels highly dynamic, responsive, and suitable for a range of biomedical and environmental applications where tunability, biocompatibility, and degradability are essential. One of the primary advantages of physically crosslinked hydrogels is their reversibility, which allows them to undergo gel–sol transitions in response to environmental stimuli, such as changes in pH, temperature, ionic strength, or mechanical stress. This reversible behavior allows these hydrogels to be self-healing, injectable, and stimuli-responsive, making them particularly attractive for applications in drug delivery, wound healing, tissue engineering, and biosensing. For example, thermoresponsive hydrogels, such as those made from poly(N-isopropylacrylamide) (PNIPAAm), can form a gel at body temperature and revert to a sol at room temperature.[100] Similarly, ionic crosslinking using divalent cations, such as calcium ions, in alginate hydrogels can produce gels that degrade or reform depending on the surrounding ionic conditions.[101] The preparation of physically crosslinked hydrogels is generally simpler and safer than that of chemically or radiation-crosslinked hydrogels. Physical methods often do not require toxic initiators, crosslinking agents, or irradiation, thereby minimizing cytotoxicity and preserving the biological activity of encapsulated cells, proteins, or drugs. This advantage makes physically crosslinked hydrogels highly suitable for cell-laden scaffolds, injectable formulations, and *in vivo* applications where preserving biological function is crucial. Physically crosslinked hydrogels, while offering remarkable features such as biocompatibility, reversibility, and stimulus-responsiveness, are generally not suitable for water treatment applications due to their structural and mechanical limitations.[102] These hydrogels form three-dimensional polymer networks through non-covalent interactions, such as hydrogen bonding, ionic interactions, hydrophobic associations, or crystallization, which are inherently weaker than covalent bonds.[103] As a result, the mechanical integrity and long-term stability of these materials in aqueous environments are significantly compromised,

especially under dynamic or harsh conditions typically encountered in water purification systems.

In water treatment, materials are often exposed to continuous flow, fluctuating pH levels, varying temperatures, and sometimes aggressive chemical agents or high ionic strengths. Physically crosslinked hydrogels tend to swell excessively, leach unbound polymer chains, or disintegrate under such stresses. For example, alginate hydrogels ionically crosslinked with Ca^{2+} may easily dissolve in the presence of chelating agents such as EDTA, which are commonly used in water purification to remove heavy metals.[104] This solubility undermines the hydrogel's reusability and operational lifespan, making it impractical for industrial-scale water treatment systems.

Furthermore, these hydrogels lack the adsorption capacity and durability required for the removal of pollutants, including heavy metals, dyes, and organic micropollutants. Chemically crosslinked hydrogels, by contrast, provide permanent network structures with higher mechanical strength, reduced solubility, and enhanced performance stability.[105] These properties make them better suited for applications such as ion-exchange resins, adsorbent membranes, and reactive filters. Radiation-crosslinked hydrogels also exhibit superior robustness and can be sterilized and tailored for specific functionalities without the need for potentially toxic chemical crosslinkers.[106]

While physically crosslinked hydrogels are promising for biomedical applications such as tissue engineering, drug delivery, and wound healing where transient stability and mild processing are advantageous, they are not engineered for the rigorous operational demands of water treatment. Attempts to improve their performance through hybrid approaches, such as incorporating nanomaterials or combining physical with chemical crosslinking, have shown some promise.[105] However, these still fall short of the structural integrity required for continuous or large-scale decontamination processes.

However, there are trade-offs. While reversible crosslinking imparts excellent dynamic properties, it often results in lower mechanical strength and stability than covalently crosslinked hydrogels. As such, physically crosslinked systems may degrade more rapidly or lose structural integrity under mechanical stress. Researchers are actively exploring hybrid strategies that combine physical and chemical crosslinking to balance stability and functionality. For instance, a dual-network hydrogel might use ionic interactions for initial gelation and mild covalent crosslinking for longer-term stability.

In contrast, chemical crosslinking methods, such as glutaraldehyde or carbodiimide chemistry, create permanent covalent bonds that are robust and mechanically strong but often require toxic reagents and complex purification steps. Similarly, radiation crosslinking uses high-energy gamma rays or electron beams to initiate free-radical polymerization and crosslinking without the need for chemical additives. Although effective, radiation methods can damage sensitive biomolecules and require specialized equipment and safety protocols, limiting their accessibility.

Physically crosslinked hydrogels are a class of soft materials composed of three-dimensional polymer networks held together by non-covalent interactions, such as hydrogen bonding, ionic interactions, hydrophobic associations, crystallization, and chain entanglement. Unlike chemically or radiation-crosslinked hydrogels, which rely on covalent bonds to form stable, irreversible networks, physically crosslinked hydrogels are dynamic and reversible. This reversibility confers stimuli-responsive behaviors, which are crucial for biomedical applications such as drug delivery, wound healing, and tissue engineering.

A key advantage of physically crosslinked hydrogels is their ability to respond to environmental cues, such as pH, temperature, ionic strength, and mechanical stress, thereby enabling reversible gel–sol transitions. This property facilitates self-healing, injectability, and controlled degradation. For instance, thermoresponsive hydrogels based on poly(N-isopropylacrylamide) (PNIPAAm) undergo a sharp sol–gel transition around 32 °C, close to body temperature, allowing for minimally invasive administration and subsequent *in situ* gelation.[107] Similarly, alginate hydrogels crosslinked with divalent calcium ions exhibit reversible gelation. Lee and Mooney[104] demonstrated that these hydrogels can dissolve in the presence of chelating agents like EDTA, offering a simple strategy for controlled drug release or cell recovery.

Another benefit of physical crosslinking lies in the mild conditions required for hydrogel formation. Unlike chemical crosslinking, which often necessitates toxic crosslinkers or initiators, physical methods avoid such reagents, making them highly suitable for encapsulating sensitive biomolecules or living cells. Despite their many advantages, physically crosslinked hydrogels often exhibit lower mechanical strength and reduced long-term stability compared to their chemically crosslinked counterparts. To address this limitation, researchers have explored hybrid hydrogels that incorporate both physical and chemical crosslinking. Jeon *et al.*[108] developed dual-crosslinked alginate hydrogels, in which initial gelation *via* calcium ions was complemented by covalent crosslinking *via* methacrylation, resulting in improved mechanical integrity while retaining injectability. Additionally, nanocomposite strategies have been employed to enhance mechanical properties without compromising the network's reversible behavior. Haraguchi *et al.*[105] introduced clay nanoplatelets into polymer matrices to create physically crosslinked nanocomposite hydrogels with enhanced toughness and elasticity.

Fig. 4 provides a comparative overview of three primary crosslinking methods used in polymer and hydrogel engineering: physical, chemical, and radiation crosslinking. Each process is analyzed based on its advantages and disadvantages, highlighting key features relevant to its practical application. Physical crosslinking, which is reversible, offers several benefits, including simplicity, non-toxicity, and the ability to form gels without chemical additives. This makes it particularly attractive for biomedical applications where biocompatibility is critical.[109] However, their poor mechanical strength and solubility are significant limitations, as these materials can easily dissolve or deform under physiological conditions. Chemical crosslinking is marked as irreversible, indicating the formation of permanent covalent bonds between polymer chains. This
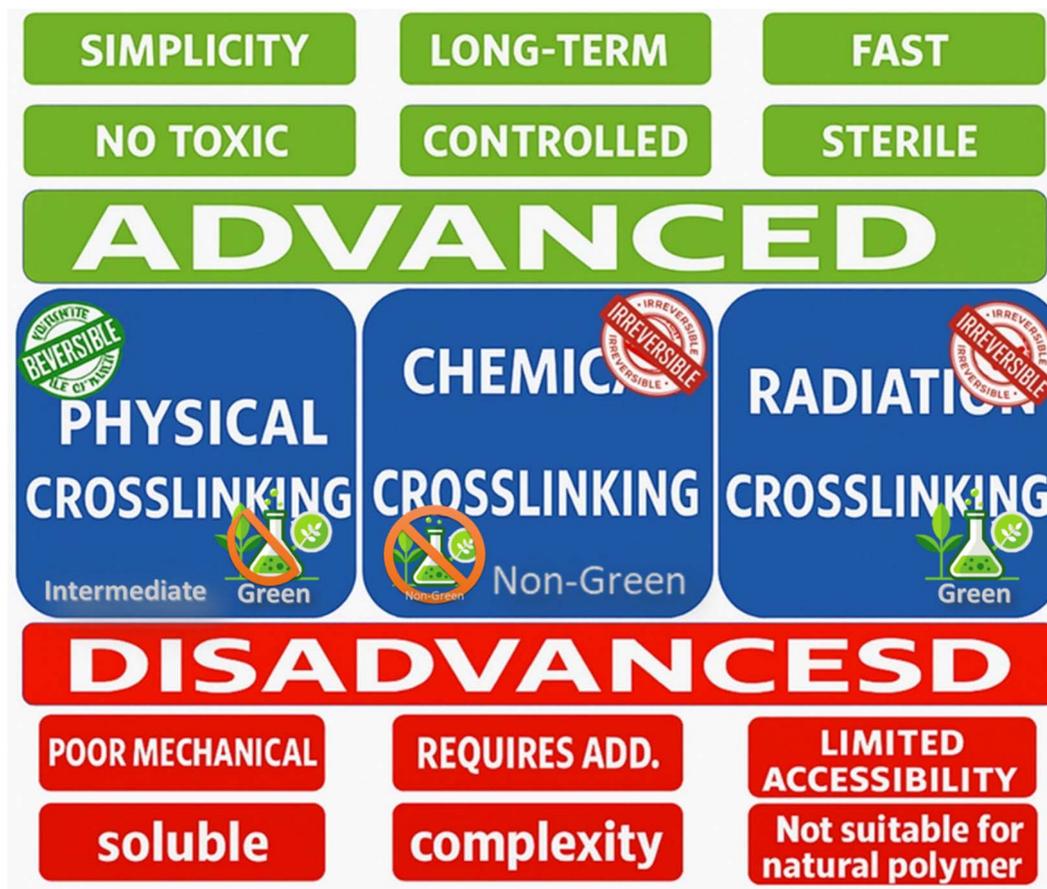
Fig. 4 Comparative analysis of crosslinking methods physical, chemical, and radiation, highlighting their reversibility, advantages, and disadvantages.

method offers controlled, long-term stability, making it suitable for applications that require durable scaffolds or drug-delivery systems. Nevertheless, chemical crosslinking often requires additional reagents, which increases complexity and can pose toxicity concerns if not properly purified. Radiation crosslinking is another irreversible method that utilizes high-energy radiation (*e.g.*, gamma rays or electron beams) to initiate crosslinking reactions. It is valued for its speed and sterility, which are advantageous for medical-grade materials. However, it has limited accessibility due to the need for specialized equipment and is generally unsuitable for natural polymers, which may degrade under radiation.

Table 2 outlines a comparison of hydrogel crosslinking methods for advanced water treatment. Chemical crosslinking is a highly scalable, established method that produces hydrogels with strong, permanent mechanical properties. It offers excellent control over the network structure, making it reproducible for various industrial applications. However, it is classified as a non-green method due to its reliance on toxic crosslinking agents and solvents. The risk of these hazardous residues leaching out, coupled with the generation of harmful chemical waste, makes it fundamentally unsuitable for large-scale water treatment. Its poor biocompatibility also prevents its use in applications involving sensitive biological

components. Radiation-induced crosslinking represents a "greener" chemical approach by creating covalent bonds without adding synthetic initiators, resulting in a pure, sterile hydrogel matrix. It provides excellent control over crosslinking density and can produce networks with high mechanical strength. Despite these advantages, its status is only intermediate due to significant drawbacks: the process is capital-intensive and energy-consuming, and it requires specialized, shielded facilities. These factors hinder scalability and raise environmental concerns about its energy footprint, making it a challenging option for widespread use in water treatment despite the purity of the final product. Physical crosslinking is unequivocally the greenest method available. It relies on non-covalent, often reversible interactions, such as ionic bonds and hydrogen bonding, using typically non-toxic, and sometimes natural, materials. This method operates under mild aqueous conditions, yielding highly biocompatible, often biodegradable hydrogels that are ideal for encapsulating sensitive biological actives, such as enzymes or microbes. While these gels are generally mechanically weaker than their covalently linked counterparts, their lack of toxic leachate, minimal environmental impact, and low cost make them the most suitable and sustainable choice for large-scale water treatment applications.

Table 2 Comparison of hydrogel crosslinking methods for advanced water treatment

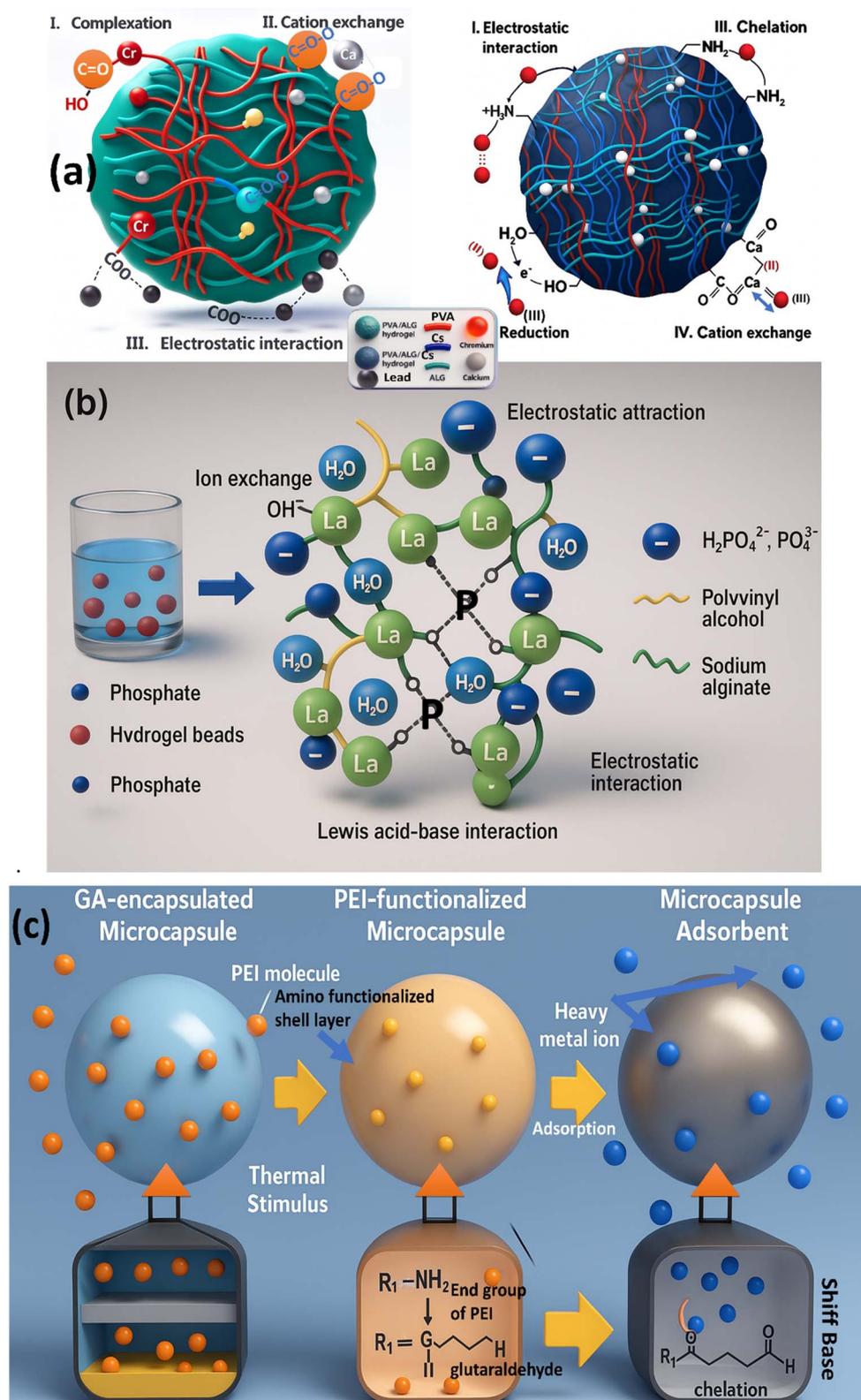| Feature	Chemical crosslinking	Radiation-induced crosslinking	Physical crosslinking
General mechanism	Covalent bonds formed via chemical crosslinkers (e.g., glutaraldehyde, EDC/NHS, genipin)	Covalent bonds formed via free radicals generated by high-energy radiation (e.g., gamma, E-beam)	Non-covalent interactions (ionic bonds, H-bonding, crystallinity, hydrophobic assembly)
Scalability	High. Easily integrated into existing chemical manufacturing processes	Moderate to low. Limited by the availability, cost, and safety protocols of radiation facilities	Variable. Ionic gelation is highly scalable; complex self-assembly may be less so
Cost	Low (material), moderate (processing). Crosslinkers are cheap, but purification adds cost	High. High capital (radiation source) and operational (energy, safety) costs	Low. Often uses abundant, cheap ions or relies on simple physical processes
Environmental impact	High (non-green). Toxic reagents and solvents; generates hazardous waste; risk of leaching	Moderate. Minimal chemical waste but high energy footprint and radioactive waste management	Low (green). Typically uses non-toxic, bio-based materials; generates minimal waste; and is often biodegradable
Suitability for large-scale water treatment	Poor. Leaching of toxic residues is a critical failure point for water safety	Moderate. The pure hydrogel matrix is a plus, but cost and public perception are significant barriers	Excellent. Ideal due to absence of toxic leachates, biocompatibility, and often renewable sources
Crosslinking density & control	High and tunable. Precise control via stoichiometry. Can lead to brittle networks	High and tunable. Controlled by radiation dose. Can be very uniform throughout the material	Low to moderate, dynamic. Difficult to control precisely. Often results in weaker, reversible networks
Hydrogel mechanical strength	Typically high. Rigid, covalent networks provide high compressive and tensile strength	High. Can form very strong, tough networks, similar to chemical crosslinking	Typically weaker. Softer, more elastic gels. Prone to deformation and dissolution under stress
Processing time & conditions	Variable. Can require hours, specific pH, temperature, and catalysts	Fast. Crosslinking occurs in seconds to minutes upon exposure	Very fast (e.g., ionic) to slow (e.g., thermal). Often occurs under mild, aqueous conditions
Biocompatibility & cytotoxicity	Low. Residual crosslinkers are often cytotoxic, requiring rigorous purification	High. No chemical initiators, resulting in a pure, highly biocompatible matrix	Very high. Inherently biocompatible due to the absence of synthetic crosslinkers
Degradability	Non-degradable or slow. Degradation depends on hydrolytically or enzymatically labile bonds	Controllable. Degradation rate can be tuned via crosslink density and polymer choice	Often readily degradable. Reversible bonds can lead to dissolution under specific conditions (e.g., pH, ion chelation)
Ability to encapsulate sensitive actives (e.g., cells, enzymes)	Poor. A harsh chemical environment and potential toxicity can denature biological actives	Poor. High-energy radiation is destructive to most biological molecules and living cells	Excellent. Mild, non-denaturing conditions are ideal for encapsulating cells, proteins, and drugs
"Green" status	Non-green method	Intermediate/"greener" chemically	Green method
Key advantages	• Strong, stable networks • High reproducibility • Wide range of applicable polymers	• Pure product (no initiators) • Simultaneous sterilization • Good penetration and uniformity	• Mild, safe conditions • Often biodegradable • Excellent biocompatibility • Stimuli-responsive
Key disadvantages	• Toxicity of reagents • Hazardous waste	• High cost and energy use • Specialized facilities required	• Generally weaker mechanics • Potential instability in complex environments
	• Risk of leaching • Irreversible	• Potential polymer degradation • Irreversible	• Less control over network structure • Reversible
References	33, 110 and 111	106 and 112	113–115

Fig. 5 Adsorption mechanisms of hydrogel particles for removal of various pollutants: (a) electrostatic interaction and ion exchange processes involved in the adsorption of Cr(VI) and Pb(II) ions by PVA/ALG/CS composite hydrogel particles at acidic pH, where amine groups are protonated and metal cations replace Ca^{2+} ions. Reproduced from ref. 116 with permission from [Elsevier], copyright 2022. (b) Electrostatic interaction, ion exchange, and Lewis acid–base interactions governing the selective adsorption of phosphorus anions ($H_2PO_4^-$, HPO_4^{2-}, and PO_4^{3-}) on PVA-alginate-La(OH)$_3$ hydrogel particles, with maximum adsorption observed at pH 4 due to surface protonation of La–OH groups. Reproduced from ref. 117 with permission from [Elsevier], copyright 2018. (c) Chelation-based adsorption of heavy metal ions (Cu^{2+}, Cd^{2+}, Zn^{2+}) on amino-functionalized microgels synthesized via Schiff-base reaction between polyethyleneimine and glutaraldehyde, where coordination bonds are formed between metal ions and nitrogen donor atoms. Reproduced from ref. 118 with permission from [Elsevier], copyright 2021.

3. Adsorption mechanisms in hydrogel-based remediation

Hydrogel-based remediation relies on a variety of adsorption mechanisms to capture and remove pollutants from aqueous environments, making them highly effective in water purification and environmental cleanup. These mechanisms include physical adsorption, ion exchange, electrostatic interactions, hydrogen bonding, and complexation or chelation with functional groups embedded in the hydrogel matrix. Hydrogels often incorporate hydrophilic and charged moieties such as carboxyl (–COOH), hydroxyl (–OH), amine (–NH$_2$), and sulfonate (–SO$_3$H) groups, which facilitate strong interactions with a wide range of contaminants, including heavy metals, dyes, and organic pollutants. The three-dimensional, porous structure of hydrogels enables high surface area and water retention, further enhancing their adsorption capacity. Additionally, the stimuli-responsive nature of certain hydrogels enables controlled adsorption and desorption, enabling the regeneration and reuse of these materials. The synergy of these mechanisms underpins the efficiency and versatility of hydrogels in environmental remediation. Electrostatic interactions have been considered among the most common and important mechanisms underlying the adsorption of ionizable pollutants onto the positively or negatively charged surfaces of hydrogel particles.[8] Fig. 5a illustrates the dual mechanisms of electrostatic interaction and ion exchange in the adsorption of heavy metal ions, specifically Cr(VI) and Pb(II), using PVA/ALG/CS composite hydrogel particles. At acidic pH levels (pH < 4), the amine groups (–NH$_2$) on the hydrogel surface become protonated to –NH$_3^+$, which facilitates the electrostatic attraction of negatively charged HCrO$_4^-$ ions (a form of Cr(VI) in acidic conditions). Simultaneously, the adsorption of Pb^{2+} occurs primarily through a cation exchange process, where Pb^{2+} ions displace Ca^{2+} ions from the hydrogel matrix. Additionally, Cr(VI) undergoes a redox transformation to Cr(III), which then participates in the ion-exchange mechanism, further enhancing adsorption efficiency.[116]

Fig. 5b focuses on the adsorption of phosphorus-containing anions using a PVA-alginate-La(OH)$_3$ hydrogel system. The primary mechanism here is electrostatic interaction, in which the La–OH groups on the hydrogel surface become protonated to La–OH$_2^+$ in acidic environments (optimal at pH 4), thereby acquiring a positive charge. This positively charged surface attracts and binds negatively charged phosphorus species, especially H$_2$PO$_4^-$, through strong electrostatic interactions. In addition, ion exchange and Lewis acid–base interactions also contribute to phosphorus adsorption, particularly when HPO$_4^{2-}$ and PO$_4^{3-}$ are present under varying pH conditions. The combination of these mechanisms enables the hydrogel to exhibit highly selective and efficient phosphorus removal, especially in acidic environments.[117]

Fig. 5c demonstrates the chelation mechanism for the adsorption of heavy metal ions such as Cu^{2+}, Cd^{2+}, and Zn^{2+} using a monodisperse microgel functionalized with polyethyleneimine (PEI). The microgel, synthesized via a Schiff base reaction between PEI and glutaraldehyde, contains abundant amine groups that serve as active chelation sites. These amine groups coordinate with metal ions through donor–acceptor interactions, forming stable chelate rings. Among the tested metals, Cu^{2+} shows the strongest binding due to its high affinity for nitrogen donor atoms, followed by Cd^{2+} and Zn^{2+}. This figure highlights the significance of functional group chemistry and metal ion properties in determining the effectiveness of chelation-based adsorption, rendering it a powerful method for removing toxic metals from aqueous environments.[118]

3.1. Physical adsorption and ion exchange

Physical adsorption and ion exchange are fundamental mechanisms by which hydrogels remove contaminants from aqueous solutions. Physical adsorption in hydrogels is primarily driven by weak, reversible interactions, such as van der Waals forces, π–π stacking, and hydrogen bonding. Unlike chemisorption, these interactions do not involve covalent bonding, enabling rapid adsorption and desorption of target molecules. Physical adsorption is particularly effective for capturing nonpolar or aromatic pollutants and can be enhanced by increasing the hydrogel network's surface area and porosity.

Ion exchange, while related to electrostatic interactions, specifically involves replacing ions originally present in the hydrogel matrix with pollutant ions from the solution. Charged functional groups, such as –COO$^-$, –SO$_3^-$, or –NH$_3^+$, act as active sites for exchanging counterions like Na$^+$, H$^+$, or Ca^{2+} with cationic or anionic contaminants. This mechanism enables selective adsorption and can contribute to the regeneration and reuse of hydrogel materials. Together, physical adsorption and ion–exchange processes provide versatile pathways for pollutant removal, complementing chemisorption and electrostatic interactions in hydrogel-based treatment systems. Both mechanisms are typically rapid and reversible, making them suitable for rapidly removing pollutants such as dyes and ions. The high water content and large surface area of hydrogels enhance the accessibility of adsorption sites, thereby increasing the adsorption rate.

In contrast, ion exchange involves replacing ions in the hydrogel with target ions from the surrounding solution. Hydrogels functionalized with ionizable groups such as carboxyl (–COO$^-$) or sulfonate (–SO$_3^-$) for cation exchange, and ammonium (–NH$_3^+$) for anion exchange facilitate this process. Ion exchange is particularly effective for capturing heavy metal ions (e.g., Pb^{2+}, Cd^{2+}) and nutrient pollutants (e.g., nitrate, phosphate) through electrostatic interactions. Both mechanisms can operate simultaneously, enhancing the overall adsorption efficiency of hydrogels in environmental remediation applications.

Cao et al.[119] developed functional ZnO/ZnFe layered double hydroxide (LDH)– alginate hydrogels to efficiently adsorb and recover phosphorus from water. The key challenge was to enhance the adsorption capacity and phosphate recovery rate while maintaining reusability. Hydrogels function through physical mechanisms, including electrostatic attraction and hydrogen bonding, as well as ion-exchange interactions

between phosphate ions and the hydroxide layers. This synergy allowed a maximum adsorption capacity of 17.06 mg g^{-1} and an outstanding phosphate recovery efficiency of 96.81% *via* simple filtration. Moreover, the hydrogel maintained over 90% of its adsorption capacity after five regeneration cycles, indicating strong durability and practical applicability.

Wang *et al.*[120] introduced alginate-based hydrogel beads hybridized with dipicolinic acid (DPA) for ultrasensitive fluorescence detection and effective adsorption of rare earth ions, specifically terbium (Tb^{3+}) and europium (Eu^{3+}). The challenge was to design a material that combines selective ion recognition with robust fluorescence response and anti-interference properties. The beads utilize physical adsorption *via* electrostatic attraction, complexation *via* DPA ligands, and ion exchange to capture target ions effectively. The optimized beads demonstrated high adsorption capacities of 270 mg g^{-1} for Tb^{3+} and 301 mg g^{-1} for Eu^{3+}, along with detection limits of 0.23 nM and 0.85 nM, respectively, confirming the material's dual sensing and removal capabilities.

Tong *et al.*[121] designed a multifunctional hydrogel composite incorporating metal–organic frameworks (MOF-on-MOF) for simultaneous uranyl ion (UO$_2^{2+}$) adsorption and ultra-sensitive fluorescence detection. The challenge was to integrate high adsorption capacity with low detection limits in aqueous environments. The composite leverages physical chelation *via* amino and carboxyl groups, ion-exchange interactions with uranyl ions, and fluorescence-quenching mechanisms, including static quenching and photoinduced electron transfer. It achieved an impressive adsorption capacity of 603 mg g^{-1} and a fluorescence detection limit of 0.551 nmol L^{-1}, retaining over 80% adsorption capacity after multiple reuse cycles. These results underscore its utility in managing radioactive pollutants.

Ramos-Martinez *et al.*[122] developed a poly(vinyl alcohol) (PVA)–citric acid crosslinked hydrogel aiming for safe and effective arsenic(v) removal without using nanoparticles. The main challenge was synthesizing a stable hydrogel with sufficient ion-exchange capacity and mechanical integrity. Ester bond crosslinking introduced carboxyl groups that facilitated ion-exchange with arsenate ions, while hydrogel swelling enhanced diffusion and physical sorption. The optimized hydrogel reached a maximum arsenic sorption capacity of 14.1 mg g^{-1} at neutral pH and 25 °C, demonstrating promising stability and reusability for water treatment applications.

Li *et al.*[123] created hybrid sodium alginate/attapulgite/zeolitic imidazolate framework-8 (ZIF-8) hydrogel beads targeting the efficient adsorption of the antibiotic norfloxacin (NOR) from water. The challenge was to enhance mechanical and thermal stability while maximizing adsorption of pharmaceutical contaminants. Adsorption mechanisms involved combined hydrogen bonding, electrostatic attraction, cation exchange, π–π electron donor–acceptor interactions, and coordination bonding *via* the active sites of ZIF-8. The beads exhibited an outstanding adsorption capacity of 1360.67 mg g^{-1} at pH 5.0, along with excellent thermal stability and anti-swelling properties, making them suitable candidates for removing antibiotics from wastewater.

Chen *et al.*[124] developed cellulose-based hydrogel composites compounded with modified kaolin aimed at simultaneous removal of heavy metals (Pb^{2+}, Cu^{2+}) and organic dyes (methylene blue) from wastewater. The challenge was to create a reusable adsorbent that maintains structural integrity while efficiently removing multiple pollutants. Removal mechanisms included ion exchange between heavy metal ions and kaolin surface functional groups, as well as electrostatic interactions that captured cationic dye molecules. The composite achieved high adsorption capacities of 879.84 mg g^{-1} for Pb^{2+}, 543.50 mg g^{-1} for Cu^{2+}, and 805.16 mg g^{-1} for methylene blue, sustaining stable performance over five adsorption/desorption cycles. These results highlight the composite's potential for broad-spectrum wastewater treatment.

Wang *et al.*[120] developed alginate-based hydrogel beads (DPA/GB) for dual-functional detection and removal of terbium and europium ions from water. The aim was to develop sustainable materials that combine visual detection with efficient adsorption capabilities for rare earth elements. The challenge addressed was achieving both functionalities simultaneously in a cost-effective material (USD 0.25 per gram). The optimal results demonstrated exceptional performance, with detection limits of 0.23 nM for Tb^{3+} and 0.85 nM for Eu^{3+}, and high adsorption capacities of 270 mg g^{-1} for Tb^{3+} and 301 mg g^{-1} for Eu^{3+} at pH 5.02. The mechanism involved synergistic effects of complexation, electrostatic interaction, and ion exchange. Tong *et al.*[121] constructed fluorescent MOF-on-MOF hydrogel complexes (Tb-MOF@ZIF-8@PAM) using a "three-in-one" synthetic strategy for simultaneous detection and removal of uranyl ions (UO$_2^{2+}$) from water. The aim was to address the threats of uranium contamination to human health and environmental security. The challenge was to develop materials with both high-sensitivity detection and superior adsorption capacity. Optimum results demonstrated remarkable performance, with an extremely low detection limit of 0.551 nmol L^{-1} and an exceptional absorption capability of 603 mg g^{-1} for UO$_2^{2+}$. The composite maintained adsorption efficiency above 80% after 4 recycling cycles, demonstrating excellent reusability through straightforward regeneration strategies.

Chen *et al.*[124] constructed cellulose-based hydrogels compounded with sulfuric acid-modified kaolin (SA/CMC/SKL) for the removal of heavy metal ions and dyes from water. The aim was to develop low-cost, environmentally friendly adsorbents from inexpensive kaolin. The challenge was to optimize the proportions of raw materials and ensure good mechanical stability while maintaining a high adsorption capacity. Optimum results achieved maximum adsorption capacities of 879.84 mg g^{-1} for Pb^{2+}, 543.50 mg g^{-1} for Cu^{2+}, and 805.16 mg g^{-1} for methylene blue, as determined by Langmuir isotherm modeling. The mechanism involved ion exchange and electrostatic attraction, with the adsorbent maintaining excellent stability and performance even after five adsorption–desorption cycles.

Gong *et al.*[125] developed semi-interpenetrating polymer network hydrogel beads (P(AM-AMPS)-CMC-Ca(ii)) using physical and chemical crosslinking approaches for efficient Cd(ii) removal. The aim was to address cadmium contamination while

overcoming the limitations of conventional adsorbents, such as poor mechanical strength and low reusability. The challenge was achieving high compressive strength while maintaining excellent adsorption performance. Optimum results showed a compressive strength of 60.0 kPa and a maximum adsorption capacity of 275.13 mg g^{-1} for Cd(II). The adsorption mechanism involved electrostatic attraction, complexation with functional groups, and ion exchange, with an adsorption efficiency of over 90% remaining after five regeneration cycles using 0.1 mol L^{-1} HCl.

Galindo et al.[126] designed novel sulfonate hydrogels by radical polymerization, with one pristine and the other hybridized with few-layer graphene (FLG) for heavy metal ion removal. The aim was to address environmental threats from non-degradable heavy metals that accumulate to toxic levels. The challenge was to maintain thermal stability while enhancing mechanical properties and adsorption capacity by incorporating graphene. Optimum results showed exceptional adsorption capacities of 631.7 mg g^{-1} for Pb^{2+}, 633.3 mg g^{-1} for Ni^{2+}, and 373.1 mg g^{-1} for Cd^{2+} in pristine hydrogels. The FLG incorporation reduced pore size, enhanced mechanical properties (Young's modulus increased from 32 to 44 kPa), and maintained high adsorption while improving swelling degree.

Cao et al.[119] developed zinc oxide/zinc–iron layered hydroxide/alginate hydrogel composites (ZnO/LDHs/Alg) to improve phosphate removal and recovery efficiency from aqueous solutions. The aim was to develop materials superior to traditional adsorbents, such as bentonite, biochar, and zeolite, for sustainable phosphorus management. The challenge was achieving both efficient removal and high recovery rates with good reusability. Optimum results demonstrated a maximum phosphate adsorption capacity of 17.06 mg g^{-1} and a recovery efficiency of 96.81% via simple filtration. The adsorption mechanisms involved electrostatic attraction, hydrogen bonding, ligand exchange, and ion exchange, with phosphate removal rates maintained above 90% after five consecutive adsorption–desorption cycles.

Salem et al.[127] prepared compatible terpolymer hydrogels (PVA/PVP/PAAm) using ionizing gamma radiation for efficient adsorption of lanthanum(III) and yttrium(III) ions. The aim was to develop simple and effective materials for the recovery of rare earth elements from aqueous solutions. The challenge involved optimizing pH conditions and understanding adsorption mechanisms while ensuring recyclability. Optimum results showed that maximum adsorption was achieved after 120 minutes, with optimal pH values of 3 and 4 for La(III) and Y(III), respectively. Physisorption was identified as the primary mechanism, with adsorption energies of 0.330385 and 0.38168 kJ mol^{-1}. The process was exothermic and spontaneous, with efficient desorption achieved using 1 M HCl, allowing for multiple recycling cycles without performance decline.

Gai et al.[128] created ZIF-8-doped sodium alginate gel beads for copper recovery and subsequent tetracycline hydrochloride removal, addressing both precious-metal recovery and emerging organic-pollutant treatment. The aim was to develop sustainable multistage treatment systems that address multiple

water contamination challenges simultaneously. The challenge was to develop stable materials capable of sequentially treating different types of pollutants while meeting safety standards. Optimum results were achieved with a Cu^{2+} adsorption capacity of 182.61 mg g^{-1} and TC removal capacity of 152.2 mg g^{-1}. The mechanisms involved electrostatic attraction, complexation, coordination, and ion exchange, with the maximum Cu^{2+} leaching concentration (1.57 mg L^{-1}) remaining below regulatory limits, confirming the safe application.

Ramos-Martinez et al.[122] developed functionalized poly(vinyl alcohol)–citric acid hydrogels for arsenic(v) removal, using citric acid as both a crosslinker and a functionalizing agent. The aim was to develop cost-effective materials for arsenic mitigation without relying on expensive nanoparticles or high-cost reagents. The challenge was to achieve effective arsenic capture while maintaining water-insolubility and scalability for real-world applications. Optimum results demonstrated maximum arsenic sorption capacity of 14.1 mg As g^{-1} when treating 13 mg As L^{-1} solutions at pH 7 and 25 °C. The removal process involved swelling–sorption, deswelling–desorption, and sorption–swelling stages, with a higher citric acid content providing more carboxylic acid groups for ligand formation with arsenic via ion-exchange mechanisms.

Li et al.[123] synthesized novel hybrid hydrogel beads composed of sodium alginate, attapulgite, and zeolitic imidazole framework-8 for the removal of norfloxacin from aqueous solutions. The aim was to overcome the limitations of conventional sodium alginate hydrogels, including their limited functional groups and poor adsorption capacity. The challenge was to enhance thermal stability and anti-swelling properties while maintaining high adsorption performance for pharmaceutical contaminants. Optimum results were achieved with a maximum theoretical adsorption capacity of 1360.67 mg g^{-1} for norfloxacin at pH 5.0, significantly higher than that of pure SA and SA/ATP hydrogels. Real water testing demonstrated 100% removal efficiency at 0.0015 mmol L^{-1} and 71% at 0.015 mmol L^{-1}. Multiple mechanisms are involved, including hydrogen bonding, electrostatic adsorption, cation exchange, π–π EDA interactions, and coordination.

Salfate et al.[129] modified lignin to obtain sulfonated methacrylated lignin combined with itaconic acid to create polymeric hydrogels (AITC/LMS) for copper(II) removal from water. The aim was to develop eco-friendly materials utilizing sustainable lignin resources for the remediation of heavy metals. The challenge involved modifying lignin structure to enhance adsorption properties while maintaining swelling capabilities and effectiveness. Optimum results showed swelling of up to 300% in water and a maximum copper sorption capacity of 67 mg g^{-1}, as predicted by the Langmuir isotherm model. The materials captured Cu(II) ions via both electrostatic attraction and chemisorption, as indicated by pseudo-first-order, pseudo-second-order, and intraparticle diffusion kinetic models, highlighting their potential as eco-friendly solutions to heavy metal contamination challenges.

Li et al.[130] integrated carbon dots with amphiphilic polyurethane to create composite hydrogels for enhanced fluorescence detection and absorption of Fe^{3+} ions in wastewater. The

aim was to develop materials with superior mechanical stability, high sensitivity, and selectivity for monitoring and treating iron contamination. The challenge was to achieve a significant improvement in detection limits while maintaining absorption capacity and mechanical properties. Optimum results showed a remarkable 103-fold enhancement in Fe^{3+} detection limit (from 0.38 μM to 0.98 nM) compared to carbon dots in solution. The composite hydrogels exhibited a 4.2-fold increase in Fe^{3+} adsorption capacity compared to pure polyurethane, attributed to the stable complexation between carbon dots and Fe^{3+} ions, offering a cost-effective solution for wastewater treatment.

Bell et al.[131] used chitosan hydrogels crosslinked with glutaraldehyde for adsorbing ethinylestradiol, a synthetic pharmaceutical steroid hormone, at environmentally realistic low concentrations. The aim was to address emerging contaminant pollution from hormonally active agents with unknown health and ecosystem effects. The challenge involved testing materials at realistic low concentrations rather than high concentrations typically used in research, while optimizing physical treatment methods. Optimum results were achieved with 62% adsorption efficiency for microwave-treated hydrogels at a low ethinylestradiol concentration (400 ng mL^{-1}) and 61% removal efficiency at higher concentrations (5000 ng mL^{-1}). Physical treatments, including microwave treatment, liquid nitrogen submersion, and overnight freezing, increased pore size and surface area, with a high moisture content enhancing performance.

Ali et al.[132] developed polysaccharide-based hydrogels from *Salvia spinosa* seeds, which were cross-linked with citric acid and subsequently converted to the sodium salt form (Na-CL-SSH) for the removal of Cd(II). The aim was to develop bio-based adsorbents from natural polysaccharides, with optimized performance achieved through the application of response surface methodology. The challenge involved optimizing adsorption conditions using a Box-Behnken design while understanding ion-exchange mechanisms to enable scalability. Optimum results demonstrated a rapid, exothermic Cd(II) adsorption process occurring through an ion-exchange mechanism, with a high coefficient of determination ($R^2 = 0.9980$) for the optimization model. Column adsorption experiments provided data useful for industrial-scale implementation, with successful regeneration capabilities and kinetic studies confirming chemisorption processes for effective cadmium removal from contaminated water systems.

Gopika et al.[133] fabricated ternary composite hydrogels using biopolymer gelatin reinforced with nano-lanthanum hydroxide-decorated graphene oxide (GLG) for hexavalent chromium detoxification. The aim was to create mesoporous spherical hydrogels with enhanced adsorption properties for the removal of toxic chromium species. The challenge was to achieve uniform dispersion of fillers throughout the gelatin matrix while maintaining stability and regenerative properties. Optimum results showed the highest adsorption rate at pH 3.5 after 120 minutes, using 0.4 g GLG2 with a 50 mg L^{-1} Cr(VI) solution at 298 K. The mechanism involved electrostatic attraction, ion exchange, and partial reduction of Cr(VI) to Cr(III).

Continuous flow system testing demonstrated a maximum bed capacity of 21.03 mg g^{-1} at a 0.5 mL min^{-1} flow rate, with remarkable performance in treating real electroplating effluent.

3.2. Electrostatic interactions and hydrogen bonding

Electrostatic interactions and hydrogen bonding play a significant role in the adsorption behavior of hydrogels toward various pollutants. Electrostatic adsorption arises from coulombic attraction between charged functional groups present on the hydrogel matrix and oppositely charged contaminants in solution. Key functional groups responsible for these interactions include carboxyl groups (–COO^-), which can bind cationic dyes and metal ions, and sulfate or sulfonate groups (–SO_3^-), which serve as strong ion-exchange sites. Additionally, protonated amino groups (–NH_3^+) can bind anionic dyes and negatively charged organic pollutants, thereby enhancing the selectivity of hydrogel adsorption.

Ion-exchange mechanisms further complement electrostatic adsorption. In these processes, charged functional groups on the hydrogel substitute their native counterions, such as Na^+, H^+, or Ca^{2+}, with pollutant ions from the surrounding medium. This exchange not only strengthens binding of the target pollutants but also enhances the hydrogel's regeneration potential in repeated adsorption cycles. Hydrogen bonding, although weaker than covalent or electrostatic interactions, can additionally stabilize the adsorption of polar molecules, providing a versatile and efficient mechanism for pollutant capture.

Wang et al.[120] aimed to develop sustainable difunctional materials for selective visual detection and efficient removal of rare earth elements (Tb^{3+} and Eu^{3+}) from water. The main challenge was achieving both detection and adsorption functionalities in a single material. Their alginate-based hydrogel beads (DPA/GB) incorporated dipicolinic acid and were calcium-crosslinked, providing high-density carboxyl groups and pyridine nitrogen atoms. The optimal results showed exceptional performance, with limits of detection of 0.23 nM for Tb^{3+} and 0.85 nM for Eu^{3+}, and maximum adsorption capacities of 270 mg g^{-1} for Tb^{3+} and 301 mg g^{-1} for Eu^{3+} at pH 5.02. The material cost was remarkably low at USD 0.25 per gram, demonstrating synergistic effects through complexation, electrostatic interactions, and ion-exchange mechanisms.

Tong et al.[121] focused on developing multifunctional materials for simultaneous adsorption and detection of uranyl ions (UO_2^{2+}) in water, addressing the threat of uranium contamination to human health and environmental security. The challenge was to create stable fluorescent materials with both high detection sensitivity and high adsorption capacity. Their novel Tb-MOF@ZIF-8@PAM hydrogel composite achieved remarkable results, with a detection limit of 0.551 nmol L^{-1} for UO_2^{2+} and a superior adsorption capacity of 603 mg g^{-1}. The material demonstrated excellent stability and recyclability, maintaining an adsorption efficiency above 80% after 4 cycles, with mechanisms involving a static quenching effect and photoinduced electron transfer for detection, combined with abundant amino and carboxyl groups for adsorption.

Chen et al.[124] aimed to develop cost-effective, environmentally friendly hydrogel adsorbents for the simultaneous removal of heavy metal ions and dyes from water, using inexpensive kaolin as a starting material. Optimizing the composition and structure for maximum adsorption efficiency while maintaining stability was the challenge. Their SA/CMC/SKL hydrogel, composed of sodium alginate, carboxymethyl cellulose, and sulfuric acid-modified kaolin, achieved exceptional adsorption capacities of 879.84 mg g^{-1} for Pb^{2+}, 543.50 mg g^{-1} for Cu^{2+}, and 805.16 mg g^{-1} for methylene blue. The material followed Langmuir isotherm and pseudo-second-order kinetic models, with ion exchange and electrostatic attraction as primary removal mechanisms, maintaining excellent stability after five adsorption–desorption cycles.

Gong et al.[125] addressed the limitations of conventional adsorbents, including poor mechanical strength, low adsorption capacity, and limited reusability for the removal of Cd(II) contamination. Their challenge was to develop a mechanically robust hydrogel with high-performance characteristics. The semi-interpenetrating polymer network hydrogel beads, P(AM-AMPS)-CMC-Ca(II), achieved a compressive strength of 60.0 kPa and a maximum adsorption capacity of 275.13 mg g^{-1} for Cd(II). The optimal results showed that the material followed the Freundlich isotherm and the pseudo-second-order kinetic model, with adsorption driven by electrostatic attraction, complexation, and ion exchange. The hydrogel maintained an efficiency above 90% after five cycles using 0.1 mol L^{-1} HCl as the desorption agent.

Galindo et al.[126] aimed to address heavy metal contamination using cost-effective radical polymerization methods incorporating sulfonate groups and few-layer graphene (FLG) to enhance performance. The challenge was to maintain a high adsorption capacity while improving mechanical properties and thermal stability. Their pristine (VBS) and hybrid FLG hydrogels (VBSG) achieved maximum uptake capacities of 631.7 mg g^{-1} for Pb^{2+}, 633.3 mg g^{-1} for Ni^{2+}, and 373.1 mg g^{-1} for Cd^{2+} in pristine hydrogels, with 540.6 mg g^{-1} for Pb^{2+}, 615.1 mg g^{-1} for Ni^{2+}, and 304.9 mg g^{-1} for Cd^{2+} in hybrid versions. The FLG incorporation reduced the pore size from 42 to 35 μm, increased Young's modulus from 32 to 44 kPa, and enhanced the swelling degree from 62 to 76%, while maintaining excellent reusability in acidic media.

Cao et al.[119] focused on developing materials for efficient phosphorus removal and recovery from aqueous solutions, addressing both environmental concerns and the potential for resource recovery. The challenge was to achieve high removal efficiency while enabling the practical recovery and reuse of phosphate. Their ZnO/LDHs/Alg composite hydrogels achieved a maximum phosphate adsorption capacity of 17.06 mg g^{-1}, surpassing traditional materials such as bentonite, biochar, and zeolite. Optimum results achieved 96.81% recovery efficiency through simple filtration, with a removal rate of over 90% maintained after five consecutive adsorption–desorption cycles. The main mechanisms involved are electrostatic attraction, hydrogen bonding, ligand exchange, and ion exchange.

Salem et al.[127] aimed to develop simple, compatible terpolymer hydrogels for efficient adsorption of lanthanum(III)

and yttrium(III) ions using gamma radiation synthesis. The challenge was to optimize conditions for maximum adsorption while ensuring recyclability and understanding the adsorption mechanisms. Their PVA/PVP/PAAm terpolymer hydrogel reached maximum adsorption and equilibrium after 120 minutes, with optimum pH values of 3 for La(III) and 4 for Y(III). The material demonstrated physisorption mechanisms with adsorption energies of 0.330385 and 0.38168 kJ mol^{-1} for La(III) and Y(III), respectively. The process was found to be exothermic and spontaneous, with efficient desorption using 1 M HCl and successful recycling for multiple cycles without performance decline.

Gai et al.[128] addressed the dual challenge of precious metal recovery and organic pollutant treatment, focusing on sustainable multistage pollutant treatment approaches. Their challenge was creating materials that could sequentially treat different types of contaminants while maintaining stability and safety. The ZIF-8@SA gel beads achieved a Cu^{2+} adsorption capacity of 182.61 mg g^{-1} via electrostatic attraction, complexation, coordination, and ion-exchange mechanisms. The subsequent ZIF-8@SA@Cu-MOF material demonstrated a maximum adsorption capacity of 152.2 mg g^{-1} for tetracycline hydrochloride. The safety evaluation revealed a Cu^{2+} leaching concentration of 1.57 mg L^{-1}, below the regulatory limit of 2 mg L^{-1}, confirming its safe application for industrial wastewater management.

Ramos-Martinez et al.[122] aimed to develop cost-effective materials for arsenic(V) capture that do not use nanoparticles or high-cost reagents, with a focus on scalable, real-world applications. The challenge was achieving effective arsenic removal using commercially available, simple materials while understanding the complex swelling–sorption mechanisms. Their citric acid-crosslinked PVOH hydrogels achieved a maximum arsenic sorption capacity of 14.1 mg As/g when treating solutions containing 13 mg As/L at pH 7 and 25 °C. The material exhibited water–insoluble properties, enabling effective separation, with a higher citric acid content providing more carboxylic acid groups for citrate–arsenic ligand formation. The process involved three stages: swelling–sorption, deswelling–desorption, and sorption–swelling, offering a cost-effective approach using readily available reagents.

Li et al.[123] aimed to overcome the limitations of sodium alginate hydrogels, including limited functional groups and poor adsorption capacity, for the removal of pharmaceutical pollutants. The challenge was to enhance thermal stability and anti-swelling properties while achieving a high adsorption capacity for norfloxacin. Their SA/ATP/ZIF-8 hybrid hydrogel beads achieved a remarkable maximum theoretical adsorption capacity of 1360.67 mg g^{-1} for norfloxacin at pH 5.0. In real Nandu River water tests, the material demonstrated 100% removal efficiency at an initial concentration of 0.0015 mmol L^{-1} and 71% at 0.015 mmol L^{-1}. The adsorption mechanisms included hydrogen bonding, electrostatic adsorption, cation exchange, π–π electron donor–acceptor interactions, and coordination, with kinetics following the pseudo-second-order model and isotherms fitting the Langmuir–Freundlich model.

Salfate et al.[129] focused on using lignin, a renewable resource, to create environmentally friendly hydrogels for heavy metal removal, addressing sustainability concerns in water treatment. The challenge was modifying lignin to enhance its functionality while maintaining cost-effectiveness and environmental benefits. Their sulfonated methacrylated lignin with itaconic acid (AITC/LMS) hydrogels achieved swelling up to 300% of their mass in water and demonstrated a maximum copper adsorption capacity (q_{max}) of 67 mg g^{-1}. The materials followed the Langmuir isotherm model and exhibited both electrostatic attractions and chemisorption mechanisms, as indicated by the PFO, PSO, and IPD kinetic models, highlighting their potential as eco-friendly materials for addressing heavy-metal contamination challenges.

Li et al.[130] aimed to develop dual-function materials that combine fluorescence detection with adsorption for Fe^{3+} ions, addressing the need for sensitive detection and effective removal. The challenge was achieving enhanced sensitivity while maintaining mechanical stability and absorption capacity. Their carbon dots-amphiphilic polyurethane composite achieved remarkable results with a 103-fold enhancement in detection limit for Fe^{3+} (from 0.38 μM to 0.98 nM) compared to carbon dots in solution. The composite showed a 4.2-fold increase in Fe^{3+} absorption capacity compared to pure polyurethane, attributed to the formation of a stable complex between carbon dots and Fe^{3+} ions. The red shift in fluorescence emission and improved stability were due to interactions between functional groups on carbon dots and the polyethylene glycol segments of the polyurethane matrix.

Bell et al.[131] addressed the emerging challenge of removing hormonally active agents, specifically ethinylestradiol, from water at environmentally realistic low concentrations. Their challenge was to optimize hydrogel properties through physical treatments while working with concentrations much lower than those typically studied. The chitosan hydrogels crosslinked with glutaraldehyde achieved optimal results, with microwave-treated materials showing 62% adsorption efficiency at a low ethinylestradiol concentration (400 ng mL^{-1}) and 61% removal efficiency at a higher concentration (5000 ng mL^{-1}) when the moisture content was high. Physical treatments, including microwave treatment, liquid nitrogen submersion, and overnight freezing, successfully increased pore size and exposed surface area. Treatments performed after synthesis proved most effective for enhancing adsorption capacity.

Ali et al.[134] aimed to develop polysaccharide-based hydrogels from natural Salvia spinosa seeds for cadmium removal, optimizing conditions through advanced statistical design. The challenge was to create effective adsorbents from natural sources while understanding ion-exchange mechanisms and maximizing their potential. Their citric acid cross-linked Salvia spinosa hydrogel (Na-CL-SSH) demonstrated excellent performance, optimized through a Box-Behnken design, with a high coefficient of determination ($R^2 = 0.9980$) and a significant F-value (358.61). The material exhibited rapid, exothermic adsorption through ion-exchange mechanisms, with successful column adsorption experiments providing useful data for industrial-scale scalability. The study revealed a non-significant
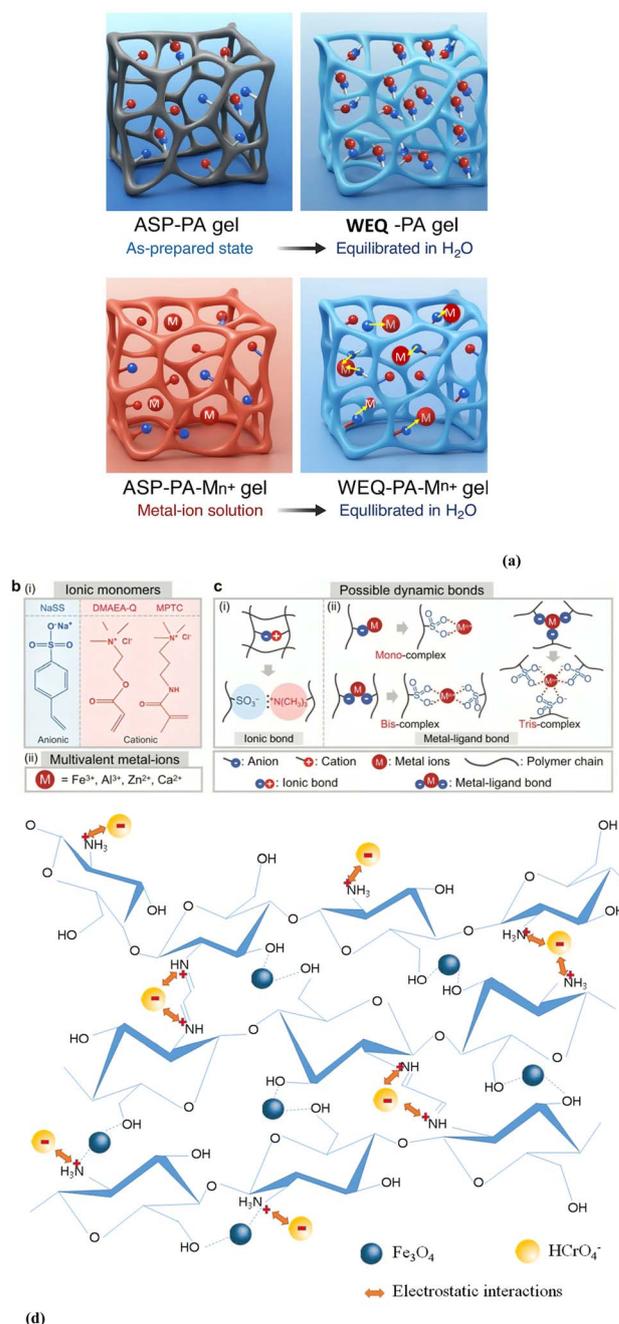

Fig. 6 Conceptual design and fabrication process of strong and tough polyampholyte (PA) hydrogels via a two-step equilibrium method leveraging electrostatic and metal−ligand interactions. (a) Schematic of the secondary equilibrium process: the as-prepared (ASP) hydrogel swells in a multivalent metal ion solution (e.g., FeCl$_3$) due to ionic bond disruption, then is equilibrated in deionized water to re-establish ionic and metal−ligand crosslinks. (b) Chemical structures of the monomers DMAEA-Q, MPTC, and NaSS and metal ions used to build the PA network. (c) Illustration of dynamic ionic and metal−ligand bonding in the restructured hydrogel network, contributing to enhanced mechanical strength, toughness, and self-recovery. Electrostatic interactions, screened and reformulated during processing, are central to the hydrogel's tunable and resilient structure. (d) The adsorption of Cr^{6+} ions onto Fe$_3$O$_4$ NPs/CS/glyoxal hydrogel film via electrostatic interactions under acidic conditions (pH 4). Reproduced from ref. 135 with permission from [Springer Nature], copyright 2017.

lack of fit, indicating excellent model fitness for the cadmium adsorption process.

Gopika et al.[133] focused on developing ternary composite hydrogels for hexavalent chromium detoxification, combining the biopolymer gelatin with nano-lanthanum hydroxide-decorated graphene oxide. The challenge was achieving efficient Cr(VI) removal while maintaining stability and demonstrating large-scale applicability. Their GLG hydrogels achieved the highest adsorption at pH 3.5 after 120 minutes, using 0.4 g GLG2 and a 50 mg L^{-1} Cr(VI) solution at 298 K. The mesoporous spherical hydrogels (average diameter, 1.993 mm) demonstrated stable regeneration for three consecutive cycles. They demonstrated remarkable performance in continuous flow systems, achieving a maximum bed capacity of 21.03 mg g^{-1} at a flow rate of 0.5 mL min^{-1}, corresponding to a total volume of 3.5 L. The comprehensive mechanism study revealed efficient uptake through electrostatic attraction, ion exchange, and partial reduction of Cr(VI) to Cr(III), with successful application to the treatment of real electroplating effluent.

Fig. 6 illustrates the conceptual design and fabrication process for strong and tough polyampholyte (PA) hydrogels, using a secondary-equilibrium approach that leverages the synergistic effects of ionic and metal–ligand interactions. Fig. 6a depicts the two-step equilibrium procedure: in the first stage, the as-prepared (ASP) PA hydrogel is immersed in a multivalent metal ion solution (e.g., FeCl$_3$), allowing the gel to swell due to the disruption of ionic bonds and the screening of electrostatic attractions by the introduced free ions. This swelling arises from an imbalance in electrostatic interactions, in which the ionic environment decouples the originally paired cationic and anionic groups within the PA network. In the second step, the swollen gel is transferred into deionized (DI) water to reach a water-equilibrated (WEQ) state. During this phase, excess free ions are dialyzed out, and the network is reconstructed by forming new ionic bonds and metal–ligand complexes, resulting in a reinforced, restructured hydrogel.

Fig. 6b presents the chemical structures of the monomers and metal ions used in the study. Specifically, two cationic monomers DMAEA-Q and MPTC are copolymerized with the anionic monomer NaSS to form the PA network. The introduction of multivalent metal ions such as Fe^{3+}, Al^{3+}, Zn^{2+}, and Ca^{2+} plays a crucial role in creating metal–ligand bonds with anionic sulfonate groups in the hydrogel. These interactions are central to the observed mechanical enhancement. Fig. 6c highlights the dynamic bonding mechanisms within the optimized PA gels, showing both ionic bonds (between oppositely charged monomer units) and metal–ligand bonds (between Fe^{3+} and negatively charged sulfonate or carboxyl groups). These bonds are dynamic, reversible, and capable of dissipating energy under deformation, which is key for toughness and self-recovery.

Electrostatic interactions play a central role in this strategy. Initially, they govern the ionic bonding within the original PA hydrogel. Upon immersion in saline or metal-ion solutions, these electrostatic interactions are screened, leading to ionic bond breaking and gel swelling an effect tied to the anti-polyelectrolyte nature of PA networks. Later, as excess salts are removed during dialysis, the electrostatic environment shifts

again, allowing ionic re-pairing and the formation of new metal–ligand interactions. Importantly, metal–ligand bonds are stronger and more tunable than hydrogen bonds, enabling a more stable and mechanically enhanced hydrogel structure. This strategy ultimately yields hydrogels with significantly enhanced modulus, tensile strength, work of tension, tearing energy, and self-recovery performance, confirming the effectiveness of utilizing electrostatic interactions, particularly through synergistic ionic and metal–ligand bonding, as a design principle for robust hydrogel materials. Fig. 6d illustrates the electrostatic adsorption mechanism of hexavalent chromium (Cr^{6+}) ions onto a hydrogel film composed of Fe$_3$O$_4$ nanoparticles, chitosan (CS), and glyoxal. In aqueous solution under acidic conditions (pH < 4), Cr^{6+} predominantly exists in the form of negatively charged hydrogen chromate ions (HCrO$_4^-$). Concurrently, the amino groups (–NH$_2$) on the chitosan backbone become protonated, forming positively charged –NH$_3^+$ groups, effectively rendering the hydrogel surface positively charged. This charge oppositeness between the hydrogel surface and the HCrO$_4^-$ ions leads to a strong electrostatic attraction, facilitating the effective adsorption of Cr^{6+} from the solution.

The adsorption mechanism shown in Fig. 6d illustrates how the surface functional groups of hydrogels dynamically interact with pollutants, depending on the pH. In acidic media, amino-containing groups like those in chitosan protonate, which enhances the hydrogel's ability to bind negatively charged species, including anionic dyes and oxyanions like HCrO$_4^-$. In this context, electrostatic interactions serve as the primary driving force, enabling selective adsorption of hazardous pollutants based on their charge.

3.3. Chemisorption and covalent binding

Chemisorption involves the formation of strong and often irreversible interactions between the hydrogel and target molecules or ions. These interactions can occur through various mechanisms, including covalent bonding (such as imine formation, Michael addition, or nucleophilic substitution), metal–ligand coordination between hydrogel donor atoms and heavy-metal ions, and surface complexation that forms inner–sphere complexes. Such strong interactions distinguish chemisorption from weaker physical adsorption processes and are critical for applications requiring high selectivity and stability. The presence of specific functional groups largely determines a hydrogel's ability to undergo chemisorption. Carboxyl groups (–COOH/–COO$^-$) can coordinate with metal ions via their oxygen donors, while amino groups (–NH$_2$) can form Schiff bases, chelate metals, or participate in nucleophilic addition reactions. Thiol groups (–SH) exhibit a strong affinity for soft metals such as Hg^{2+}, Ag$^+$, and Pb^{2+}, making them particularly useful in heavy-metal capture. Hydroxyl groups (–OH) also contribute by complexing with transition metals, and aldehyde or ketone groups can react with amines to form imine bonds, as in Schiff base hydrogels. The combination of these functional groups enables hydrogels to efficiently bind and immobilize a wide range of target species through chemisorption. This

mechanism is especially relevant for organic pollutants and can be achieved through several pathways. Enzymatic cross-linking represents one approach in which enzymes immobilized within a hydrogel catalyze covalent bond formation with target pollutants. For instance, peroxidase enzymes can catalyze the coupling of phenolic compounds to the polymer backbone through C–C or C–O bond formation. Photo-initiated covalent binding utilizes light-activated reactions to create permanent bonds. Hydrogels containing photosensitive groups can form covalent bonds with organic contaminants upon exposure to UV radiation, effectively trapping pollutants within the network. The chemical nature of these interactions provides several advantages over physical adsorption.

The binding strength is significantly higher, reducing the likelihood of contaminant desorption and secondary pollution. This permanence is particularly valuable for treating persistent organic pollutants or toxic heavy metals, where complete removal is critical. Selectivity is another key benefit, as the chemical specificity of functional groups enables the targeted removal of specific contaminants. This selectivity can be enhanced through molecular imprinting, in which the hydrogel is synthesized in the presence of target molecules, thereby creating complementary binding sites. Successful implementation requires careful consideration of both the hydrogel's architecture and chemistry. The cross-linking density affects both the accessibility of binding sites and the mechanical stability of the material. Higher cross-linking generally increases selectivity but may reduce diffusion rates and total binding capacity. pH conditions significantly influence both chemisorption and covalent binding efficiency. The protonation state of functional groups affects their binding affinity, while solution pH can alter the speciation of metal contaminants and their availability for binding. Temperature effects are also important, as elevated temperatures can enhance reaction kinetics for covalent binding but may also increase the risk of bond breaking for some chemisorbed species. While the strength of chemical binding is advantageous for contaminant removal, it poses challenges for hydrogel regeneration. Traditional desorption methods, such as pH changes or competing ions, may be insufficient to break covalent bonds. Advanced regeneration techniques such as thermal treatment, chemical reduction, or enzymatic cleavage may be necessary. Some systems incorporate reversible covalent bonds, such as disulfide bridges or pH-sensitive linkages, that allow for controlled release and regeneration under specific conditions. This approach strikes a balance between the benefits of strong binding and the practical need for material reuse. The integration of chemisorption and covalent binding mechanisms makes hydrogels powerful tools for water treatment, offering high efficiency, selectivity, and permanence in contaminant removal while presenting opportunities for innovative design approaches tailored to specific water treatment challenges.

Wang et al.[120] aimed to develop sustainable difunctional materials for selective visual detection and efficient removal of rare earth elements (REE^{3+}), addressing the challenge of achieving both functionalities simultaneously. They fabricated unique hydrogel beads (DPA/GB) by hybridizing dipicolinic acid with sodium alginate and then cross-linking with calcium. The optimum results demonstrated exceptional performance, with limits of detection of 0.23 and 0.85 nM for Tb^{3++} and Eu^3, respectively, and superior adsorption capacities of 270 mg g^{-1} for Tb^{3+} and 301 mg g^{-1} for Eu^{3+} at pH 5.02, with remarkable cost-effectiveness at USD 0.25 per gram.

Zhang et al.[136] focused on fabricating ion/pH dual-responsive semi-interpenetrating network hydrogel microspheres for efficient dye removal, addressing the challenge of creating materials with excellent stimulus response and reusability. They utilized inverse suspension polymerization with diacetone acrylamide and zwitterionic sulfobetaine methacrylate as monomers. The optimum results showed a maximum adsorption capacity of 330.56 ± 3.64 mg g^{-1} for Eosin Y, with the microspheres demonstrating excellent cycling repeatability, antifouling properties, and spontaneous adsorption, as indicated by pseudo-second-order kinetics and Langmuir isotherm models.

Huang et al.[137] aimed to develop efficient adsorbents for Ga(III) recovery using geochemical principles to address the challenge of selective metal recovery from complex matrices. They created a sodium alginate-montmorillonite nanosheet hydrogel via electrostatic interactions and Ca^{2+} complexation. The optimum results achieved a maximum adsorption capacity of 85.95 mg g^{-1}, following the Langmuir isotherm model, with the hydrogel maintaining a capacity of 65.4 mg g^{-1} after four cycles. This demonstrates good selectivity for Ga(III) in quaternary ion systems through ion exchange, chelation, and electrostatic interactions.

Tong et al.[121] aimed to construct multifunctional MOF-on-MOF hydrogel complexes for simultaneous adsorption and sensitive detection of uranyl ions, addressing the challenge posed by uranium contamination to human health and environmental security. They developed Tb-MOF@ZIF-8@PAM using a "three-in-one" synthetic strategy combining ZIF-8 with Tb-MOF. The optimal results demonstrated exceptional sensitivity (LOD of 0.551 nmol L^{-1}) and remarkable adsorption capacity of 603 mg g^{-1} for UO$_2^{2+}$, maintaining above 80% adsorption efficiency after four cycles with a straightforward recycling strategy.

Han et al.[138] aimed to develop effective solutions for removing microplastics from drinking water, addressing the significant health concerns posed by micro- and nanoplastics in food systems. They created a polydopamine-modified sodium alginate hydrogel (PMSAH) via surface modification. Optimum results showed that PMSAH5 achieved approximately 99.6% removal efficiency for microplastics, regardless of size or surface charge, driven by multilayer adsorption via combined forces. This demonstrated higher elasticity and thermal stability compared to unmodified hydrogels.

Guo et al.[139] aimed to address the difficulty of specific separation of natural flavonoids while providing environmental remediation solutions, tackling the challenge of accurate recognition in complex environmental matrices. They developed hyperbranched imprinted-covalent organic frameworks hydrogel (PHs@RCOFs@H-MIPs) via Pickering emulsion microreactors for the extraction of naringin. The optimum

results achieved a high affinity site number (70.86 μmol g^{-1}), recognition capability (53.20 μmol g^{-1}), rapid mass transfer (180 min), a selectivity coefficient (IF = 1.69), remarkable stability (93.50% after six cycles), and an extraction efficiency of 92.00% for commercial naringin treatment.

Tai et al.[140] aimed to develop sustainable removal technologies for toxic textile dyes, addressing the challenge of poor mechanical strength and limited adsorption efficiency in conventional hydrogel designs. They created bio-based hydrogel composites by reinforcing polyacrylamide with bacterial cellulose and human hair keratin intermediate filaments. The optimal results demonstrated high dye removal efficiency of 60 mg g^{-1} for methylene blue over 12 hours, rapid adsorption equilibrium (15 seconds) under continuous flow, compressive strength of 0.4 MPa, and successful multiple adsorption–desorption cycles via electrostatic interactions and π–π stacking.

Seleka and Makhado[141] aimed to address global water pollution problems through innovative nanocomposite adsorbents, tackling the challenge of excessive and inappropriate use of pollutants. They fabricated a xanthan gum/acrylic acid/acrylamide hydrogel nanocomposite modified with graphene oxide via free radical polymerization for the removal of methylene blue. The optimum results achieved a maximum adsorption capacity of 1008 mg g^{-1} using 250 mg L^{-1} MB^{-1} dye at pH 7 within 1 hour, followed by pseudo-second-order kinetics and excellent recyclability across 5 successive cycles; electrostatic attraction was identified as the primary adsorption mechanism.

Kong et al.[142] aimed to develop efficient uranium recovery systems from radioactive wastewater, addressing the challenge of simultaneously recycling uranium resources and conserving the environment. They created a high-strength double-network poly(acrylamide-acrylic acid) hydrogel that is synergistic with UiO-66-NH-AO through both chemical covalent and physical crosslinking. The optimal results achieved an uranium-uptake capacity of 275.42 mg g^{-1} at 298 K, with a 93% removal rate in simulated nuclear wastewater within three days, maintaining reproducible stability after five cycles and high selectivity amid 10 competing metal ions through coordination of amidoxime, carboxyl, and amino groups.

Dou et al.[143] aimed to develop effective erythromycin removal systems addressing antibiotic overuse threats to ecosystems and human health, tackling the challenge of creating dual-functional adsorption–catalysis processes. They created copper peroxide nanoparticles@ZIF-8/polyacrylic acid/chitosan (CPNs@ZIF-8/PA/CS) hydrogel Fenton-like catalyst through a novel coupling adsorption-catalysis (CAC) process. The optimal results demonstrated adsorption efficiency 4 times higher than that of CS alone and degradation efficiency 2 times higher than that of CPNs@ZIF-8 alone, with significant advantages in recyclability, stability, and sustained catalytic degradation, maintaining high performance after 5 cycles.

Sharma et al.[144] aimed to address water scarcity and pollution challenges through sustainable solutions, emphasizing the need for efficient contaminant removal from water systems. They comprehensively reviewed cellulose-based materials, including membranes, hydrogels, and aerogels, for water treatment applications, addressing the advantages of biodegradability, hydrophilicity, and non-toxicity. Optimal findings revealed significant efficacy in eliminating heavy metals, oil, microorganisms, dyes, and other pollutants from wastewater, with various modification techniques, such as nanoparticle incorporation and polymer grafting, enhancing water treatment potential while maintaining environmental sustainability and cost-effectiveness.

Obsa et al.[145] aimed to develop eco-friendly composite hydrogels for lead removal from wastewater, addressing the challenge of toxic heavy metal contamination in water systems. They created a cellulose–bentonite composite hydrogel via uniform dispersion techniques, thereby enhancing both its swelling capacity and mechanical strength. The optimum results achieved a maximum adsorption capacity of 110.64 mg g^{-1} for Pb^{2+}, with kinetics and isotherm data best described by the pseudo-second-order model ($R^2 = 0.999$) and the Sips model ($R^2 = 0.996$), demonstrating selectivity for Pb^{2+} over Cd^{2+} and good reusability after five adsorption–desorption cycles.

Wang et al.[146] aimed to develop efficient adsorbents for the removal of diclofenac sodium from aqueous solutions, addressing the challenge of pharmaceutical contamination in water systems. They fabricated chitosan/microcrystalline cellulose@polyethyleneimine (CS/MCC@PEI) composite gel spheres through blending and grafting modifications. The optimal results demonstrated a high adsorption capacity of 274.84 mg g^{-1} for diclofenac sodium, following pseudo-second-order kinetics and a Freundlich isotherm model, with minimal interference from co-existing anions and humic acid, excellent reusability (>77% removal after five cycles), and cost-effective, sustainable performance.

S. Mukhopadhyay[147] aimed to optimize the synthesis of β-cyclodextrin/guar gum hydrogel for dual-dye removal, addressing the challenge of achieving both maximum swelling percentage and strength through systematic parameter optimization. They employed Response Surface Methodology with a Central Composite Design, using epichlorohydrin as the crosslinking agent, with optimized factors including temperature, reaction time, crosslinker amount, solvent amount, backbone ratio, and pH. The optimum results achieved a maximum adsorption capacity of 453 mg g^{-1} for methylene blue and 899 mg g^{-1} for fuchsin acid, with outstanding reusability, maintaining 43.6% and 39.76% removal efficiencies, respectively, after five cycles.

Salfate et al.[129] aimed to develop eco-friendly materials for copper removal from water systems, addressing the challenge of heavy-metal contamination through sustainable lignin-based approaches. They modified lignin to obtain sulfonated methacrylated lignin (LMS) and itaconic acid (AITC) for the formation of a polymeric hydrogel via free radical polymerization. Optimal results demonstrated hydrogel swelling of up to 300% in water and Cu(II) capture via electrostatic attraction and chemisorption, in accordance with PFO, PSO, and IPD kinetic models. A Langmuir isotherm model with a q_{max} of 67 mg g^{-1} was also observed, showcasing the effectiveness of this material as an eco-friendly option for heavy metal removal.

Table 3 Physisorption *vs.* chemisorption in hydrogel-based wastewater treatment

Parameter	Physisorption	Chemisorption	Ref.
Interaction forces	Van der Waals forces, hydrogen bonding, dipole–dipole interactions, π–π interactions, hydrophobic interactions	Chemical bonds (covalent or ionic), electron exchange, coordination interactions	155–157
Bond strength/energy range	Weak, typically <0.8 eV (<18.45 kJ mol^{-1} to 40 kJ mol^{-1})	Strong, typically 40–800 kJ mol^{-1}	157–159
Reversibility	Reversible and desorptive process; easily reversed by variations in temperature, pH, or pressure	Irreversible or difficult to reverse; requires high activation energy for desorption, typically occurs at elevated temperatures	155 and 158
Monolayer formation	Multilayer adsorption possible due to weak forces	Monolayer coverage; at most one molecular layer forms on adsorbent surface	158 and 159
Temperature dependence	Decreases with increasing temperature; favored at low temperatures	May increase with temperature to certain extent; requires higher activation energy; temperature-dependent	158 and 159
Activation energy	No or minimal activation energy required; spontaneous process	High activation energy required; activated adsorption process	158 and 159
Surface specificity	Non-selective; nearly any molecule can physically adsorb to any surface	Highly selective; occurs only with specific adsorbate–adsorbent combinations based on chemical compatibility	155, 158 and 159
Rate-limiting mechanism	Controlled by diffusion of adsorbate on adsorbent surface; particle diffusion-dominated	Controlled by chemical reaction and surface interaction; chemisorption site-dominated	160 and 161
Common hydrogel types	Chitosan, cellulose, starch-based hydrogels (combined physisorption–chemisorption); GO/PEI hydrogels	Chitosan (NH$_3^+$ groups), starch-based (acid-base interactions), PEI (electrostatic), and chitin-based through coordination	156 and 162
Typical pollutants	Organic dyes (MB, CV, CR, MO), VOCs, neutral molecules; some antibiotics and pharmaceuticals	Heavy metal ions (Fe, Pb, Cu, Cd, Ni), anionic dyes, acidic pollutants, and specific organic contaminants	156, 162 and 163
pH dependence	Less pH-sensitive; adsorption relatively uniform across pH ranges	Highly pH-sensitive; adsorption depends critically on pH-dependent surface charge and pollutant protonation state	162 and 163
Pseudo-first-order (PFO) kinetics	Better fits physisorption-dominated processes; R^2 typically 0.85–0.90; k_1 range: 10^{-5}–10^{-2} min^{-1}	Does not typically fit well; lower R^2 values indicate physisorption is not rate-limiting	160, 161 and 164
Pseudo-second-order (PSO) kinetics	Poor fit; lower R^2 correlations	Excellent fit; R^2 typically 0.99+; k_2 range: 0.88×10^{-5} to 3.97×10^{-5} g mg^{-1} min^{-1} (for dyes); predominant model in 89% of hydrogel literature	160, 165 and 166
Intraparticle diffusion model	Often controls the process; linear plots indicate pore diffusion contribution	May contribute, but not rate-limiting; surface reaction dominates over diffusion	160 and 161
Adsorption capacity	Lower to moderate; depends on surface area and weak interaction strength	Higher; ranges 50–400+ mg g^{-1} depending on hydrogel type and pollutant	162 and 167–169
Contact time	Rapid initial adsorption; reaches equilibrium in 30–60 minutes	Slower approach to equilibrium; may require 60–120+ minutes for complete removal	156 and 162
Removal efficiency	Moderate efficiency (60–85%) for non-selective pollutants	High efficiency (80–98%); more selective pollutant removal; COD removal 76–89% reported	157 and 162
Reusability/regeneration	Easily regenerated; multiple adsorption–desorption cycles (5–7+ cycles reported); minimal hydrogel degradation	Difficult to regenerate; chemisorbed species strongly bound; typically 5+ cycles with gradual efficiency loss	162
Mechanistic pathway	Physical transport and surface structure change	Electron transfer, valence force interactions, formation of surface complexes, possible ionic or covalent bonding	155
Common wastewater applications	Air purification, VOC removal, neutral molecular adsorption, initial rapid capture stages	Heavy metal remediation, acidic dye removal, persistent organic pollutant removal, targeted contaminant capture	156, 158 and 163
Thermodynamic character	Negative ΔH (exothermic) with low magnitude; typically $\Delta H = -2$ to -10 kJ mol^{-1}	Negative ΔH (exothermic) with higher magnitude; typically $\Delta H = -20$ to -200 kJ mol; spontaneous and endothermic in some cases	162 and 165
Industrial scale feasibility	High feasibility for bulk gas/vapor treatment; good scalability; lower operating costs	Good for targeted pollutant removal; regeneration challenges increase costs; suitable for specific wastewater streams	156 and 159
Recommended use	Pre-treatment, continuous flow systems, non-polar organic compounds, odor/VOC removal	Main treatment for heavy metals, anionic dyes, persistent pollutants; batch systems or fixed-bed configurations	156 and 163

Raj et al.[148] aimed to provide comprehensive insights into the development of lignin-based hydrogels for wastewater treatment, addressing the challenge of creating sustainable alternatives to petroleum-based plastics for water remediation. They reviewed lignin as the primary renewable aromatic material on Earth, examining its synthesis methods, characteristics, and applications in water treatment, with a focus on structurally cross-linked polymers enriched with hydrophilic functional groups. The optimal findings highlighted lignin's biocompatibility, affordability, eco-friendliness, and biodegradability. They provided a detailed examination of various lignin extraction methods from different raw materials, along with future research prospects for the sustainable elimination of aquatic contaminants.

Cheng et al.[149] aimed to develop high-affinity adsorbents for bisphenol A detection in environmental samples, addressing the challenge of trace detection in complicated matrices due to low affinity and poor selectivity of existing adsorbents. They engineered an N-methacryloyl-L-lysine-NH$_2$ (MLys)-based hydrogel copolymer (HP 17) through structure-based design and screening guided by molecular mechanisms from a focused polymer library. The optimum results achieved high adsorption capacity (349.4 mg g^{-1}) for BPA under a wide pH (3.0–10.0) and ionic strength (0–150 mM) range, with the MSPE–HPLC method showing a wide linear range (2.5–100 ng mL^{-1}), a detection limit of 0.22 ng mL^{-1}, and excellent accuracy (92.6–103.0%).

Zhang et al.[150] aimed to develop efficient and selective removal systems for ciprofloxacin in actual water environments, addressing the challenge of poor treatment efficiency for antibiotic-contaminated wastewater. They synthesized carboxylated COF (TzAm COF) via a "one-step" Schiff base reaction, incorporating multiple functional binding sites, including triazine rings and carboxyl groups. Optimum results achieved a high ciprofloxacin adsorption capacity of 217.86 mg g^{-1}, good thermal and pH stability, strong resistance to ionic interference, and excellent regenerability and selectivity, with monolayer chemisorption confirmed through π–π interactions, electrostatic attraction, hydrogen bonding, and channel adsorption mechanisms.

Chaurasiya et al.[151] aimed to examine efficient, cost-effective, and selective heavy metal ion removal from synthetic and real wastewater, addressing the challenge of developing mesoporous, reusable, and biodegradable materials. They prepared novel starch-functionalized hydrogels (SMHs) via free-radical polymerization with varying concentrations of N, N'-methylenebisacrylamide crosslinker, while maintaining fixed monomer ratios. The optimum results with SMHs-3 hydrogel achieved a swelling ratio of 305.55 g/g, removal percentages of 95.81% for Ni^{2+} and 98.67% for Cu^{2+} at pH 7, adsorption capacities following the Langmuir model of 521.35 mg g^{-1} for Ni^{2+} and 563.30 mg g^{-1} for Cu^{2+}, with desorption efficiencies of 94.24% and 97.15%, respectively.

Verma et al.[152] aimed to explore cellulose-based hydrogel innovations for enhanced wastewater treatment by elucidating comprehensive adsorption mechanisms, addressing the challenge of developing versatile, biodegradable materials with tunable properties for water purification applications. They examined the extraction and modification of cellulose, the functional and structural properties of cellulose derivatives, and synthesis techniques for cellulose-based hydrogels, with a focus on adsorption mechanisms for heavy metals and dyes. The optimal findings revealed exceptional adsorption capacity and reusability under demanding environmental conditions, with a detailed analysis of factors influencing adsorption behavior, including crosslink density, pollutant concentration, pH, temperature, and ionic strength, to support sustainable wastewater remediation solutions.

Al-Hazmi et al.[153] aimed to enhance stability and efficacy in bivalent nickel ion removal by integrating cerium metal–organic framework, addressing the challenge of developing stable composite materials with enhanced structural integrity for water purification. They utilized a Ce-MOF encapsulated within a food-grade algal matrix, integrated into a dual-layer hydrogel containing chitosan and carboxymethyl cellulose, cross-linked with epichlorohydrin. The Box-Behnken design optimization yielded optimal conditions at pH 5, a dosage of 0.02 g per 25 mL solution, and an adsorption capacity of 301.05 mg g^{-1} for Ni(II), following pseudo-second-order kinetics and a Langmuir isotherm model, with significant stability over six successive adsorption–desorption cycles.

Alshangiti et al.[154] aimed to develop a novel semi-permeable membrane for efficient water purification from dyes by incorporating organoclay into a PS/PEVA polymer blend and using γ-radiation to induce crosslinking and in situ polymerization. The main challenge addressed was how to enhance bentonite clay's adsorptive capacity and improve its integration with polymer matrices for practical membrane formation. Through chemical modification with aniline and gamma radiation exposure, the team created a composite membrane that achieved over 99% removal of Toluidine Blue (TB) in just 15 seconds, highlighting its potential for fast, efficient water remediation.

Table 3 highlights the fundamental differences between physisorption and chemisorption mechanisms in hydrogel-based wastewater treatment. Physisorption relies on weak physical interactions, such as van der Waals forces, hydrogen bonding, and π–π interactions, resulting in relatively low bond strength, multilayer adsorption, rapid uptake, and reversible behavior, making it suitable for non-selective pollutant removal, neutral molecules, and rapid pre-treatment applications. In contrast, chemisorption involves stronger chemical interactions, including covalent or ionic bonding, electron exchange, and coordination, which result in higher adsorption capacities, monolayer formation, slower equilibration, and greater selectivity, particularly for heavy metals and acidic dyes. Chemisorption processes are highly dependent on pH, temperature, and the chemical nature of both the hydrogel and the pollutant, whereas physisorption is comparatively less sensitive to environmental conditions. Kinetic modeling reveals these differences: physisorption often fits pseudo-first-order models, whereas chemisorption typically follows pseudo-second-order kinetics, indicating stronger, more specific adsorbate–hydrogel interactions. Overall, the table illustrates that physisorption is advantageous for rapid, reversible, and broad-spectrum pollutant removal. In contrast, chemisorption
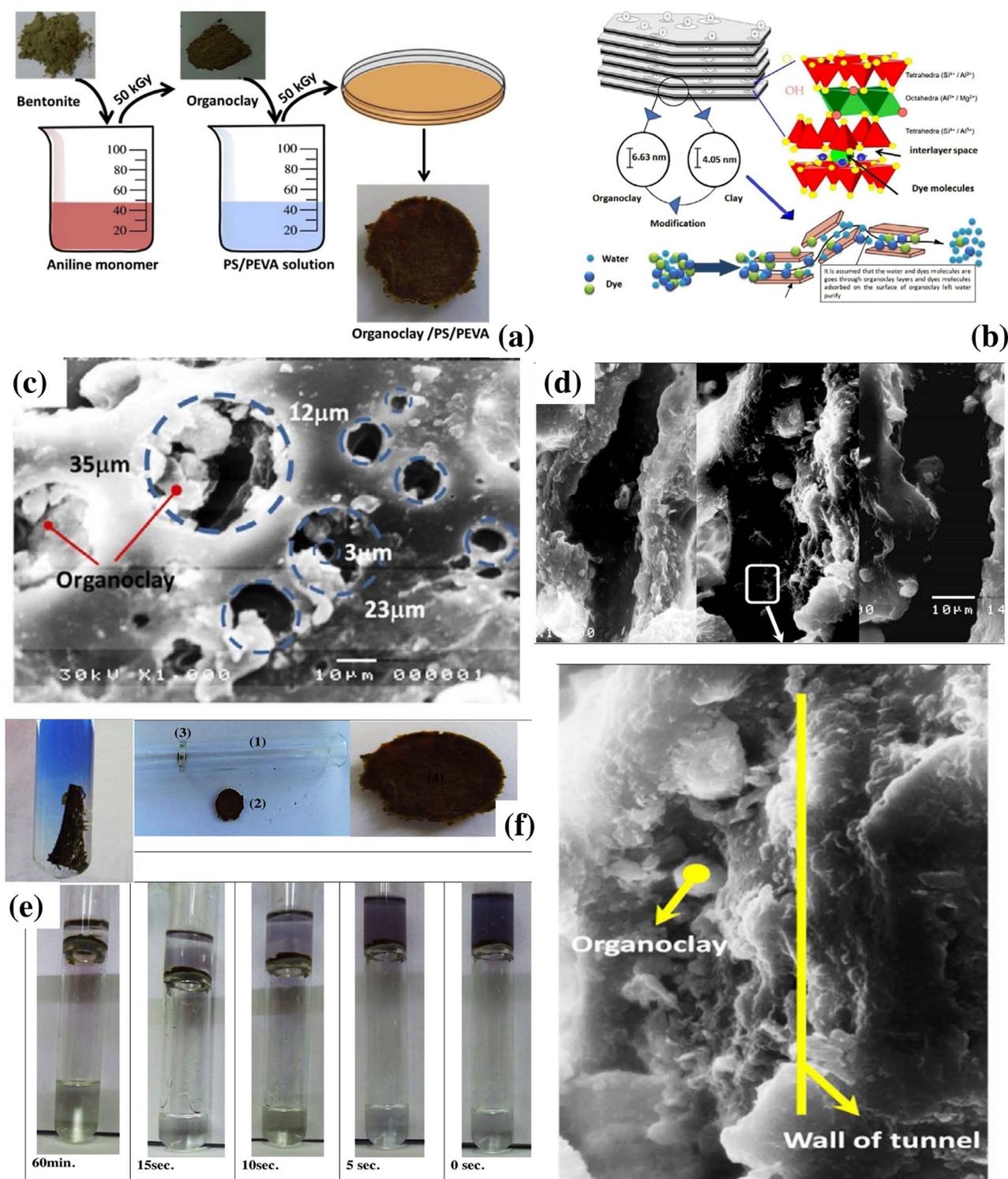
Fig. 7 Fabrication, structural characterization, and dye adsorption performance of γ-irradiated organoclay/PS/PEVA semi-permeable membrane for water purification. (a) Schematic illustration of the membrane preparation process. (b) XRD-based model showing interlayer expansion from 4.05 nm (raw bentonite) to 6.63 nm (organoclay), indicating successful aniline intercalation. (c) SEM image of the membrane surface showing an irregular, interconnected porous structure. (d) Cross-sectional SEM revealing tunnel-like structures within the membrane and strong incorporation of organoclay particles along the polymer walls. (e) Visual confirmation of dye adsorption: a membrane slice placed in a TB dye solution (2×10^{-5} M) without agitation shows a clear concentration gradient, indicating strong passive adsorption. (f) Dialysis performance test: the membrane, positioned in a vertical tube containing TB dye, results in the progressive decolorization of the solution within 60 minutes, confirming the membrane's adsorption efficiency and semi-permeable behavior. Reproduced from ref. 154 with permission from [Elsevier], copyright 2019.

Table 4 Factors influencing hydrogel adsorption mechanisms

Factor	Influence on mechanism	Key considerations	Example systems & outcomes	Ref.
Solution pH	Controls the ionization state of hydrogel functional groups and pollutant speciation; dictates electrostatic interactions	- Low pH: protonation of $-NH_2$ to $-NH_3^+$ enhances cation repulsion but anion attraction - High pH: deprotonation of $-COOH$ to $-COO^-$ increases negative charge density - Pollutant speciation changes (e.g., Cr(vi): $HCrO_4^-$ at pH < 6 vs. CrO_4^{2-} at pH > 6) - Optimal pH maximizes electrostatic attraction between hydrogel and target pollutant	- Chitosan-based hydrogels show maximum Cr(vi) adsorption at pH 2–3 due to electrostatic attraction between $-NH_3^+$ and $HCrO_4^-$ - Alginate hydrogels exhibit enhanced Cu^{2+} removal at pH 5–6 where $-COO^-$ groups are deprotonated - Cationic dye (methylene blue) adsorption peaks at alkaline pH on carboxylated hydrogels	170–172
Hydrogel functionalization	Determines available binding sites and mechanism selectivity; creates multi-mechanistic adsorption platforms	- Amine-rich polymers (PEI, chitosan): chelation and electrostatic attraction for metal cations - Carboxyl-rich polymers (alginate, PAA): ion exchange and coordination with divalent metals - Sulfonate groups: strong cation exchange capacity - Nanomaterial integration (graphene, MOFs, MXenes): adds π–π interactions, Lewis acid–base sites, and coordination centers	- PEI-grafted hydrogels achieve 95% Pb^{2+} removal via chelation with nitrogen donors - $La(OH)_3$-loaded hydrogels show selective phosphate capture (>200 mg g^{-1}) through Lewis acid–base interactions - MOF-embedded hydrogels demonstrate enhanced organic pollutant removal via host–guest interactions - Graphene oxide composites enable simultaneous electrostatic and π–π stacking mechanisms	173–175
Pollutant properties	Dictates mechanism pathway based on chemical hardness/softness, molecular structure, and charge characteristics	- Hard metal ions (Pb^{2+}, Cd^{2+}, Cu^{2+}): prefer oxygen-donor ligands (carboxylates, hydroxyl groups) - Soft metal ions (Hg^{2+}, Ag^+): prefer nitrogen/sulfur-donor ligands (amines, thiols) - Aromatic pollutants: facilitate π–π interactions and hydrophobic interactions - Charged organic molecules: enable electrostatic attraction/repulsion - Size and geometry: affect pore accessibility and steric hindrance	- Pb^{2+} shows stronger binding to carboxylated hydrogels (HSAB principle) with adsorption capacity >400 mg g^{-1} - Hg^{2+} preferentially binds to thiol-functionalized hydrogels via covalent-like coordination - Methylene blue (aromatic dye) adsorption enhanced on graphene–hydrogel composites via π–π stacking - Perfluorinated compounds show hydrophobic partitioning in hydrophobic polymer networks	176–179
Ionic strength	Affects electrostatic shielding and competition for binding sites; influences hydrogel swelling	- High ionic strength: compresses electrical double layer, reduces electrostatic attraction range - Background electrolytes compete for binding sites - Salt concentration affects hydrogel network expansion/contraction - Divalent ions (Ca^{2+}, Mg^{2+}) cause greater interference than monovalent ions	- 50% reduction in Cd^{2+} adsorption when NaCl concentration increases from 0 to 0.1 M - Seawater conditions reduce heavy metal removal efficiency by 30–60% - Alginate hydrogels undergo significant deswelling in high Ca^{2+} environments, reducing accessible sites	180–183

Table 4 (Contd.)

Factor	Influence on mechanism	Key considerations	Example systems & outcomes	Ref.
Temperature	Influences adsorption thermodynamics, polymer chain mobility, and diffusion kinetics	- Endothermic processes: adsorption increases with temperature (chemisorption, some chelation) - Exothermic processes: adsorption decreases with temperature (physisorption, electrostatic attraction) - Higher temperature increases intraparticle diffusion rates - Polymer chain flexibility and pore accessibility improve at elevated temperatures	- Heavy metal adsorption on chitosan hydrogels shows positive ΔH° (15–40 kJ mol^{-1}), indicating endothermic chelation - Dye adsorption often exothermic ($\Delta H^{\circ} = -10$ to -30 kJ mol^{-1}), favored at lower temperatures - Temperature increase from 25 °C to 45 °C enhances Cr(vi) adsorption by 35% on amine-functionalized hydrogels	184 and 185

is ideal for targeted, high-capacity, and selective contaminant remediation in wastewater systems.

Fig. 7a illustrates the step-by-step fabrication of the organoclay-based semi-permeable membrane. Bentonite clay was first modified with aniline monomer (5 mL aniline mixed with 5 g bentonite) and left to interact overnight. After repeated washing, the mixture was irradiated with gamma rays (50 kGy), inducing *in situ* polymerization of aniline and forming organoclay, which visibly changed color from light brown to reddish brown. Separately, polystyrene (PS) and polyethylene vinyl acetate (PEVA) were dissolved in toluene and mixed with 33 wt% organoclay. The composite was again exposed to 50 kGy γ-radiation to enhance compatibility, and the resulting material was cast into Petri dishes to form membranes. Fig. 7b compares bentonite's interlayer spacing before and after modification. XRD analysis revealed that unmodified bentonite exhibited a basal spacing of 4.05 nm, which expanded to 6.63 nm after intercalation with aniline and irradiation an indication of successful formation of organoclay. This expanded spacing facilitates adsorption by increasing surface area and accessibility for dye molecules, making it ideal for pollutant removal applications. Fig. 7c Scanning Electron Microscopy (SEM) of the OC/PS/PEVA membrane shows an irregular pore structure, with pore diameters ranging between 3 and 35 μm. The image shows that the organoclay is well-distributed and embedded within the polymer network. This porous architecture is crucial for semi-permeability, enabling the membrane to perform effective dye adsorption and filtration. In Fig. 7d, the SEM cross-section reveals a tunnel-like membrane structure with irregular, interconnected channels. Organoclay particles are visibly adhered within the polymer matrix, suggesting successful entrapment and mechanical stability. These tunnels remain open, with pore sizes reduced by ~10–80% but not blocked, allowing for continuous diffusion and making the membrane suitable for dialysis or water remediation without clogging. Fig. 7e shows a membrane slice placed into a test tube containing TB dye (2×10^5 M). Without agitation, the dye concentration near the membrane decreased significantly within 10 minutes, confirming strong dye binding. The visible gradient in dye color from the bottom to the top of the solution indicates efficient adsorption and transport into the membrane, even under passive conditions. Fig. 7f represents an experiment that further assesses the membrane's dialysis function. A square piece of membrane was vertically positioned in a tube containing TB dye. Over 60 minutes, the solution became clear, demonstrating that the dye molecules diffused through the membrane and were effectively adsorbed. This validates the membrane's semi-permeable nature and its practical applicability for removing soluble contaminants in continuous or batch systems.

As outlined in Table 3, the adsorption performance of hydrogels for water treatment is strongly influenced by multiple interrelated factors, including solution pH, hydrogel functionalization, pollutant properties, ionic strength, temperature, and contact time. Solution pH governs the ionization of hydrogel functional groups and the speciation of pollutants, thereby modulating electrostatic interactions, as seen with chitosan-based hydrogels for Cr(vi) removal at acidic pH. Hydrogel

functionalization with amine, carboxyl, or sulfonate groups enables selective binding *via* mechanisms such as chelation, ion exchange, and π–π interactions. At the same time, nano-material incorporation enhances adsorption performance by providing additional binding sites. Pollutant properties, including hardness, molecular structure, and charge, dictate the preferred hydrogel interaction pathway, influencing adsorption efficiency. Ionic strength and background electrolytes can shield charges and compete for binding sites, affecting swelling and uptake capacity. Temperature affects both thermodynamics and kinetics: endothermic processes benefit from elevated temperatures, whereas exothermic adsorption favors cooler conditions. Finally, contact time and adsorption kinetics reveal the dominant mechanism, distinguishing between surface adsorption, intraparticle diffusion, and chemisorption. Optimizing these parameters enables the design of high-performance hydrogel systems for the selective and efficient removal of heavy metals, dyes, and organic pollutants from water (Table 4).

4. Polymeric hydrogels for microbial inactivation

Polymeric hydrogels offer several advantages for microbial inactivation applications. Their high-water content and three-dimensional network structure make them excellent platforms for incorporating antimicrobial agents while maintaining biocompatibility. The hydrogel matrix can provide controlled release of active compounds, extended contact time with microorganisms, and mechanical stability. Several mechanisms are commonly employed in these systems. Contact-killing hydrogels incorporate cationic polymers or quaternary ammonium compounds that disrupt microbial cell membranes through electrostatic interactions. Release-based systems gradually release antimicrobial agents, such as silver nanoparticles, antibiotics, or antimicrobial peptides. Some hydrogels generate reactive oxygen species through photodynamic or catalytic processes, while others create unfavorable environments through pH modulation or metal ion chelation.

Standard polymer bases include chitosan, which has inherent antimicrobial properties due to its cationic nature, and polyvinyl alcohol, polyethylene glycol, and alginate, which serve as excellent carriers for antimicrobial additives. Stimuli-responsive hydrogels based on poly(*N*-isopropylacrylamide) or other smart polymers can provide triggered release mechanisms.

These materials have applications in wound dressings, where sustained antimicrobial activity is crucial; in medical device coatings to prevent biofilm formation; in water treatment systems for pathogen removal; and in food packaging to extend shelf life. Hydrogels employ a variety of mechanisms to achieve microbial inactivation, each targeting different aspects of microbial physiology and structural integrity. These mechanisms can be broadly categorized into physical, chemical, and biological pathways. Physically, hydrogels can disrupt microbial membranes by incorporating nanostructures or by applying mechanical stress that compromises cell wall integrity. Chemically, hydrogels can be loaded with antimicrobial agents, such as silver nanoparticles, quaternary ammonium compounds, or reactive oxygen species, which interfere with microbial metabolic processes, induce oxidative stress, or cause DNA damage. Some hydrogels function through pH-sensitive or stimuli-responsive release systems that deliver antimicrobial compounds in a controlled manner at the site of infection. In addition, hydrogels with inherent antimicrobial properties, such as those made from chitosan or cationic polymers, interact electrostatically with the negatively charged membranes of microbes, leading to membrane disruption and leakage of intracellular contents. Biologically, hydrogels may incorporate enzymes or peptides that inhibit microbial growth or degrade essential cellular components. These multifunctional strategies enhance the efficacy of hydrogels in various applications, including wound dressings, drug delivery systems, and implant coatings. The ability to tailor the composition and structure of hydrogels enables the design of materials that not only prevent infection but also promote tissue regeneration, making them highly valuable for biomedical applications.

4.1. Membrane disruption mechanisms

The most prevalent mechanism involves electrostatic interactions between cationic components and negatively charged microbial cell membranes. Cationic polymers such as chitosan, poly(diallyldimethylammonium chloride), and quaternary ammonium-functionalized networks bind to bacterial cell walls and cytoplasmic membranes. This binding disrupts membrane integrity, leading to the leakage of intracellular contents and ultimately resulting in cell death. The effectiveness depends on charge density, molecular weight, and the specific cationic functionality present in the hydrogel matrix.

Guo *et al.*[186] addressed the critical challenge of simultaneously removing various contaminants from water with minimal energy consumption through innovative bacterial cellulose hydrogel (BCH) technology. The researchers developed a dual-format approach by synthesizing ZnO nanoflowers within three-dimensional BCH networks *via in situ* synthesis, creating both aerogel (BCA/ZnO-3) and membrane (BCM/ZnO-3) variants *via* freeze-drying and heat-drying, respectively. The aerogel demonstrated exceptional performance, with a treatment capacity of 773.8 L m^{-2} in injection-driven filtration systems for real contaminated water. In contrast, the membrane variant achieved a flux of 29.19 L m^{-2} h^{-1} at 2.5 bar, along with a treatment capacity of 674 L m^{-2}. Both systems effectively eliminate microorganisms, heavy metals, and organic molecules through combined ultrafiltration and adsorption mechanisms that involve size screening, electrostatic interactions, and hydrogen bonding, and offer environmentally sustainable alternatives to petroleum-based membranes.

Yang *et al.*[187] tackled the significant challenge of detecting low-level human norovirus (HuNoV) contamination in food and environmental samples through innovative hydrogel digital reverse transcription loop-mediated isothermal amplification (HD RT-LAMP) technology. The research team developed an

evaporation-enhanced system that incorporates *in situ* enrichment and interfacial enzymatic reactions to overcome the sensitivity limitations inherent to traditional nucleic acid detection methods. Their optimized approach achieved a remarkable 20-fold increase in sensitivity by strategically concentrating samples *via* evaporation on chamber-array chips, with nanoconfined hydrogel spaces enabling rapid quantification within 15 minutes. The system successfully demonstrated universality across multiple pathogens and incorporated deep learning algorithms with smartphone applications for automated analysis. Testing across diverse real-world samples, including lake water, strawberries, tap water, and drinking water, validated the system's practical applicability for comprehensive food safety monitoring and environmental surveillance programs.

Nyadroh *et al.*[188] addressed the global water scarcity crisis affecting 2.8 billion people by developing innovative microbial desalination cells (MDCs) incorporating 3D-printed bioelectrodes with immobilized electroactive bacteria. The research challenged conventional energy-intensive reverse osmosis methods by integrating wastewater treatment with bioenergy generation, thereby overcoming traditional MDC limitations, including poor anode performance and membrane biofouling. Three distinct bio-ink formulations were investigated: sodium alginate-graphene nanoplatelets (SAGNP), sodium alginate (SA), and gelatin methacrylate (GelMA), each with *Shewanella oneidensis* added for immobilization. The SAGNP bioelectrode achieved superior performance, with desalination rates of 0.84 mS h^{-1} for brackish water and 0.63 mS h^{-1} for artificial seawater, generating a maximum power density of 22 mW m^{-2} while maintaining 84.4% COD removal efficiency. The 33-day fed-batch operation demonstrated significant improvements over conventional membrane distillation cells (MDCs), establishing 3D-printed bioelectrodes as promising, sustainable solutions for energy-efficient water desalination applications.

Fang *et al.*[189] addressed the persistent challenges of insufficient light absorption, suboptimal energy conversion, and microbial contamination in solar-driven interfacial water evaporation systems by developing an innovative Au@ZIF-8/$Ti_3C_2T_x$ nanocomposite. The research integrated gold nanoparticles into three-dimensional alginate hydrogel networks to enhance light-to-heat conversion while establishing Schottky junctions between ZIF-8 and $Ti_3C_2T_x$ to generate reactive oxygen species. This dual-mechanism approach achieved an exceptional antibacterial efficiency of 99.54% against *E. coli* and 97.22% against *S. aureus* through the combined effects of photothermal therapy and photocatalytic ROS production, including superoxide radicals and singlet oxygen. The optimized hydrogel demonstrated an impressive evaporation rate of 1.589 kg m^{-2} h^{-1} and 100% steam sterilization effectiveness under single-sun illumination. These results establish the Au@ZIF-8/$Ti_3C_2T_x$ alginate hydrogel as a cost-effective, efficient sterilization strategy suitable for water purification, desalination, and disinfection applications in off-grid and specialized environments.

Tang *et al.*[190] investigated the application of super adsorbent polymer hydrogels for microalgal biomass concentration and harvesting in open culture systems, addressing contamination challenges from bacteria and non-algal impurities that compromise harvesting efficiency and product quality. The research systematically evaluated poly(sodium acrylate-acrylamide) hydrogels with varying monomer ratios to optimize biomass-harvesting performance under realistic open-system conditions. The optimal formulation (WSA : WAM = 10 : 0) achieved remarkable results, with a 417.9% increase in chlorophyll a concentration, a 3.7% improvement in the Chl-a/VSS ratio, and a 9.5% reduction in extracellular polymeric substances compared to pre-harvest conditions. Mechanistic analysis revealed that hydrogel pore size and structure functioned as molecular sieves, effectively separating microalgal cells from water, bacterial cells, and EPS through differential hydrophilicity interactions. The system demonstrated excellent reusability while simultaneously achieving concentration and purification of microalgal biomass, providing valuable theoretical foundation for sustainable microalgae cultivation and harvesting applications.

Souza *et al.*[191] addressed the economic viability challenges of microbial fuel cells (MFCs) by developing cost-effective, environmentally friendly proton exchange membranes (PEMs) using bacterial nanocellulose/hydroxyapatite hybrid systems. The research focused on developing sustainable alternatives to expensive conventional PEM materials while maintaining efficiency in bioelectricity generation from the biodegradation of organic matter by microorganisms. BNC/HAp hybrid membranes were synthesized *via* biomimetic mineralization using BNC hydrogel scaffolds, and comprehensive characterization by SEM, XRD, FTIR, and TGA confirmed their successful formation. The optimized BNC/HAp membrane achieved a promising power density of approximately 31 mW m^{-2} within 10 days of MFC operation, demonstrating enhanced proton-conductive pathways through HAp integration. While porosity reduction occurred with HAp synthesis, the crystalline calcium phosphate successfully enhanced membrane performance. These results establish BNC/HAp hybrid membranes as economically viable, environmentally sustainable PEM alternatives for advancing MFC technology toward practical bioelectricity generation applications. Chi *et al.*[192] addressed the challenge of extending the shelf life of fresh food by developing polyvinyl alcohol/sodium alginate/*Artemisia sphaerocephala Krasch* gum (PVA/SA/ASKG) hydrogels, which exhibit excellent water-absorption properties for fish fillet preservation. The research incorporated the natural high-molecular-weight polysaccharide ASKG into PVA and SA matrices using a crosslinking approach to create porous network structures *via* esterification and chelation reactions. The addition of ASKG significantly improved the water absorption, retention, porosity, and thermal stability of the hydrogels, with water absorption kinetics following the Schott second-order kinetic model, indicating simple diffusion behavior. The optimized 5P-5S-6A-1C-$0.025Ca^{2+}$ hydrogel formulation exhibited superior mechanical properties and a porous network structure, which depended on the PVA/SA ratios. Applied as a packaging material for

Lateolabrax Japonicus fillets, the hydrogel pad effectively absorbed exudates, maintained fillet cleanliness, inhibited microbial growth and protein oxidation, successfully extending shelf life from 6.8 to 9.1 days.

4.2. Reactive oxygen species generation

Photocatalytic hydrogels incorporate titanium dioxide nanoparticles, zinc oxide, or organic photosensitizers that generate reactive oxygen species (ROS) upon exposure to light. These ROS, including hydroxyl radicals, superoxide anions, and singlet oxygen, cause oxidative damage to microbial DNA, proteins, and lipids. Some hydrogels also employ enzymatic systems, such as glucose oxidase or peroxidase, to continuously generate hydrogen peroxide.

Guo et al.[193] developed anti-bacterial hydrogels incorporating catechol-enabled hydrogen peroxide generators and quinone-anchored activated carbon particles to address the critical challenge of providing safe water access in resource-limited settings where energy-intensive pasteurization is impractical. Their innovative molecular engineering approach achieved remarkable water disinfection efficiency, exceeding 99.999% within 60 minutes, without requiring external energy input, while simultaneously enabling solar-driven vapor generation for sustained water purification. The synergistic bactericidal mechanism, combining hydrogen peroxide and quinone groups, effectively disrupts bacterial cell components and metabolism, producing no harmful byproducts and allowing for easy tablet removal. The dual-functionality hydrogel platform demonstrates exceptional promise for point-of-use water treatment in remote areas and during emergencies, with lower energy and chemical demands than conventional methods.

Wang et al.[194] addressed the urgent problems of antibiotic resistance and biofilm impermeability by engineering kanamycin-sulfate-derived carbon nanodots (KCDs) and integrating them into injectable, self-healing hydrogels to create a novel anti-infection strategy. Their research aimed to overcome the limitations of conventional antibiotic therapy through reactive oxygen species-enhanced biofilm disruption mechanisms. The multifunctional CG-KCDs hydrogel demonstrated superior antibacterial activity under laser irradiation, effectively damaging bacterial biofilms through ROS-dependent pathways while retaining the active structure of kanamycin and generating five new surface-modified components that inhibit key bacterial enzymes. *In vivo* wound infection models confirmed the therapeutic efficacy for wound healing and tissue remodeling, validating the potential of replacing traditional antibiotics with this innovative anti-infective approach that circumvents resistance mechanisms.

Nayak et al.[195] pioneered the development of carbon-dot-crosslinked polyvinylpyrrolidone hybrid hydrogels to address the complex challenge of simultaneously removing organic pollutants and eliminating bacteria from wastewater using a single treatment system. Their research addressed the need for cost-effective, environmentally friendly water treatment solutions that can simultaneously handle multiple contaminants. The innovative hydrogel demonstrated exceptional performance in both cationic and anionic dye adsorption, following pseudo-second-order kinetics. Additionally, sunlight-induced generation of reactive oxygen species from embedded carbon dots enabled concurrent photodegradation and bacterial elimination within 10 minutes. The hybrid material demonstrated remarkable recyclability for up to 4 photocatalytic cycles with simple acid-wash regeneration, offering a sustainable approach to comprehensive wastewater treatment using readily available materials and solar energy activation. Zhuang et al.[196] investigated enhanced antibiotic removal through dual-reaction-center Fenton-like processes in three-dimensional graphene-based hydrogels to address the growing concern of pharmaceutical contamination in aquatic environments. Their study aimed to overcome the limitations of conventional Fenton processes by developing self-generating reactive oxygen species systems that do not require exogenous hydrogen peroxide. The ethylene glycol-promoted α-FeOOH/reduced graphene oxide hydrogels exhibited superior structural properties, including higher porosity, a larger surface area, and stronger Fe–O–C bonds, which enabled enhanced tetracycline degradation through novel π–π interactions coupled with π–Fe interactions. Density functional theory calculations revealed electron-transfer mechanisms from tetracycline nitrogen sites to material iron centers, establishing a highly efficient pollutant-removal method that advances understanding of environmental nanomaterial design and mechanistic pathways for pharmaceutical contamination remediation.

Liu et al.[197] developed bio-inspired redox-cycling antimicrobial films to address the critical need for safe and effective wound dressing materials capable of sustained reactive oxygen species generation for infection prevention. Their research challenged traditional approaches by creating catechol-modified chitosan films that mimic the features of melanin capsules in insect immune responses, thereby providing continuous antimicrobial activity without external intervention. The biomimetic film exhibited remarkable redox activity, catalyzing electron transfer from physiological ascorbate to oxygen, thereby sustaining ROS generation and conferring ascorbate-dependent antimicrobial properties. *In vivo* studies using rat subcutaneous and mouse wound-healing models confirmed bacterial growth inhibition and reduced inflammation. They accelerated wound healing, establishing this innovative approach as a promising solution for localized, sustained antimicrobial protection that potentially enlists ROS-mediated healing mechanisms for comprehensive wound management applications.

4.3. Metal ion-based inactivation

Silver, copper, and zinc ions incorporated into hydrogel networks exhibit broad-spectrum antimicrobial activity. Silver ions interact with sulfur-containing proteins and DNA, disrupting cellular respiration and DNA replication. Copper ions catalyze the formation of reactive oxygen species (ROS) while also binding to essential enzymes. The hydrogel matrix provides

controlled release of these ions, maintaining therapeutic concentrations while minimizing cytotoxicity.

Goswami *et al.*[198] addressed the critical challenge of removing emerging micro-pollutants and pathogenic bacteria from water supplies, which poses significant risks to human health and agricultural applications. The research aimed to develop an effective and affordable water treatment strategy using natural clay minerals enhanced with synthetic components. The authors created a novel fibrous composite by grafting poly(ethylene glycol) (PEG) onto attapulgite clay, followed by *in situ* decoration with green-synthesized silver nanoparticles. This innovative approach provided a high specific surface area and mesoporous structure, enhancing adsorption capabilities. The optimum results demonstrated an exceptional removal efficiency for ciprofloxacin and 17α-ethinylestradiol micro-pollutants, while simultaneously eliminating both Gram-positive *Bacillus subtilis* and Gram-negative *Pseudomonas aeruginosa* bacteria. The composite material demonstrated excellent regeneration capabilities through gentle washing processes, without compromising performance, making it highly suitable for practical water purification applications.

Abd El-Lateef *et al.*[199] tackled the urgent need for effective disinfection systems to eliminate waterborne pathogens in wastewater treatment facilities. The primary challenge was to develop a biocompatible, sustainable material that provides broad-spectrum antimicrobial activity while maintaining environmental safety. The research aimed to develop a multifunctional hydrogel system combining the biocompatibility of carboxymethyl cellulose with the photocatalytic properties of titanium oxide nanoparticles. The authors synthesized TiO_2 NPs *via* hydrolysis and peptization, then incorporated them into a CMC matrix crosslinked with calcium chloride. Optimum results showed remarkable antimicrobial efficacy against diverse pathogens, including *Salmonella typhi*, *E. coli* O157, *Shigella dysenteriae*, *Enterococcus faecalis*, *Bacillus cereus*, and *Candida albicans*, with inhibition zones reaching 29 mm for *S. typhi*. The hydrogel achieved a 2.7-log reduction in microbial counts within 120 minutes and complete pathogen inactivation at a 2× MIC concentration within 180 minutes, demonstrating excellent biofilm inhibition rates of 87.6% against *B. cereus*.

Luo *et al.*[200] confronted the challenge of developing sustainable, eco-friendly silver-based nanocomposites for point-of-use water disinfection while minimizing silver leaching and environmental impact. The research objective was to develop a smart material system that combines effective bactericidal properties, anti-biofouling capabilities, and controlled silver release. The authors developed an innovative approach that utilizes the graft copolymerization of sulfobetaine methacrylate onto chitosan chains, followed by *in situ* immobilization of silver nanoparticles *via* a drop method. This resulted in thermo-responsive CS-g-PSBMA hydrogel beads with temperature-controlled silver release. The optimal results demonstrated an exceptional silver loading capacity of 122.63 mg g^{-1} in the material, with minimal silver leaching of only 0.015% after 14 days of incubation. The temperature-responsive behavior enabled controlled silver release, with maximum concentrations ranging from 33.1 to 52.3 µg L^{-1} at

temperatures of 25–60 °C. The hydrogel beads exhibited outstanding bactericidal efficacy against *Escherichia coli* while maintaining superior anti-biofouling capabilities and excellent reusability, making them highly promising for practical water disinfection applications.

Sboui *et al.*[201] addressed the growing demand for multifunctional biomaterials capable of simultaneously treating wastewater, purifying air, and disinfecting microbes using solar energy. The main challenge was developing a versatile photocatalytic system that could effectively degrade organic pollutants in both liquid and gas phases while exhibiting antimicrobial activity under visible-light irradiation. The research aimed to develop a cellulose-based biocomposite film incorporating $Cu_2O/H_2Ti_3O_7$ heterojunction photocatalysts for comprehensive environmental decontamination. The authors employed a solvothermal method combined with an impregnation-reduction process to synthesize Cu_2O nanoparticles decorated on $H_2Ti_3O_7$ nanosheets, which were then immobilized onto a cellulose paper substrate. The optimal results demonstrated enhanced photocatalytic efficiency for removing aniline from the liquid phase and 1-propanol from the gaseous phase compared to $H_2Ti_3O_7$/CP alone. The synergistic effect between Cu_2O and $H_2Ti_3O_7$ effectively suppressed charge-carrier recombination and enhanced mobility, resulting in excellent visible-light responsiveness. The biocomposite film exhibited remarkable stability across multiple reuse cycles and demonstrated effective antimicrobial activity against *Escherichia coli*, demonstrating its versatility for diverse environmental applications. Fig. 8 presents a comprehensive analysis of the CS/GO/Ag hydrogel-based continuous-flow water disinfection reactor, demonstrating its practical application and optimization for real-world water treatment scenarios. Fig. 8a provides a schematic representation of the CS/GO/Ag hydrogels functioning as a column filter in a continuous-flow disinfection reactor. This user-friendly flow-through assembly features tailored functionality that does not require specialized technical skills for operation, making it accessible for practical water treatment applications. The design emphasizes the simplicity and effectiveness of the hydrogel-based filtration system for continuous water disinfection processes. Fig. 8b illustrates the hydrogel's remarkable capacity to disinfect water, reaching complete exhaustion across multiple runs with three distinct water samples: deionized water, rainwater, and river water. The results demonstrate that the median disinfection capacity was highest in ultrapure water (3800 runs), followed by river water (3500 runs), and rainwater (3400 runs) before reaching complete exhaustion. Despite slight variances in maximum disinfection potential across different water sources, the overall biocidal effectiveness remained consistent, highlighting the strong permeation capacity of the hydrogel network and its ability to preserve immobilized silver nanoparticles from surface oxidation even under environmentally relevant conditions. Fig. 8c presents a mechanistic overview of continuous-flow water disinfection, illustrating how the hydrogel's shielding mechanism facilitates more profound interactions between bacteria and AgNPs as water traverses the porous bed. This optimization of contact area facilitates rapid contact-driven
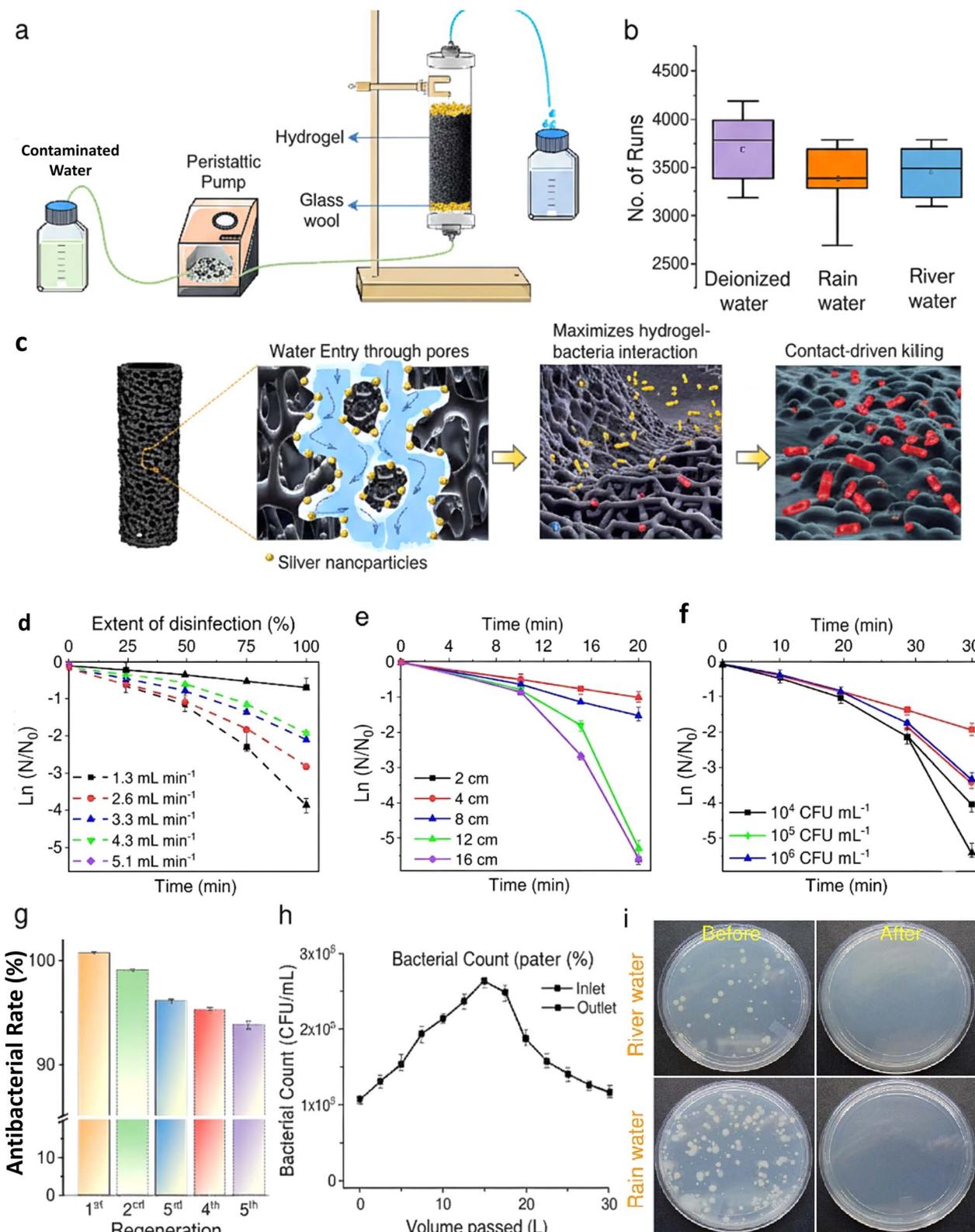
Fig. 8   (a) Schematic representation of CS/GO/Ag hydrogels as a column filter in a continuous-flow disinfection reactor. (b) Hydrogel's capacity to disinfect water until complete exhaustion across multiple runs in distinct water samples: deionized water, rainwater, and river water. (c) A mechanistic overview of continuous-flow water disinfection. Effect of process parameters (d) water flow rate, (e) filter bed height, and (f) initial bacterial load in the inlet on disinfection performance. (g) Reuse potential of the hydrogel-column filter for the number of runs until exhibiting an antibacterial rate of >90%. (h) Column data for the disinfection of *E. coli* contaminated water. (i) Culture plates displaying indigenous micro-flora in natural water samples and their subsequent removal using hydrogel-based reactor operated under optimized conditions (flow-rate 2.6 mL min^{-1}, 8 cm bed height, ~3 min). Adapted from ref. 202 with permission from [Elsevier], copyright 2024.

disinfection responses, even in the presence of ionic species such as chlorides, sulfates, and carbonates commonly found in natural water sources. Fig. 8d illustrates the effect of water flow rate on disinfection performance, showing that antibacterial rates decrease gradually with increasing water flow rates (1.3–5.1 mL min^{-1}). Higher flow rates significantly reduce the hydraulic residence time, thereby reducing the likelihood of direct contact between the hydrogel and contaminated water. Although greater than 99% antibacterial activity could be achieved at both 1.3- and 2.6 mL min^{-1} flow rates, the optimal flow rate of 2.6 mL min^{-1}, with an approximately 3-minute hydraulic residence time, was selected for its balance of efficiency and practical operation considerations. Fig. 8e illustrates the effect of filter bed height on disinfection performance, demonstrating that increased bed height enhances antibacterial rates. The optimization studies revealed that an 8 cm bed height provided optimal disinfection results, striking a balance between effectiveness and practical implementation considerations. Fig. 8f illustrates how the initial bacterial load in the inlet affects disinfection performance, with the system maintaining high efficiency across different initial bacterial concentrations. An initial bacterial count of 10^3 CFU mL^{-1} was determined to be the optimized value for achieving the desired level of disinfection under the experimental conditions. Fig. 8g illustrates the reuse potential of the hydrogel-column filter, showing the number of runs required for the system to exhibit an antibacterial rate of ≥90%. The hydrogel-based reactor yielded excellent results in disinfecting river water during each regeneration cycle, with a freshly installed hydrogel capable of disinfecting approximately 10 L of water without regeneration. The system demonstrated reusability for up to 5 regeneration cycles before its antibacterial activity dropped below the 90% threshold, indicating a practical lifespan and sustainable functionality. Fig. 8h presents column data for the disinfection of *E. coli*-contaminated water, demonstrating the system's capability to handle specific pathogenic bacteria. The data show the hydrogel nanocomposite's resilience against natural resources, exemplified by its ability to disinfect large volumes of rainwater (up to 30 L) with a microbial load of 10^5 CFU mL^{-1} without requiring regeneration. Fig. 8i displays culture plates showing the indigenous microflora in natural water samples and their subsequent removal using the hydrogel-based reactor operated under optimized conditions (flow rate: 2.6 mL min^{-1}, 8 cm bed height, approximately 3 minutes contact time). The chosen samples of river water and rainwater, which encompass diverse microbial communities across vast and complex habitats with varying physicochemical parameters, were sterilized entirely by the CS/

GO/Ag hydrogel filter within 20 minutes, demonstrating complete killing of all natural contaminants and validating the system's effectiveness for real-world water treatment applications.

5. Photothermal hygroscopic hydrogel for water treatment and power generation

Photothermal hygroscopic hydrogels represent a promising class of multifunctional materials capable of simultaneously generating clean water and electricity by integrating solar-driven evaporation with moisture-harvesting and energy-conversion mechanisms. Their unique polymer networks, embedded with photothermal agents, efficiently absorb solar radiation and convert it into localized heat, accelerating water evaporation while minimizing thermal losses. At the same time, the hygroscopic components continuously capture atmospheric moisture, enabling a stable water supply even under low-humidity conditions. When coupled with ion-rich gradients, asymmetric structures, or triboelectric interfaces, these hydrogels can also harvest ambient energy, generating electricity alongside freshwater. The synergy between photothermal conversion, moisture absorption, and energy harvesting positions photothermal hygroscopic hydrogels as innovative platforms for integrated water-energy systems, offering sustainable solutions for off-grid environments and resource-limited regions.

Table 5 presents a comparative overview of six innovative hydrogel systems designed to harvest atmospheric moisture while simultaneously generating electrical power. These materials demonstrate remarkable versatility in converting humidity gradients into usable electricity *via* mechanisms such as ion migration, triboelectric effects, and moisture-induced charge separation. The PA/CNT/PC hydrogel exhibits exceptional durability with 100 operational cycles, though with modest power output (0.36 nW cm^{-2}). In contrast, the H-PSS membrane achieves the highest power density of 13 mW cm^{-2}, representing an approximately 36-million-fold improvement over the PA/CNT/PC system. Operating conditions vary significantly, with relative humidity requirements ranging from 55% to 95%, demonstrating adaptability across diverse environments. The MXene aerogel-based system demonstrates outstanding operational stability (15 days of continuous operation). It operates across the widest humidity range (20–95% RH), making it

Table 5 Hydrogel-based AWH systems for electricity generation

Material	Max power density	Output voltage	Current density	RH (%)	Durability	Ref.
PA/CNT/PC hydrogel	0.36 nW cm^{-2}	∼50 mV	7.2 nA cm^{-2}	90%	100 cycles	203
H-PSS membrane	13 mW cm^{-2}	0.8 V	0.12 mA cm^{-2}	90%	NA	204
Ink PAM-CaCl$_2$ hydrogel	124 mW m^{-2}	241 mV	NA	86%	5 cycles	205
PAAm hydrogel	12.6 nW cm^{-2}	0.22 V	0.3 A	55%	80 h	206
PVA-QC/PVA-LS/PVA hydrogel	73.71 μW cm^{-2}	1.3 V	150 μA cm^{-2}	80%	30 min	207
MXene aerogel-on-organo hydrogel	24.8 μW cm^{-2}	430 mV	1160 μA cm^{-2}	20–95%	15 days	208

particularly suitable for real-world applications in fluctuating climates.

Despite the potential advantages, several challenges must be addressed to realize an efficient hybrid water and energy generation system. First, the design of adsorbent materials that can efficiently capture water from low-humidity air is nontrivial, as conventional desiccants may have limited absorption capacity or slow kinetics of water uptake and release. Moreover, ensuring effective solar-driven desorption for water recovery requires photothermal materials that can efficiently convert solar radiation into heat while minimizing energy loss. Second, coupling water harvesting with thermoelectric power generation introduces additional complexity: the temperature gradient required for electricity production must be maintained without compromising water evaporation. Material stability is also a concern, as repeated absorption and desorption cycles may lead to structural degradation or loss of hygroscopic performance. Additionally, system-level optimization is necessary to balance water productivity, electricity generation, and energy efficiency, particularly under varying environmental conditions such as fluctuating solar intensity and ambient humidity. Overcoming these challenges requires a material design that is low-cost, mechanically robust, highly hygroscopic, and capable of photothermal energy conversion, as well as a system architecture that can synergistically integrate both water harvesting and thermoelectric processes.

To address these challenges, a photothermal hygroscopic hydrogel-based hybrid system was designed and implemented by T. Ren *et al.*[205] The core component of this system is a hydrogel ink composed of polyacrylamide (PAM) and calcium chloride ($CaCl_2$), which combines the high water absorption capacity of $CaCl_2$ with the structural and mechanical properties of a crosslinked polymer network. The hydrogel ink was prepared *via in situ* polymerization using acrylamide as the monomer and ammonium persulfate as the thermal initiator. This preparation method ensures uniform distribution of the hygroscopic component within the polymer network, resulting in high water uptake efficiency and mechanical stability. During daytime operation, the hydrogel absorbs solar energy through its inherent photothermal properties and induces water evaporation from its internal structure, yielding fresh water. Concurrently, the heat generated during evaporation is partially captured and directed to a thermoelectric panel, which produces electricity *via* the Seebeck effect by maintaining a temperature gradient across the panel. At night, when solar radiation is absent, the hydrogel regenerates by adsorbing water vapor from ambient air, enabling continuous, cyclic operation. To understand the underlying physical processes and optimize system performance, a theoretical model was developed to describe heat flow, water desorption kinetics, and thermoelectric generation, enabling the prediction of water and energy outputs under various operational and environmental conditions. The hybrid hydrogel system demonstrates significant performance under controlled experimental conditions. The photothermal hygroscopic hydrogel achieved a water production rate of 0.33 kg m^{-2} h^{-1} at 1 kW m^{-2} solar intensity, a competitive value compared to other atmospheric water-

harvesting systems. In parallel, the residual heat from the evaporation process enabled the thermoelectric panel to generate an additional electrical output of 124 mW m^{-2}, effectively utilizing otherwise wasted thermal energy. The system's performance highlights the synergistic advantage of combining water harvesting with energy recovery: the heat used for evaporation does not merely dissipate but contributes to electricity generation, improving overall energy efficiency. Theoretical modeling results closely align with experimental data, confirming the reliability of the heat flow and thermoelectric generation analyses. Moreover, the hydrogel demonstrated excellent stability over multiple absorption–desorption cycles, with negligible loss in water uptake capacity or photothermal efficiency, indicating suitability for long-term field deployment.

Environmental factors, such as ambient humidity and solar intensity, were found to influence both water and electricity production, with optimal performance observed under moderate humidity and high solar irradiation, conditions characteristic of desert regions. In summary, the proposed photothermal hygroscopic hydrogel-based hybrid system provides a compelling approach for simultaneous freshwater and electrical energy generation in arid environments. By integrating solar-driven water harvesting with thermoelectric power generation, this strategy maximizes solar energy use and addresses the dual challenges of water and energy scarcity. The low-cost PAM-$CaCl_2$ hydrogel, prepared *via in situ* polymerization, offers high water absorption, rapid solar-driven desorption, and mechanical robustness for cyclic operation. Experimental results confirm that the system can produce 0.33 kg m^{-2} h^{-1} of fresh water while simultaneously generating 124 mW m^{-2} of electricity under standard solar illumination. Theoretical modeling supports these findings and provides insights into optimizing system architecture and operational parameters. Overall, this study demonstrates a practical, scalable solution for sustainable water and energy replenishment in regions with abundant solar resources, offering a pathway toward resilient, multifunctional infrastructure for water- and energy-limited environments. Future work may focus on enhancing the hydrogel's photothermal conversion efficiency, expanding its surface area to improve water uptake, and integrating modular designs to enable large-scale deployment in arid or desert landscapes.

The main aim of the work by Mu *et al.*[209] is to design and implement a thermoelectricity–freshwater cogenerator capable of maximizing solar energy utilization while harvesting additional scavenging energy from the environment. By integrating a thermoelectric generator (TEG) with a high-capacity starch-polyacrylamide (S-PAM) hydrogel, this study seeks to enhance both water evaporation rates and thermoelectric performance, creating a hybrid system that efficiently converts solar and environmental energy into dual outputs freshwater and electricity thereby offering a sustainable and multifunctional solution to global water-energy challenges. Despite the promising concept, implementing such a hybrid cogeneration system faces several challenges. First, conventional thermoelectric generators often suffer from low efficiency due to limited temperature differences between the hot and cold sides, which

constrains electricity output. Achieving a sufficient thermal gradient while simultaneously maintaining high evaporation rates for water production is a critical hurdle. Second, the effective utilization of solar energy requires materials with high absorptance and low emissivity to capture as much sunlight as possible while minimizing radiative heat loss. Third, water evaporation itself induces cooling at the cold side, which can inadvertently reduce the thermal gradient if not properly managed. Additionally, conventional hydrogels may experience slow water transport or insufficient heat absorption, limiting their ability to facilitate evaporation and enhance thermoelectric performance simultaneously. Managing conductive heat loss from the system to the surrounding environment or to the bulk water is another challenge, as unmitigated heat transfer can significantly reduce both the net energy gain and the system's efficiency. Addressing these multifaceted challenges requires careful selection of materials, innovative system design to optimize heat transfer, and a mechanism to exploit environmental energy while maintaining continuous and high-performance operation. To overcome these challenges, a hybrid thermoelectricity–freshwater cogenerator was designed based on a TEG coupled with a starch-polyacrylamide (S-PAM) hydrogel. The hot side of the TEG is covered with a commercial $TiNO_x$ blue membrane, selected for its high solar absorptance and low thermal emissivity, serving as the primary solar absorber to maximize energy input. The cold side of the TEG is overlaid with the hydrophilic, porous 3D S-PAM hydrogel, which performs dual functions: it absorbs waste heat from the TEG and facilitates water evaporation. The hydrogel's structure allows it to retain substantial water, enabling continuous heat absorption during evaporation and maintaining a low surface temperature, thereby enhancing the thermal gradient across the TEG. The system further incorporates optimized heat-transfer channels on the cold side, allowing the evaporation surface to drop below ambient temperature and enabling additional net energy harvesting from the environment. To minimize conductive heat loss from the purifier to the bulk water, a rapid water spraying approach is applied, enhancing heat exchange at the hydrogel interface and further boosting electricity generation. This multistage utilization of solar and scavenging energy capturing energy at the hot side, recycling waste heat at the cold side, and harvesting environmental energy forms the core innovation of the system, providing an integrated strategy for simultaneous water and power generation. The hybrid cogenerator demonstrates outstanding performance under controlled experimental conditions, achieving a record evaporation rate of 1.79 kg m^{-2} h^{-1} under one-sun illumination when water spraying is applied for two minutes. This high evaporation rate significantly surpasses those of most previously reported TEG-based cogeneration systems, demonstrating the effectiveness of multistage energy utilization and the superior water-transport capability of the S-PAM hydrogel. Simultaneously, the system achieves a maximum output power density of 11.39 W m^{-2}, which represents a benchmark for TEG-based hybrid cogenerators. The enhanced electricity generation is attributed to several synergistic factors: maintaining a large temperature difference between the hot and cold sides of the TEG, effective heat absorption by the S-PAM hydrogel, and rapid heat exchange enabled by water spraying. By integrating solar energy absorption, waste heat recovery, and environmental energy scavenging, the system maximizes energy utilization at multiple stages, improving overall efficiency. Theoretical modeling and experimental validation confirm that the optimized heat transfer channels, low-emissivity solar absorber, and hydrophilic porous hydrogel network collectively enable high-performance cogeneration, ensuring stable operation over repeated cycles and under varying environmental conditions. In conclusion, the thermoelectricity–freshwater hybrid cogenerator based on a TEG and an S-PAM hydrogel provides a highly efficient, sustainable, and multifunctional solution to address the dual challenges of water scarcity and energy shortages. By leveraging a commercial $TiNO_x$ solar absorber, a hydrophilic porous hydrogel, and an optimized heat-transfer design, the system achieves record evaporation and electricity generation rates, demonstrating the successful integration of solar energy harvesting, waste heat utilization, and environmental energy scavenging. The S-PAM hydrogel plays a critical role in facilitating rapid water evaporation while maintaining a low temperature at the cold side of the TEG, creating a large temperature gradient and enhancing thermoelectric output. The multistage energy utilization strategy maximizes the utilization of solar and ambient energy, establishing a practical blueprint for high-efficiency, decentralized water-energy cogeneration. Overall, this pioneering work highlights the potential for combining thermoelectric and hydrogel-based technologies to create hybrid systems capable of sustainably producing freshwater and electricity, offering a scalable approach suitable for remote, arid, or energy-limited regions. Future developments may focus on further improving the hydrogel's water retention and thermal conductivity, expanding the system's modularity for large-scale deployment, and integrating advanced heat management strategies to achieve even higher efficiency and continuous operation in diverse environmental conditions.

The rapid development of photovoltaic (PV) technology has revolutionized the way solar energy is harnessed, offering a clean, renewable, and environmentally friendly solution to global energy demands. PV panels convert sunlight directly into electricity with high sustainability and minimal environmental footprint. Despite these advantages, the photon-to-electron conversion efficiency (PCE) of PV panels is inherently limited by the residual heat generated during solar absorption. This excess thermal energy not only reduces the electrical efficiency of PV panels but also accelerates material degradation over time, affecting long-term stability. Addressing this challenge requires effective thermal management strategies that can simultaneously enhance energy conversion and maintain stable operation. In this context, the present study aims to design and implement a dual-function device the photovoltaic cooling-water generator (PVC-WG) that achieves two objectives simultaneously: (1) reducing the operating temperature of PV panels to improve electricity output and longevity, and (2) harvesting freshwater from the atmosphere using hygroscopic hydrogels. This integrated approach enables simultaneous utilization of

solar energy for electricity generation, cooling, and water harvesting, offering a multifunctional solution to energy and water challenges in both laboratory and real-world settings. The realization of such a dual-function system presents several key challenges. First, achieving significant cooling of PV panels under high solar intensity without affecting electrical output requires a material or system that efficiently transfers heat away from the panel surface. Traditional cooling methods, such as active water cooling or fans, are energy-intensive and may not be suitable for off-grid applications. Second, atmospheric water harvesting in arid and semi-arid regions is inherently limited by low ambient humidity, necessitating highly hygroscopic materials that can rapidly absorb and release water. Third, integrating a cooling system with water harvesting introduces additional complexity: the heat extracted from PV panels must be sufficient to drive evaporation for water generation while maintaining a stable thermal gradient for optimal PV performance.

Furthermore, the system must demonstrate durability and cyclic reusability, as the hygroscopic hydrogel will undergo repeated absorption–desorption cycles. Environmental variability, such as fluctuating solar intensity, ambient temperature, and humidity, further complicates system optimization, requiring a design that can maintain stable performance under both laboratory and outdoor conditions. To address these challenges, Zhou et al.[210] developed a photovoltaic cooling-water generator (PVC-WG) by combining a standard PV panel with an overlaid hygroscopic hydrogel layer. The hydrogel acts as a passive, evaporative cooling medium that absorbs heat from the PV panel surface, reducing its operating temperature, while simultaneously promoting water evaporation. The hydrogel's hygroscopic nature allows it to absorb water molecules from the atmosphere during nighttime regeneration, ensuring continuous cyclic operation without manual intervention or external water input. The system is designed to maximize thermal contact between the PV panel and the hydrogel, allowing efficient heat transfer for cooling. In laboratory tests, the device was exposed to a solar intensity of 1 kW m^{-2}, enabling controlled evaluation of both cooling performance and freshwater generation. The hydrophilic hydrogel's porosity and water–retention properties were optimized to maximize evaporation rates while maintaining mechanical stability across multiple cycles. In outdoor trials, the system was exposed to natural sunlight and ambient conditions, allowing assessment of practical performance metrics, including temperature reduction, water collection rate, and hydrogel reusability over extended periods. The dual-function design ensures that both PV electricity generation and freshwater production occur synergistically, enhancing overall solar energy utilization.

The PVC-WG system demonstrated excellent performance in both laboratory and real-world environments. In the laboratory, the hydrogel-enabled evaporative cooling reduced the PV panel's operating temperature by up to 8 °C under a solar irradiance of 1 kW m^{-2}, directly enhancing electrical efficiency and reducing thermal stress on the panel. Simultaneously, the hygroscopic hydrogel facilitated a freshwater generation rate of 122.32 g m^{-2} h^{-1}, indicating effective moisture harvesting from the ambient air. The hydrogel also exhibited excellent self-regeneration at night, absorbing atmospheric water molecules and restoring its capacity for subsequent cycles, confirming long-term reusability. Outdoor experiments validated these results under realistic environmental conditions: a maximum cooling effect of 9.2 °C was recorded, accompanied by a stable freshwater generation rate of 98.08 g m^{-2} day^{-1}. These results highlight the robustness and practicality of the system, demonstrating that it can effectively maintain PV panel efficiency while producing freshwater, even under variable temperature, sunlight, and humidity. The combined thermal management and water harvesting functions represent an effective approach to maximizing the utilization of solar energy across multiple applications.

In conclusion, the photovoltaic cooling-water generator (PVC-WG) offers a highly effective, dual-function approach to addressing both energy and water challenges in arid and semi-arid regions. By integrating a hygroscopic hydrogel with a conventional PV panel, the system achieves significant cooling of the PV surface up to 9.2 °C reduction in outdoor conditions improving electrical efficiency and prolonging the operational lifespan of the panels. Simultaneously, the hydrogel enables atmospheric water harvesting, producing freshwater at rates exceeding 98 g m^{-2} day^{-1} under outdoor conditions, with reliable self-regeneration during nighttime cycles. The system's passive, energy-efficient operation eliminates the need for additional cooling infrastructure, making it suitable for off-grid or decentralized applications. Moreover, the multifunctional design leverages the entire spectrum of solar energy, converting it into electricity, heat management, and potable water, thereby improving overall solar energy utilization. This study provides a practical blueprint for integrating renewable energy generation with freshwater production, highlighting the potential of hydrogel-based evaporative cooling as a sustainable, scalable, and environmentally friendly approach. Future improvements may focus on enhancing hydrogel water uptake capacity, optimizing panel-hydrogel thermal coupling, and developing modular designs for large-scale deployment in diverse climatic conditions, further advancing the role of PV-based dual-function systems in sustainable energy and water management.

In the field of solar thermal electricity, achieving both efficient solar energy utilization during the day and continuous power generation throughout the day and night remains a major technical challenge. Conventional photothermal systems are typically limited to daytime operation, as electricity production is largely dependent on solar irradiation. Nighttime operations often require external energy storage, which adds complexity and cost. The multifunctional hybrid system is capable of harvesting solar energy during the day, efficiently utilizing waste heat, and generating electricity continuously at night. This approach combines photothermal power generation, water evaporation, and hygroscopic exothermic electricity generation within a single integrated architecture. By leveraging the synergistic properties of composite hydrogels, thermoelectric generators, and hydrophilic porous foams, the system aims to maximize multi-stage energy utilization while providing sustainable, continuous electricity output during both daytime

and nighttime conditions. Despite the potential of this concept, several technical challenges must be addressed to realize a highly efficient and continuous solar-to-electricity system. First, daytime photothermal electricity generation requires materials that efficiently absorb sunlight and convert it into heat with minimal radiative or conductive losses. Second, the system must effectively utilize the waste heat from the thermoelectric generator to drive additional processes, such as water evaporation, without reducing the temperature gradient required for electricity generation. Third, nighttime operation requires materials capable of hygroscopic energy harvesting, absorbing ambient moisture, and releasing heat to maintain a temperature difference across the thermoelectric generator. Achieving continuous electricity generation while balancing water evaporation, heat transfer, and thermal regulation requires careful integration of materials with complementary properties. Finally, mechanical stability, cyclic durability, and high overall energy efficiency are critical for practical application, particularly when combining hydrogels, porous foams, and thermoelectric devices, all of which can degrade or lose performance under repeated cycling or environmental exposure. To overcome these challenges, Long et al.[211] designed an integrated hybrid system comprising three functional layers: a multifunctional composite hydrogel on top, a thermoelectric generator in the middle, and a hydrophilic porous foam at the bottom. The hydrogel is a crosslinked sodium alginate (SA) network loaded with the photothermal material polypyrrole (PPy) and the hygroscopic salt $CaCl_2$. During the daytime, PPy absorbs sunlight and converts it into heat, increasing the temperature of the hydrogel and the hot side of the thermoelectric generator, thereby driving electricity generation. Simultaneously, waste heat from the thermoelectric generator is transferred to the hydrophilic porous PDMS foam below, promoting water evaporation. This multi-stage energy utilization allows solar energy to be harvested both as electricity and as latent heat for water evaporation. At night, the $CaCl_2$ and SA in the hydrogel absorb moisture from the surrounding air, releasing exothermic heat. This heat generates a temperature gradient across the thermoelectric generator, allowing continuous electricity generation even in the absence of solar input. The porous foam, treated via pore formation and oxygen plasma, enhances water transport and thermal conductivity, ensuring efficient daytime evaporation and improving the system's overall energy efficiency. Laboratory experiments were conducted to evaluate power output, evaporation rate, and system efficiency under controlled environmental conditions, validating performance during both daytime and nighttime conditions. The integrated system demonstrates impressive performance under both daytime and nighttime conditions. During the day, the PPy-loaded hydrogel efficiently converts sunlight into heat, driving the thermoelectric generator to achieve a power output of 141.8 mW m^{-2}. The waste heat from the thermoelectric generator is effectively used to evaporate water from the porous PDMS layer, achieving a water evaporation rate of 1.311 kg m^{-2} h^{-1}. This multi-stage utilization of solar energy results in an overall energy conversion efficiency of approximately 80%, significantly higher than conventional

photothermal or thermoelectric systems alone. At night, the $CaCl_2$ and SA components of the hydrogel absorb atmospheric moisture and release exothermic heat, enabling the thermoelectric generator to produce continuous electricity with a power output of 15.1 mW m^{-2}. The system exhibits stable cyclic performance, with the hydrogel and porous foam maintaining mechanical integrity and functional performance over repeated absorption–desorption and heating–cooling cycles. By combining daytime photothermal conversion, waste heat utilization, and nighttime hygroscopic exothermic electricity generation, the hybrid system provides continuous electricity output and efficient multi-stage energy utilization, demonstrating a versatile and practical solution for sustainable solar thermal energy harvesting. In conclusion, the integrated hybrid system presented in this study provides a highly efficient, multifunctional approach for solar energy utilization and continuous electricity generation. By combining a multifunctional composite hydrogel, a thermoelectric generator, and a hydrophilic porous foam, the system achieves multi-stage energy harvesting: daytime solar-to-electricity conversion via PPy photothermal absorption, waste-heat-driven water evaporation via porous PDMS, and nighttime hygroscopic exothermic electricity generation via $CaCl_2$ and SA. Laboratory experiments confirm that the system achieves a daytime electricity output of 141.8 mW m^{-2}, a water evaporation rate of 1.311 kg m^{-2} h^{-1}, and nighttime electricity generation of 15.1 mW m^{-2}, with an overall energy efficiency of 80%. The design enables continuous day-and-night electricity production while simultaneously utilizing solar energy for secondary processes such as water evaporation, demonstrating the potential for sustainable energy-water cogeneration in off-grid or resource-limited environments. This integrated system represents a promising blueprint for multi-functional solar thermal energy devices, offering both high efficiency and continuous operation. Future work may focus on scaling the system for larger applications, optimizing hydrogel composition to enhance moisture absorption, and further improving thermal management strategies to maximize energy harvesting during both daytime and nighttime conditions across diverse environments.

Duan et al.[212] created a hybrid hydrogel combining black phosphorus nanosheets with polyvinyl alcohol to enhance solar-to-electric energy conversion alongside water evaporation. Their system achieved an evaporation rate of 2.7 kg m^{-2} h^{-1} and generated a voltage of 0.41 V. Key challenges included integrating photothermal components without compromising material stability. The device retained excellent performance across 20 operational cycles, highlighting its durability for sustainable solar-driven evaporation and power generation.

Cheng et al.[213] engineered a layered hydrogel platform with a photothermal top layer and a thermoelectric bottom layer for simultaneous water purification and voltage generation. The top layer rapidly vaporized water at a rate of 2.1 kg m^{-2} h^{-1}. At the same time, the bottom created a thermal gradient, producing 0.2 V. Their integrated design minimized heat loss, thereby improving overall energy conversion efficiency. This dual-mode system efficiently combined water treatment and power harvesting in a compact hydrogel architecture. Zhao

et al.[214] fabricated a nanocomposite hydrogel embedding reduced graphene oxide and PEDOT : PSS to enable simultaneous water evaporation and electrical output. The hydrogel achieved an evaporation rate of 2.8 kg m^{-2} h^{-1} and generated a voltage of 0.37 V. A major challenge was balancing electrical resistance while maintaining high water flux. The hydrogel demonstrated excellent stability for outdoor applications, proving its potential for efficient solar–thermal–electrical integrated systems.

Zhang et al.[215] designed a Janus hydrogel combining photothermal Fe_3O_4 nanoparticles with an ionic gel base to achieve synergistic water evaporation and power generation. The hydrogel exhibited an evaporation rate of 2.9 kg m^{-2} h^{-1} and generated a voltage of 0.29 V. The primary difficulty was maintaining the interfacial integrity during prolonged exposure to sunlight and moisture. Despite this, the system maintained

consistent dual functionality for over 25 hours, demonstrating strong durability and energy-conversion performance. He et al.[216] introduced a hybrid polymer hydrogel infused with bismuth oxychloride nanosheets to enhance photothermal conversion and ionic conduction. Their system showed a water evaporation rate of 2.6 kg m^{-2} h^{-1} and an output voltage of 0.35 V. The hydrogel maintained stable operation over 10 cycles and demonstrated sufficient flexibility for wearable, adaptable energy-water devices. The design strikes a balance between efficient solar absorption and sustained ionic mobility.

Cao et al.[217] prepared a soft, conductive hydrogel composed of MXene and polyacrylamide for high-output simultaneous solar evaporation and power generation. Their hydrogel achieved an evaporation rate of 3.05 kg m^{-2} h^{-1} and an electrical output of 0.44 V. The primary challenge was mechanical fatigue resulting from repeated thermal cycling; however, the hydrogel
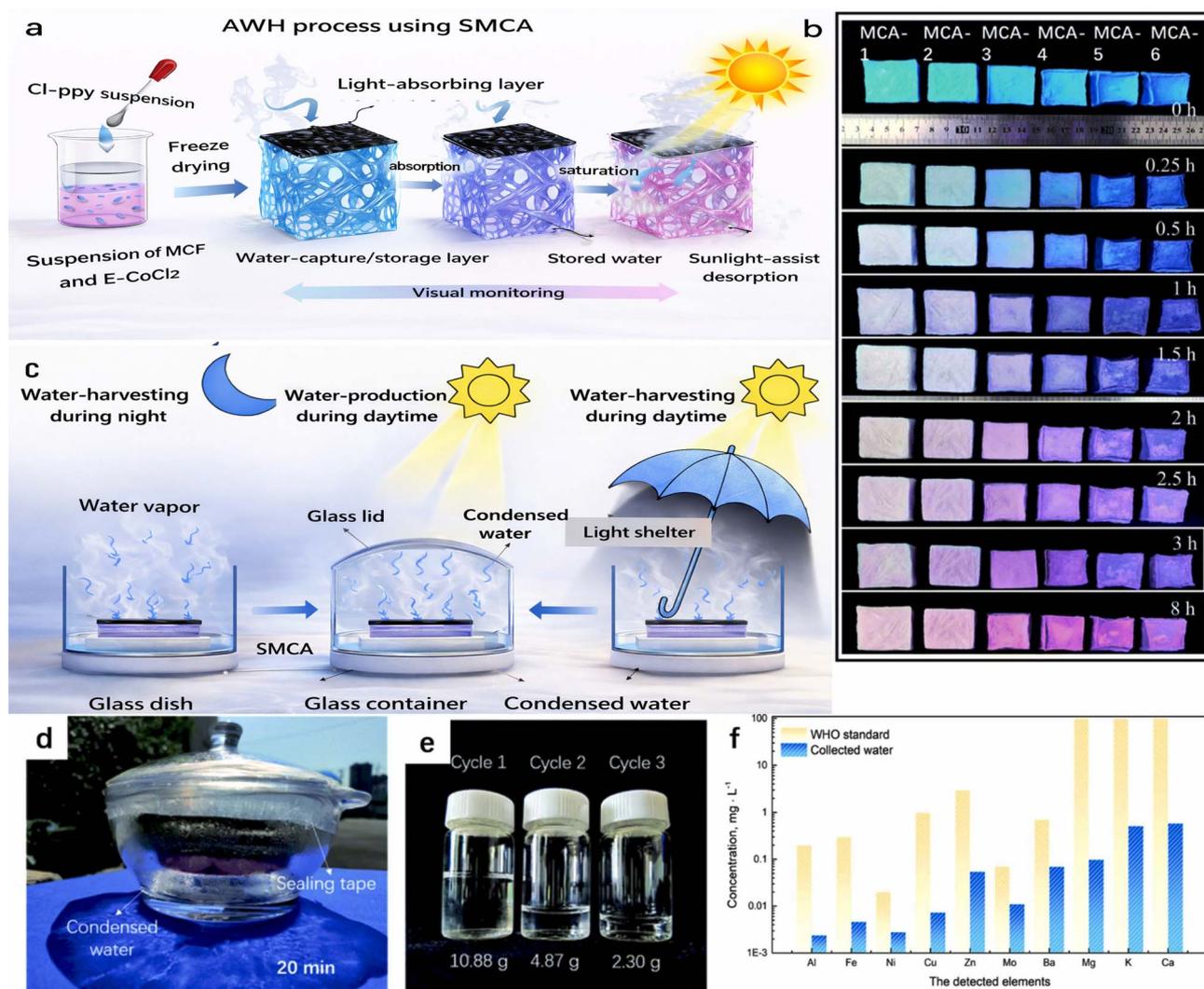

Fig. 9 (a) Preparation schematic of the solar-driven cellulose aerogel (SMCA) and its application in atmospheric water harvesting (AWH). (b) Photographs showing the moisture-induced color change of $CoCl_2$-doped aerogel (MCA-x) from blue (dry) to pink (wet) at 65% RH. (c) Schematic illustration of the AWH device's three operational modes: night-time water harvesting, daytime solar-driven water production with a glass lid, and daytime harvesting with the lid removed. (d) Photograph of the AWH device collecting water during the day. (e) Accumulated water collected over three cycles in one day (2.81 kg water/kg sorbent). (f) Quality assessment of harvested water meeting World Health Organization (WHO) drinking standards. Reproduced from ref. 220 with permission from [Elsevier], copyright 2023.

remained mechanically robust during 12 hours of continuous operation, underscoring its suitability for durable solar energy systems. Yang et al.[218] developed a high-transparency hydrogel embedding silver nanowires and ionic salts to optimize light transmission and voltage generation. The design delivered 1.9 kg m^{-2} h^{-1} water evaporation and 0.21 V output voltage. The primary challenge was to prevent silver nanowire oxidation while maintaining both transparency and conductivity. The system successfully endured 10 sun exposure cycles, demonstrating promising stability for transparent, multifunctional solar-harvesting hydrogels.

Gomes et al.[219] created a carbon nanodot-doped hydrogel blended with ionic liquids to optimize water evaporation and energy conversion. Their hydrogel exhibited a water evaporation rate of 2.75 kg m^{-2} h^{-1} and generated 0.36 V. The design optimized ionic conductivity by balancing ion mobility and water content, achieving repeatable performance over 10 cycles. This balanced dual-function system enhances efficiency for both water purification and power generation.

Fig. 9 illustrates an innovative solar-driven cellulose aerogel (SMCA) designed for atmospheric water harvesting (AWH). Fig. 9a illustrates the preparation of the solar-driven cellulose aerogel (SMCA), which integrates a moisture-sensitive indicator within its structure. The diagram shows the doping of cellulose aerogel with cobalt chloride (CoCl$_2$), which imparts moisture-responsive color change properties. The schematic also depicts the application of SMCA in an atmospheric water harvesting (AWH) system, highlighting how the aerogel captures moisture from ambient air and releases it when irradiated by sunlight. This design utilizes solar energy to drive desorption, while the moisture indicator enables real-time monitoring of water uptake, facilitating more efficient, cyclic water harvesting. Fig. 9b presents a series of photographs demonstrating the moisture-dependent color transition of the CoCl$_2$-doped aerogel (MCA-x). In dry conditions, the aerogel appears blue, indicating its dehydrated state. Upon exposure to moisture at 65% relative humidity, it absorbs water and turns pink. This visible color change is crucial for practical applications, as it allows users to visually monitor moisture content and know precisely when the aerogel is saturated or sufficiently dry for desorption. This real-time indication enhances the operational efficiency of AWH devices.

Fig. 9c explains the three operational modes of the AWH device using the SMCA aerogel. At night, the device operates in water-harvesting mode, capturing atmospheric moisture when humidity levels are higher. During the daytime, the water production mode is activated by covering the container with a glass lid, allowing solar irradiation to heat the aerogel and desorb absorbed water. Finally, the glass lid is removed for daytime water harvesting, protecting the aerogel from direct sunlight and enabling continuous moisture capture. This cycle maximizes water yield and reduces the time required for absorption and desorption. Fig. 9d features a digital photograph of the real AWH device in operation during daytime water collection. The photo shows the device setup, including the aerogel housed in the container and the transparent glass lid that enables solar-driven water desorption. The practical demonstration confirms the system's feasibility outside the laboratory and under natural sunlight. The device's compact design and integration of the moisture-indicating aerogel support rapid cycling, enabling multiple absorption/desorption cycles per day and improving total water output from atmospheric moisture. Fig. 9e illustrates the accumulated volume of liquid water produced from three complete absorption/desorption cycles of the SMCA-based AWH device during one day. Impressively, the system achieved a total water yield of 2.81 kg per kilogram of sorbent. The fast-cycling capability completing three cycles in just nine hours demonstrates a significant improvement over traditional AWH systems that rely on longer, fixed-duration cycles. This high throughput underscores the device's potential for practical applications in water-scarce regions, where rapid, repeated atmospheric moisture harvesting is essential. Fig. 9f evaluates the quality of the water collected by the AWH device, showing that it meets the World Health Organization (WHO) standards for safe drinking water. The analysis includes tests for key parameters such as pH, turbidity, and contaminant levels, confirming that the harvested water is potable. This is a critical validation for real-world use, ensuring the water produced by the moisture-responsive SMCA aerogel system is not only abundant but also safe for human consumption. The combination of high yield and water quality underscores the system's promise as a sustainable solution for clean water access.

6. Conclusion

Functionalized adsorbent hydrogels are emerging as a groundbreaking class of materials poised to address critical global issues of water pollution and freshwater scarcity. Their intrinsic properties such as high water content, porosity, large surface area, and the ability to be chemically tailored with specific functional groups, make them exceptionally suited for the selective removal of a broad spectrum of waterborne contaminants, including heavy metals, organic dyes, pharmaceutical residues, and microbial pathogens. The incorporation of nanomaterials (e.g., graphene oxide, metal–organic frameworks, and magnetic nanoparticles) into hydrogel matrices has significantly amplified their adsorption efficiency, selectivity, and responsiveness to environmental stimuli, such as pH, temperature, and light. In particular, recent advancements in hydrogel synthesis strategies such as click chemistry, ionotropic gelation, and radiation-induced polymerization have provided enhanced control over network architecture and functionalization density, resulting in robust, reusable, and high-capacity adsorbents. Beyond traditional water purification, novel applications such as solar-assisted water remediation, hydrogel-based atmospheric water harvesting, and point-of-use filtration systems are expanding the boundaries of hydrogel functionality toward sustainable and decentralized water treatment solutions. These innovative approaches harness ambient energy and environmental moisture, offering low-energy, scalable solutions for communities without access to centralized water infrastructure. Despite these advantages, significant challenges persist. Scalability remains a barrier due to the high cost of raw

materials, complex synthesis processes, and batch-to-batch variability in hydrogel properties. Long-term environmental impacts, such as degradation byproducts and material stability under prolonged use, also raise concerns regarding ecological safety. Furthermore, integration into existing water treatment systems demands hydrogels that exhibit mechanical resilience, antifouling properties, and cost-effectiveness under real-world operating conditions. Addressing these challenges requires interdisciplinary efforts that span materials science, environmental engineering, polymer chemistry, and public policy. Future research must focus on developing eco-friendly, biodegradable hydrogel components, leveraging green synthesis methods, and exploring modular design strategies for multifunctional and regenerative systems. The integration of real-time sensing, self-healing, and responsive release mechanisms could further extend the utility of hydrogels into smart water purification platforms. Additionally, future research on functionalized adsorbent hydrogels is expected to move toward fully biodegradable, environmentally benign hydrogel systems that minimize secondary pollution and offer closed-loop life-cycle sustainability. Another promising direction is the design of hybrid hydrogel architectures coupled with advanced oxidation processes (AOPs), including photocatalysis, Fenton-like reactions, persulfate activation, and plasma-activated water, which can enable simultaneous adsorption and catalytic degradation of persistent organic pollutants. The emergence of multifunctional hydrogels integrating photothermal conversion, solar-driven evaporation, antimicrobial action, and energy harvesting will further expand their applicability for off-grid water purification. At the microstructural level, nano-reinforced and micro-patterned hydrogels offer opportunities for tunable mass transport, selective adsorption, and enhanced mechanical stability. Interdisciplinary approaches combining polymer science, green chemistry, biotechnology, computational modeling, and machine learning will accelerate the rational design of next-generation hydrogels with predictable performance. Additionally, integrating hydrogels with microfluidic devices, membrane technologies, and real-time sensor platforms presents a pathway toward smart, adaptive water treatment systems. These future directions emphasize the importance of designing hydrogels that are not only highly efficient but also scalable, renewable, and compatible with future circular-economy water-treatment infrastructure.

Conflicts of interest

The authors declare that they have no conflicts of interest.

List of abbreviations

BCA	Bacterial Cellulose Aerogel
BCH	Bacterial Cellulose Hydrogel
BNC	Bacterial Nanocellulose
CMC	Carboxymethyl Cellulose
CP	Conductive Polymer
CPH	Cationic Photothermal Hydrogel
CS	Chitosan
CuS	Copper Sulfide
DA	Diels–Alder
DLP	Digital Light Processing
EPS	Extracellular Polymeric Substances
FTIR	Fourier Transform Infrared Spectroscopy
GO	Graphene Oxide
HD RT-LAMP	Hydrogel Digital Reverse Transcription Loop-Mediated Isothermal Amplification
HRP	Horseradish Peroxidase
ISVG	Interfacial Solar Vapor Generation
METAC	[2-(Methacryloyloxy)ethyl] Trimethylammonium Chloride
MDC	Microbial Desalination Cell
MoS_2	Molybdenum Disulfide
MXene	2D Transition Metal Carbide/Nitride (e.g., $Ti_3C_2T_x$)
PAA	Poly(acrylic acid)
PAM	Polyacrylamide
PAMAM	Poly(amidoamine)
PAMPS	Poly(2-acrylamido-2-methylpropane sulfonic acid)
PBAT	Poly(butylene adipate-co-terephthalate)
PCL	Polycaprolactone
PEG	Polyethylene Glycol
PEGDA	Poly(ethylene glycol) Diacrylate
PEM	Proton Exchange Membrane
PETMP	Pentaerythritol Tetrathiol
PSS	Poly(styrene sulfonate)
PPy	Polypyrrole
PVDF	Polyvinylidene Fluoride
PVA	Polyvinyl Alcohol
RAFT	Reversible Addition-Fragmentation Chain-Transfer Polymerization
rGO	Reduced Graphene Oxide
SA	Sodium Alginate
SAGNP	Sodium Alginate-Graphene Nanoplatelet
SEM	Scanning Electron Microscopy
SMCA	Silica-Modified $CoCl_2$ Aerogel
S-PAM	Sulfonated Polyacrylamide
UV	Ultraviolet
ZnO	Zinc Oxide

Data availability

No primary research results, software or code have been included and no new data were generated or analysed as part of this research article.

Acknowledgements

References

1 A. Mishra and D. W. Tushaus, in *Legal Analytics*, Chapman and Hall/CRC, 2022, pp. 105–116.

2 S. E. Haque, in *Current Directions in Water Scarcity Research*, Elsevier, 2022, vol. 6, pp. 21–43.

3 A. Saravanan, P. S. Kumar, S. Jeevanantham, S. Karishma, B. Tajsabreen, P. Yaashikaa and B. Reshma, *Chemosphere*, 2021, **280**, 130595.

4 G. Muhammad, M. M. Iqbal, M. Shahid, R. S. Ashraf, M. Altaf, M. A. Hussain and M. A. Raza, *Green Sustainable Process Chem. Environ. Eng. Sci.*, 2023, 69–112.

5 S. Bashir, M. Hina, J. Iqbal, A. Rajpar, M. Mujtaba, N. Alghamdi, S. Wageh, K. Ramesh and S. Ramesh, *Polymers*, 2020, **12**, 2702.

6 N. Kumar, R. Gusain, S. Pandey and S. S. Ray, *Adv. Mater. Interfaces*, 2023, **10**, 2201375.

7 L. Lin, W. Wang, D. Li, S. Xu, Y. Sun, L. Li, K. Fan, C. Xing, L. Zhang and J. Li, *Chem. Eng. J.*, 2023, **478**, 147249.

8 V. Van Tran, V.-D. Phung and H. H. Do, *Chem. Eng. J.*, 2024, 150324.

9 C. Zhao, Z. Chen, R. Shi, X. Yang and T. Zhang, *Adv. Mater.*, 2020, **32**, 1907296.

10 J. Rosiak, I. Janik, S. Kadlubowski, M. Kozicki, P. Kujawa, P. Stasica and P. Ulanski, *Nucl. Instrum. Methods Phys. Res., Sect. B*, 2003, **208**, 325–330.

11 K. He, J. Qu and Y. Cao, *Polym. Rev.*, 2025, 1–31.

12 R. Galante, T. J. Pinto, R. Colaco and A. P. Serro, *J. Biomed. Mater. Res., Part B*, 2018, **106**, 2472–2492.

13 J. M. Rosiak, *J. Controlled Release*, 1994, **31**, 9–19.

14 S. N. Haque, M. M. Bhuyan and J.-H. Jeong, *Gels*, 2024, **10**, 375.

15 I. Călina, M. Demeter, A. Scărișoreanu, V. Sătulu and B. Mitu, *Int. J. Mol. Sci.*, 2020, **21**, 9236.

16 M. M. Bhuyan and J.-H. Jeong, *Gels*, 2023, **9**, 159.

17 P. Y. Takinami, N. L. d. Mastro, A. Ashfaq and M. Al-Sheikhly, *Polymers*, 2023, **15**, 4128.

18 H. Jiang, X. Wang, C. Li, D. Gu, T. Jiang, C. Nie, D. Yuan, H. Wu and B. Wang, *Renewable Energy*, 2021, **176**, 388–401.

19 M. Ahmaruzzaman, P. Roy, A. Bonilla-Petriciolet, M. Badawi, S. V. Ganachari, N. P. Shetti and T. M. Aminabhavi, *Chemosphere*, 2023, **331**, 138743.

20 K. Patra, S. Dey, C. Solanki, A. Sengupta and V. K. Mittal, *ACS Appl. Eng. Mater.*, 2025, **3**, 1130–1165.

21 B. Fadeel, C. Bussy, S. Merino, E. Vázquez, E. Flahaut, F. Mouchet, L. Evariste, L. Gauthier, A. J. Koivisto and U. Vogel, *ACS Nano*, 2018, **12**, 10582–10620.

22 Z. Mao, Y. Yao, Y. He, Z. Yu, Y. Han, J. Shen, X. Tang, F. Lyu, M. Miao and Y. Xu, *Adv. Mater.*, 2025, e05002.

23 L. Alsaka, L. Alsaka, A. Altaee, S. J. Zaidi, J. Zhou and T. Kazwini, *Separations*, 2025, **12**, 51.

24 M. Chelu, A. M. Musuc, M. Popa and J. M. Calderon Moreno, *Gels*, 2023, **9**, 664.

25 L. Weerasundara, B. Gabriele, A. Figoli, Y.-S. Ok and J. Bundschuh, *Crit. Rev. Environ. Sci. Technol.*, 2021, **51**, 1970–2014.

26 M. F. Akhtar, M. Hanif and N. M. Ranjha, *Saudi Pharm. J.*, 2016, **24**, 554–559.

27 F. Ali, I. Khan, J. Chen, K. Akhtar, E. M. Bakhsh and S. B. Khan, *Gels*, 2022, **8**, 205.

28 M. S. Ahmed, M. Islam, M. K. Hasan and K.-W. Nam, *Gels*, 2024, **10**, 381.

29 G. Irmukhametova, D. Kazybayeva, G. Mun and V. Khutoryanskiy, in *Hydrogels in Drug Delivery*, Elsevier, 2025, pp. 1–37.

30 A. Pattnaik, P. Ghosh and A. K. Poonia, *J. Mol. Liq.*, 2025, 127120.

31 N. A. Peppas, P. Bures, W. Leobandung and H. Ichikawa, *Eur. J. Pharm. Biopharm.*, 2000, **50**, 27–46.

32 E. Caló and V. V. Khutoryanskiy, *Eur. Polym. J.*, 2015, **65**, 252–267.

33 E. M. Ahmed, *J. Adv. Res.*, 2015, **6**, 105–121.

34 D. Seliktar, *Science*, 2012, **336**, 1124–1128.

35 D. P. Nair, M. Podgorski, S. Chatani, T. Gong, W. Xi, C. R. Fenoli and C. N. Bowman, *Chem. Mater.*, 2014, **26**, 724–744.

36 W. Tomal and J. Ortyl, *Polymers*, 2020, **12**, 1073.

37 K. T. Nguyen and J. L. West, *Biomaterials*, 2002, **23**, 4307–4314.

38 X. Wang and Q. Wang, *Acc. Chem. Res.*, 2021, **54**, 1274–1287.

39 J. Shen, W. Jiao, Z. Chen, C. Wang, X. Song, L. Ma, Z. Tang, W. Yan, H. Xie and B. Yuan, *Carbohydr. Polym.*, 2023, **316**, 121024.

40 C. E. Hoyle and C. N. Bowman, *Angew. Chem., Int. Ed.*, 2010, **49**, 1540–1573.

41 M. Kamaci, *Eur. Polym. J.*, 2020, **123**, 109444.

42 A. C. Madl and D. Myung, *Gels*, 2021, **7**, 163.

43 J.-Y. Sun, X. Zhao, W. R. Illeperuma, O. Chaudhuri, K. H. Oh, D. J. Mooney, J. J. Vlassak and Z. Suo, *Nature*, 2012, **489**, 133–136.

44 R. Barbucci, B. Zavan, R. Cortivo and G. Abatangelo, *Hydrogels: Biological Properties and Applications*, 2009, pp. 1–8.

45 K. Li, D. Fong, E. Meichsner and A. Adronov, *Chem.–Eur. J.*, 2021, **27**, 5057–5073.

46 D. A. Ossipov and J. Hilborn, *Macromolecules*, 2006, **39**, 1709–1718.

47 C.-C. Lin and K. S. Anseth, *Pharm. Res.*, 2009, **26**, 631–643.

48 B. D. Fairbanks, S. P. Singh, C. N. Bowman and K. S. Anseth, *Macromolecules*, 2011, **44**, 2444–2450.

49 C. A. DeForest and K. S. Anseth, *Nat. Chem.*, 2011, **3**, 925–931.

50 M. Podgórski, S. Chatani and C. N. Bowman, *Macromol. Rapid Commun.*, 2014, **35**, 1497–1502.

51 K. Yue, G. Trujillo-de Santiago, M. M. Alvarez, A. Tamayol, N. Annabi and A. Khademhosseini, *Biomaterials*, 2015, **73**, 254–271.

52 Y. Wang, N. Han, X.-L. Li, R.-Z. Wang and L.-B. Xing, *ACS Appl. Mater. Interfaces*, 2022, **14**, 45734–45741.

53 V. Castro, H. Rodríguez and F. Albericio, *ACS Comb. Sci.*, 2016, **18**, 1–14.

54 A. B. Lowe, *Polym. Chem.*, 2014, **5**, 4820–4870.

55 F. Orozco, J. Li, U. Ezekiel, Z. Niyazov, L. Floyd, G. M. R. Lima, J. G. M. Winkelman, I. Moreno-Villoslada, F. Picchioni and R. K. Bose, *Eur. Polym. J.*, 2020, **135**, 109882.

56 A. R. Sayed, O. D. McNair and J. S. Wiggins, in *High Performance Plant Phenol-Based Polymers*, Elsevier, 2024, pp. 95–133.

57 O. Türünç, M. Firdaus, G. Klein and M. A. R. Meier, *Green Chem.*, 2012, **14**, 2577–2583.

58 J.-M. Noy, Y. Li, W. Smolan and P. J. Roth, *Macromolecules*, 2019, **52**, 3083–3091.

59 L. A. Pérez, R. Hernández, J. M. Alonso, R. Pérez-González and V. Sáez-Martínez, *Biomedicines*, 2021, **9**, 1113.

60 A. Dömling and I. Ugi, *Angew. Chem., Int. Ed.*, 2000, **39**, 3168–3210.

61 E. Hui, J. L. Sumey and S. R. Caliari, *Mol. Syst. Des. Eng.*, 2021, **6**, 670–707.

62 A. Sehlinger and M. A. R. Meier, *Multi-component and Sequential Reactions in Polymer Synthesis*, 2015, pp. 61–86.

63 R. Yang, W. Li, R. Mo and X. Zhang, *ACS Appl. Polym. Mater.*, 2023, **5**, 2553–2561.

64 S. Luleburgaz, E. Cakmakci, H. Durmaz and U. Tunca, *Eur. Polym. J.*, 2024, 112897.

65 B. Liu, M. Ianosi-Irimie and S. Thayumanavan, *ACS Nano*, 2019, **13**, 9408–9420.

66 A. Khan, *Chem. Commun.*, 2023, **59**, 11028–11044.

67 Y. Kim, Y. Hu, J.-p. Jeong and S. Jung, *Carbohydr. Polym.*, 2022, **284**, 119195.

68 F. Li, J. Li, X. Song, T. Sun, L. Mi, J. Liu, X. Xia, N. Bai and X. Li, *Int. J. Nanomed.*, 2022, **17**, 6561.

69 G. Deng, F. Li, H. Yu, F. Liu, C. Liu, W. Sun, H. Jiang and Y. Chen, *ACS Macro Lett.*, 2012, **1**, 275–279.

70 Y. Zhao, R. Li, Y. Liu, L. Song, Z. Gao, Z. Li, X. Peng and P. Wang, *Int. J. Biol. Macromol.*, 2023, **250**, 126282.

71 X. Chen, Y. Li, Y.-L. Qiu, G.-L. Zhang, H. Hao, H.-M. Hou and J. Bi, *Food Chem.*, 2023, **428**, 136775.

72 M. Zhang, Q. Ye, Z. Zhu, S. Shi, C. Xu, R. Xie and Y. Li, *Gels*, 2024, **10**, 703.

73 X. Liu, C. Wang, X. Wang, C. Tian, Y. Shen and M. Zhu, *Mater. Sci. Eng., C*, 2021, **118**, 111455.

74 Y. Zhong, Y. Yu, Y. Peng, Z. Su, Y. Mao, Y. Chen, L. Wang, M. Xin and M. Li, *Int. J. Biol. Macromol.*, 2025, **316**, 144478.

75 S. Liu, N. Jiang, Y. Chi, Q. Peng, G. Dai, L. Qian, K. Xu, W. Zhong and W. Yue, *ACS Biomater. Sci. Eng.*, 2022, **8**, 3754–3764.

76 R. Yang, W. Xue, H. Liao, F. Wu, H. Guo, W. Zhang, P. Wang, X. Tan, H. Xu and B. Chi, *Int. J. Biol. Macromol.*, 2022, **223**, 950–960.

77 M. Ehrbar, S. C. Rizzi, R. Hlushchuk, V. Djonov, A. H. Zisch, J. A. Hubbell, F. E. Weber and M. P. Lutolf, *Biomaterials*, 2007, **28**, 3856–3866.

78 C. W. Yung, L. Q. Wu, J. A. Tullman, G. F. Payne, W. E. Bentley and T. A. Barbari, *J. Biomed. Mater. Res., Part A*, 2007, **83**, 1039–1046.

79 M. Farokhi, M. Aleemardani, A. Solouk, H. Mirzadeh, A. H. Teuschl and H. Redl, *Biomed. Mater.*, 2021, **16**, 022004.

80 S. Sakai, T. Matsuyama, K. Hirose and K. Kawakami, *Biomacromolecules*, 2010, **11**, 1370–1375.

81 C. Rodríguez and J. Martínez-González, *Cells*, 2019, **8**, 1483.

82 N. Pishesha, J. R. Ingram and H. L. Ploegh, *Annu. Rev. Cell Dev. Biol.*, 2018, **34**, 163–188.

83 Z. Zhang, S. Ai, Z. Yang and X. Li, *Adv. Drug Deliv. Rev.*, 2021, **174**, 482–503.

84 C. Schneider-Barthold, S. Baganz, M. Wilhelmi, T. Scheper and I. Pepelanova, *BioNanoMaterials*, 2016, **17**, 3–12.

85 D. Jaros, M. Jacob, C. Otto and H. Rohm, *Int. Dairy J.*, 2010, **20**, 321–327.

86 Z. Gu, T. T. Dang, M. Ma, B. C. Tang, H. Cheng, S. Jiang, Y. Dong, Y. Zhang and D. G. Anderson, *ACS Nano*, 2013, **7**, 6758–6766.

87 N. V. Gupta and H. Shivakumar, *Daru, J. Pharm. Sci.*, 2010, **18**, 200.

88 M. R. Guilherme, F. A. Aouada, A. R. Fajardo, A. F. Martins, A. T. Paulino, M. F. Davi, A. F. Rubira and E. C. Muniz, *Eur. Polym. J.*, 2015, **72**, 365–385.

89 O. Güven, M. Şen, E. Karadağ and D. Saraydın, *Radiat. Phys. Chem.*, 1999, **56**, 381–386.

90 H. Shoukat, F. Pervaiz and S. Noreen, *Global Pharmaceutical Sciences Review*, 2016, **1**, 1–5.

91 M. Casimiro, M. Gil and J. Leal, *Int. J. Pharm.*, 2010, **395**, 142–146.

92 B. Singh and L. Pal, *Int. J. Biol. Macromol.*, 2011, **48**, 501–510.

93 J. L. Drury and D. J. Mooney, *Biomaterials*, 2003, **24**, 4337–4351.

94 A. I. Van Den Bulcke, B. Bogdanov, N. De Rooze, E. H. Schacht, M. Cornelissen and H. Berghmans, *Biomacromolecules*, 2000, **1**, 31–38.

95 R. Barbucci, S. Lamponi, A. Borzacchiello, L. Ambrosio, M. Fini, P. Torricelli and R. Giardino, *Biomaterials*, 2002, **23**, 4503–4513.

96 M. A. Raza, J.-O. Jeong and S. H. Park, *Front. Mater.*, 2021, **8**, 769436.

97 M. Demeter, I. Călina, A. Scărișoreanu and M. Micutz, *Gels*, 2021, **8**, 27.

98 T. Gupta, E. Strelcov, G. Holland, J. Schumacher, Y. Yang, M. Esch, V. Aksyuk, P. Zeller, M. Amati and L. Gregoratti, arXiv, 2019, preprint, arXiv:1904.01652, DOI: 10.48550/arXiv.1904.01652.

99 Q. Ge, Z. Chen, J. Cheng, B. Zhang, Y.-F. Zhang, H. Li, X. He, C. Yuan, J. Liu and S. Magdassi, *Sci. Adv.*, 2021, **7**, eaba4261.

100 M. J. Taylor, P. Tomlins and T. S. Sahota, *Gels*, 2017, **3**, 4.

101 P. Tordi, F. Ridi, P. Samorì and M. Bonini, *Adv. Funct. Mater.*, 2025, **35**, 2416390.

102 A. I. Visan and I. Negut, *Gels*, 2025, **11**, 72.

103 E. A. Appel, J. del Barrio, X. J. Loh and O. A. Scherman, *Chem. Soc. Rev.*, 2012, **41**, 6195–6214.

104 K. Y. Lee and D. J. Mooney, *Prog. Polym. Sci.*, 2012, **37**, 106–126.

105 K. Haraguchi and T. Takehisa, *Adv. Mater.*, 2002, **14**, 1120–1124.

106 J. M. Rosiak and F. Yoshii, *Nucl. Instrum. Methods Phys. Res., Sect. B*, 1999, **151**, 56–64.

107 Z. Wei, J. H. Yang, J. Zhou, F. Xu, M. Zrínyi, P. H. Dussault, Y. Osada and Y. M. Chen, *Chem. Soc. Rev.*, 2014, **43**, 8114–8131.

108 O. Jeon, D. S. Alt, S. M. Ahmed and E. Alsberg, *Biomaterials*, 2012, **33**, 3503–3514.

109 S. M. Kassem, M. I. A. A. Maksoud, M. M. Ghobashy, A. M. El Sayed, S. Ebraheem, A. I. Helal and Y. Y. Ebaid, *Radiat. Phys. Chem.*, 2023, **209**, 110953.

110 M. A. Waqar, N. Mubarak, A. M. Khan, F. Shaheen, M. A. Mustafa and T. Riaz, *Int. J. Polym. Mater. Polym. Biomater.*, 2025, **74**, 265–284.

111 A. M. Rangel-Garcia, M. A. Alvarez-Perez, F. Rivera-Torres and M. C. Piña-Barba, *Biomedical Materials & Devices*, 2025, pp. 1–10.

112 K. Szafulera, R. A. Wach, A. K. Olejnik, J. M. Rosiak and P. Ulański, *Radiat. Phys. Chem.*, 2018, **142**, 115–120.

113 D. A. Gyles, L. D. Castro, J. O. C. Silva Jr and R. M. Ribeiro-Costa, *Eur. Polym. J.*, 2017, **88**, 373–392.

114 S. Thakur and O. Arotiba, *Adsorpt. Sci. Technol.*, 2018, **36**, 458–477.

115 B. F. Bukit, A. W. Pratama, E. Frida, B. B. Sedayu, D. Fransiska, D. Purnomo, E. Rochima, I. Rahmawati, S. Suhartana and F. A. Syamani, *South Afr. J. Chem. Eng.*, 2025, **51**, 254–264.

116 P. Zhang, K. Zou, L. Yuan, J. Liu, B. Liu, T.-P. Qing and B. Feng, *Sep. Purif. Technol.*, 2022, **301**, 122050.

117 A. Zhou, C. Zhu, W. Chen, J. Wan, T. Tao, T. C. Zhang and P. Xie, *Colloids Surf., A*, 2018, **554**, 237–244.

118 S. Cho, J.-H. Kim, K. S. Yang and M. Chang, *Chem. Eng. J.*, 2021, **425**, 130645.

119 S. Cao, X. Zhang, S. Xie, C. Wang, J. Bai, X. Li, R. Zhang, X. Xiao, J. Hu and X. Jiang, *J. Environ. Chem. Eng.*, 2025, **13**, 115091.

120 J. Wang, X. Lan, W. Shi and Z. Chen, *Carbohydr. Polym.*, 2025, **353**, 123258.

121 W. Tong, J. Liu, S. Liu, Z. Huang, Z. Huang, D. Chen, F. Xiao and S. Yang, *Talanta*, 2025, 128299.

122 V. H. Ramos-Martinez, V. A. Escobar-Barrios and J. Oliva-Uc, *J. Environ. Chem. Eng.*, 2025, **13**, 115680.

123 N. Li, S. Wen and C. Yu, *Colloids Surf., A*, 2025, 136344.

124 J. Chen, X. Wang, X. Huang, Z. Tong, J. Zhou, Y. Shen and C. Hao, *Int. J. Biol. Macromol.*, 2025, **306**, 141398.

125 Z. Gong, M. Zhao, D. Ma, Z. Sun and J. Hu, *Int. J. Biol. Macromol.*, 2025, **306**, 141498.

126 J. M. Galindo, C. M. Andreu, S. Merino, M. A. Herrero, E. Vázquez, A. M. Sánchez-Migallón and G. Castañeda, *Ecotoxicol. Environ. Saf.*, 2025, **292**, 117934.

127 A. R. Salem, E.-S. A. Haggag, M. M. Mohamed and G. A. Mahmoud, *Surf. Interfaces*, 2025, **59**, 105801.

128 S. Gai, Z. Feng, S. Wang, X. Xu, W. Liang, Y. Hu, F. Lou, K. Cheng and F. Yang, *Sep. Purif. Technol.*, 2025, **367**, 132900.

129 G. Salfate, C. Negrete-Vergara and J. Sanchez, *Chem. Eng. Sci.*, 2025, **309**, 121440.

130 T.-X. Li, N. Zhang, X.-t. Lan, F. Wu, Y.-h. Xie, D. Feng, Y. Liu, Y. Mei and D. Xie, *Colloids Surf., A*, 2025, **715**, 136611.

131 T. Bell, J. R. Tavares and M.-J. Dumont, *J. Water Proc. Eng.*, 2025, **73**, 107709.

132 A. Ali, M. A. Hussain, M. T. Haseeb, S. N. A. Bukhari, T. Tabassum, M. Farid-ul-Haq and F. A. Sheikh, *J. Drug Delivery Sci. Technol.*, 2022, **69**, 103144.

133 G. Gopika, A. Sathish and K. Nithya, *J. Water Proc. Eng.*, 2025, **71**, 107183.

134 A. Ali, A. Akram, M. A. Bakar, H. M. Amin, L. Zohra, A. Abbas, M. Sher, M. A. Hussain, M. T. Haseeb and M. Imran, *J. Ind. Eng. Chem.*, 2025, **151**, 746–761.

135 M. Mirabedini, M. Z. Kassaee and S. Poorsadeghi, *Arabian J. Sci. Eng.*, 2017, **42**, 115–124.

136 B. Zhang, K. Chang, S. Qin, H. Wei, Q. Zhang, G. Wang, T. Guo and M. Yan, *Colloids Surf., A*, 2025, **716**, 136755.

137 Y. Huang, L. Wu, L. Chang, W. Peng, W. Wang and Y. Cao, *Int. J. Biol. Macromol.*, 2025, **295**, 139474.

138 M. Han, Z. Wang, Z. Xie, M. Hou and Z. Gao, *Int. J. Biol. Macromol.*, 2025, **297**, 139947.

139 D. Guo, B. Bai, J. Hu, X. Zhang, X. Yan and S. Liu, *Sep. Purif. Technol.*, 2025, **361**, 131482.

140 Y.-W. Tai, P. Khamwongsa, X.-T. Chen, Y.-S. Lin, Z.-J. Lee, S. Ummartyotin and Y. Wei, *Int. J. Biol. Macromol.*, 2025, **308**, 142458.

141 W. M. Seleka and E. Makhado, *Int. J. Biol. Macromol.*, 2025, 141015.

142 X. Kong, Z. Huang, C. Wang, D. Wang, W. Lan, T. Gong and H. Wang, *J. Environ. Sci.*, 2025, **160**, 777–788.

143 D. Dou, Y. Zhao, C. Yang, J. Deng, L. Lian and T. Zhou, *Sep. Purif. Technol.*, 2025, **366**, 132823.

144 K. Sharma, P. Choudhary, A. Majeed, S. Guleria, M. Kumar, A. K. Rana and G. Rajauria, *Ind. Crops Prod.*, 2025, **225**, 120474.

145 A. L. Obsa, N. T. Shibeshi, E. Mulugeta and G. A. Workeneh, *Carbohydr. Polym. Technol. Appl.*, 2025, **9**, 100637.

146 H. Wang, H. Xiao, Y. Xie, X. Tan, W. Guo, L. Li, R. Chen, B. Wang, M. Wang and D. Zhou, *J. Environ. Sci.*, 2026, **159**, 480–489.

147 S. Mukhopadhyay, *Polymer*, 2025, **324**, 128270.

148 K. Raj, T. Vora, G. PadmaPriya, B. Lal, A. Devi, R. Sharma, M. Chahar, L. Sudhakar, R. Suman and R. Nagraik, *Int. J. Biol. Macromol.*, 2025, 139963.

149 Q. Cheng, Y. Yu, Z. Wan, M. Zhou, W. Tang, W. Tan and M. Liu, *Talanta*, 2025, **283**, 127178.

150 S. Zhang, D. Mei, K. Li and B. Yan, *Colloids Surf., A*, 2025, 136304.

151 A. Chaurasiya, P. P. Pande, R. Shankar and P. Khare, *Chem. Eng. J.*, 2025, **515**, 163631.

152 A. Verma, K. Aljohani, B. S. Aljohani, B. Lal, Y. Jadeja, S. Ballal, M. Chahar and R. Suman, *Int. J. Biol. Macromol.*, 2025, **303**, 140660.

153 G. A. Al-Hazmi, N. H. Elsayed, J. S. Alnawmasi, K. B. Alomari, A. H. Alessa, S. A. Alshareef and A. El-Bindary, *Int. J. Biol. Macromol.*, 2025, 140019.

154 D. M. Alshangiti, M. M. Ghobashy, S. A. Alkhursani, F. S. Shokr, S. A. Al-Gahtany and M. M. Madani, *J. Mater. Res. Technol.*, 2019, **8**, 6134–6145.

155 O. D. Agboola and N. U. Benson, *Front. Environ. Sci.*, 2021, **9**, 678574.

156 L. A. Shah and S. A. Khan, *Environmental Chemistry and Recent Pollution Control Approaches*, 2019, vol. 69.

157 M. F. Mubarak and A. M. Saleh, *Sci. Rep.*, 2025, **15**, 42542.

158 A. H. Berger and A. S. Bhown, *Energy Procedia*, 2011, **4**, 562–567.

159 W. Lv, R. Zhang, F. Sun, Y. Guo, W. Jiao, H. Wang, X. Hou, R. Qin, W. Pan and B. Lv, *Kinet. Catal.*, 2025, 1–26.

160 J. Wang and X. Guo, *Crit. Rev. Environ. Sci. Technol.*, 2023, **53**, 1837–1865.

161 E. D. Revellame, D. L. Fortela, W. Sharp, R. Hernandez and M. E. Zappi, *Clean Eng. Technol.*, 2020, **1**, 100032.

162 Z. Darban, S. Shahabuddin, R. Gaur, I. Ahmad and N. Sridewi, *Gels*, 2022, **8**, 263.

163 M.-C. Stanciu and C.-A. Teacă, *Gels*, 2024, **10**, 243.

164 S. Domínguez Beltrán, G. Miranda Piña, E. E. Granda Gutiérrez, R. Alejo Eleuterio, J. L. García Rivas and A. Reyes García, *Modelling*, 2025, **6**, 149.

165 N. F. Al-Harby, E. F. Albahly and N. A. Mohamed, *Polymers*, 2021, **13**, 4446.

166 J. Huang, F. Liu and J. Zhang, *Sep. Purif. Technol.*, 2021, **255**, 117713.

167 J. Lin and L. Wang, *Front. Environ. Sci. Eng. China*, 2009, **3**, 320–324.

168 K. H. Chu, J.-C. Bollinger and J. Kierczak, *Environ. Surf. Interfaces*, 2025, **3**, 191–195.

169 R. Ezzati, *J. Dispersion Sci. Technol.*, 2025, **46**, 222–229.

170 G. Zhao, X. Wu, X. Tan and X. Wang, *Open Colloid Sci. J.*, 2011, **4**, 19–31.

171 G. Crini and P.-M. Badot, *Prog. Polym. Sci.*, 2008, **33**, 399–447.

172 B. E. G. Lucier, S. Chen and Y. Huang, *Acc. Chem. Res.*, 2018, **51**, 319–330.

173 D. Wu, L. Hu, Y. Wang, Q. Wei, L. Yan, T. Yan, Y. Li and B. Du, *J. Colloid Interface Sci.*, 2018, **523**, 56–64.

174 I. Ahmed and S. H. Jhung, *J. Hazard Mater.*, 2016, **301**, 259–276.

175 G. K. Ramesha, A. V. Kumara, H. B. Muralidhara and S. Sampath, *J. Colloid Interface Sci.*, 2011, **361**, 270–277.

176 R. Say, E. Birlik, Z. Erdemgil, A. Denizli and A. Ersöz, *J. Hazard. Mater.*, 2008, **150**, 560–564.

177 Z. Du, S. Deng, Y. Bei, Q. Huang, B. Wang, J. Huang and G. Yu, *J. Hazard Mater.*, 2014, **274**, 443–454.

178 F. Liu, S. Chung, G. Oh and T. S. Seo, *ACS Appl. Mater. Interfaces*, 2012, **4**, 922–927.

179 R. G. Pearson, *J. Am. Chem. Soc.*, 1963, **85**, 3533–3539.

180 F. G. Helfferich and J. S. Dranoff, *Ion Exchange*, McGraw-Hill, New York, 1963, p. 624.

181 Y. Qiu and K. Park, *Adv. Drug Deliv. Rev.*, 2001, **53**, 321–339.

182 B. Padhan, J. Lee, B. K. Maiti, R. Karmakar, J. K. Dash, M. Patel and R. Patel, *Polym.-Plast. Technol. Mater.*, 2025, **64**, 2613–2636.

183 Y. Li, P. Bai, Y. Yan, W. Yan, W. Shi and R. Xu, *Microporous Mesoporous Mater.*, 2019, **273**, 203–211.

184 D. Sarkar and D. K. Chattoraj, *Adv. Colloid Interface Sci.*, 1993, **43**, 1.

185 L. Liu, Y. Wan, Y. Xie, R. Zhai, B. Zhang and J. Liu, *Chem. Eng. J.*, 2012, **187**, 210–216.

186 Y. Guo, M. Li, T. Zhou, Q. Wu, C. Liu, S. Li, Q. Feng, H. Wang and Z. Li, *J. Environ. Chem. Eng.*, 2025, **13**, 116023.

187 T. Yang, L. Xue, Z. Luo, J. Lin, X. Zhang, F. Xiao, Y. Liu, D. Li and X. Lin, *J. Hazard. Mater.*, 2025, 137325.

188 C. Nyadroh, T. Keshavarz and G. Kyazze, *Desalination Water Treat.*, 2025, 101235.

189 Z. Fang, Y. Liu, J. Qi, M. Yu, Y. Wang, Y. Qiu, Z. Ma and S. Liu, *Mater. Today Chem.*, 2025, **43**, 102467.

190 C.-C. Tang, Y.-Q. Cheng, S.-L. Chen, Y.-R. Hu, Z.-W. He, Z.-H. Li, Y. Tian and X. C. Wang, *J. Environ. Manage.*, 2025, **383**, 125489.

191 L. Souza, D. Recouvreux, E. Watzko, W. Taufemback, C. Carminatti, R. Antônio, T. Pineda-Vásquez and D. Hotza, *Int. J. Biol. Macromol.*, 2025, **307**, 141569.

192 S. Chi, X. Liu, J. Wu, Q. Feng, L. Wang, J. Li and T. Sun, *Int. J. Biol. Macromol.*, 2025, **308**, 141824.

193 Y. Guo, C. M. Dundas, X. Zhou, K. P. Johnston and G. Yu, *Adv. Mater.*, 2021, **33**, 2102994.

194 Z. Wang, P. Zhang, C. Yin, Y. Li, Z. Liao, C. Yang, H. Liu, W. Wang, C. Fan and D. Sun, *Adv. Funct. Mater.*, 2023, **33**, 2300341.

195 S. Nayak, S. R. Prasad, D. Mandal and P. Das, *J. Hazard Mater.*, 2020, **392**, 122287.

196 Y. Zhuang, Q. Liu, Y. Kong, C. Shen, H. Hao, D. D. Dionysiou and B. Shi, *Environ. Sci.: Nano*, 2019, **6**, 388–398.

197 H. Liu, X. Qu, E. Kim, M. Lei, K. Dai, X. Tan, M. Xu, J. Li, Y. Liu and X. Shi, *Biomaterials*, 2018, **162**, 109–122.

198 S. Goswami, D. Dutta, S. Pandey, P. Chattopadhyay, R. Dubey and D. Tiwari, *J. Environ. Manage.*, 2024, **359**, 121063.

199 H. M. Abd El-Lateef, M. M. Khalaf, M. A. Alsaeed, M. F. Abou Taleb and M. Gouda, *Int. J. Biol. Macromol.*, 2024, **282**, 137410.

200 H. Luo, J. Zeng, M. Xu, Q. Tang, T. Liu, S. Wu, S. Li and H. Rong, *Int. J. Biol. Macromol.*, 2025, **289**, 138872.

201 M. Sboui, M. A. Hussein, K. A. Alamry, Y. O. Al-Ghamdi, H. Gan, Z. Ji, M. Swaminathan, K. Zhang, Z. Li and Z. Yao, *Chem. Eng. Sci.*, 2025, **302**, 120902.

202 N. K. Dhiman, S. Agnihotri and M. S. Reddy, *Chem. Eng. J.*, 2024, **489**, 151335.

203 W. Lu, T. Ding, X. Wang, C. Zhang, T. Li, K. Zeng and G. W. Ho, *Nano Energy*, 2022, **104**, 107892.

204 Y. Huang, K. Zhou, H. Cheng, T. He, H. Wang, J. Bai, C. Yang, T. Guang, H. Yao and F. Li, *Adv. Funct. Mater.*, 2024, **34**, 2308620.

205 T. Ren, L. Huang, S. Xie, G. Chen, P. Liu and L. Chen, *Sci. China Technol. Sci.*, 2023, **66**, 2958–2967.

206 X. Li, Z. Liao, J. Niu, C. Hu, L. Li, J. Li, J. Zhou, H. Shen, J. Yin and W. Guo, *Sci. China Mater.*, 2022, **65**, 2889–2893.

207 X. Pan, Q. Wang, D. Benetti, L. Jin, Y. Ni and F. Rosei, *J. Mater. Chem. A*, 2023, **11**, 19506–19513.

208 K. Zhao, J. W. Lee, Z. G. Yu, W. Jiang, J. W. Oh, G. Kim, H. Han, Y. Kim, K. Lee and S. Lee, *ACS Nano*, 2023, **17**, 5472–5485.

209 X. Mu, J. Zhou, P. Wang, H. Chen, T. Yang, S. Chen, L. Miao and T. Mori, *Energy Environ. Sci.*, 2022, **15**, 3388–3399.

210 Z. Zhou, Y. Zhang, W. Liu, C. Gui, L. Huang, H. Huang, K. Fan, Y. Huang, Y. Gong and A. Chen, *Desalination*, 2024, **583**, 117685.

211 Y. Long, X. Li, Y. Li, L. Wang, H. Zhu and G. Shi, *Chem. Eng. J.*, 2024, **494**, 152615.

212 J. Duan, X. Yan, K. Lei, J. Cheng, Y. Wang, Q. Su, S. Xu, J. Li and Q. Ma, *J. Energy Storage*, 2024, **97**, 112778.

213 X. Cheng, Y. Hu, P. Chen, H. Qi and A. Lu, *Chem. Eng. J.*, 2024, **498**, 155161.

214 Q. Zhao, J. Liu, Z. Wu, X. Xu, H. Ma, J. Hou, Q. Xu, R. Yang, K. Zhang and M. Zhang, *Chem. Eng. J.*, 2022, **442**, 136284.

215 B. Wang, K. Yang, B. Cai, J. Zhang, C. Wei and A. Zhou, *Chem. Eng. J.*, 2023, **465**, 142944.

216 T. He, S. Lv, D. Wei, R. Feng, J. Yang, Y. Yan, L. Liu and L. Wu, *Chem. Rec.*, 2023, **23**, e202300184.

217 Y. Cao, B. Xu, Z. Li and H. Fu, *Adv. Funct. Mater.*, 2023, **33**, 2301420.

218 L. Yang, X. Huang, H. Wu, Y. Liang, M. Ye, W. Liu, F. Li, T. Xu and H. Wang, *Eng. Sci.*, 2023, **23**, 808.

219 V. Gomes, S. R. Veloso, M. A. Correa-Duarte, P. M. Ferreira and E. M. Castanheira, *Int. J. Mol. Sci.*, 2022, **24**, 186.

220 J. Sun, T. Wu, H. Wu, W. Li, L. Li, S. Liu, J. Wang, W. J. Malfait and S. Zhao, *Mater. Sci. Eng. R Rep.*, 2023, **154**, 100735.